MODEL-BASED AND DATA-DRIVEN H_∞ CONTROLLER SYNTHESIS FOR STABILIZED PLATFORMS

STABİLİZE PLATFORMLAR İÇİN MODEL TABANLI VE VERİYE DAYALI H_∞ KONTROLCÜ SENTEZİ

AYHAN ARDA ARAZ

ASSOC. PROF. DR. SELAHATTİN ÇAĞLAR BAŞLAMIŞLI

Supervisor

Submitted to

Graduate School of Science and Engineering of Hacettepe University

as a Partial Fulfillment to the Requirements

for the Award of the Degree of Master

in Mechanical Engineering

2020

To my family…

ABSTRACT

MODEL-BASED AND DATA-DRIVEN H$_\infty$ CONTROLLER SYNTHESIS FOR STABILIZED PLATFORMS

Ayhan Arda ARAZ

Master of Science, Department of Mechanical Engineering

Supervisor: Assoc. Prof. Dr. Selahattin Çağlar BAŞLAMIŞLI

January 2020, 104 pages

In this study, model-based and data-driven H_∞ robust controller synthesis methods are developed for line of sight control problem of stabilized platforms. Within the scope of the study, frequency response functions of the platform are obtained by using the input/output signals obtained by open-loop system identification tests. The parameters of the nominal plant model to be used in the design of model-based controllers are determined with the help of defined optimization problems. Full-order and fixed-order model-based H_∞ robust controller synthesis processes are discussed within the framework of the $S/KS/T$ mixed-sensitivity problem. On the other hand, the synthesis of fixed-order data-driven H_∞ robust controller is realized by means of a novel two-step method that is developed within the scope thesis study. The stability and performance characteristics of the designed controllers are determined by examining the frequency domain responses of closed-loop transfer functions. Finally, reference tracking and

disturbance rejection performances of the designed controllers are compared by real-time experiments carried out with the stabilized platform used in military applications.

Key Words: stabilized platform, line of sight stabilization, H_∞ robust control, model-based control, data-driven control

ÖZET

STABİLİZE PLATFORMLAR İÇİN MODEL TABANLI VE VERİYE DAYALI H∞ KONTROLCÜ SENTEZİ

Ayhan Arda ARAZ

Yüksek Lisans, Makina Mühendisliği Bölümü

Tez Danışmanı: Doç. Dr. Selahattin Çağlar BAŞLAMIŞLI

Ocak 2020, 104 sayfa

Bu çalışmada, stabilize platformların görüş hattı stabilizasyonu kontrol problemine yönelik, model tabanlı ve veriye dahalı H_∞ gürbüz kontrolcü sentez yöntemleri geliştirilmiştir. Gerçekleştirilen çalışma kapsamında, açık döngü sistem tanılama testleri ile elde edilen giriş/çıkış sinyalleri kullanılarak, platformun frekans tepki fonksiyonları elde edilmiştir. Model tabanlı kontrolcülerin tasarımında kullanılacak nominal tesis modelinin parametreleri, tanımlanan optimizasyon problemleri yardımıyla belirlenmiştir. Tam dereceli ve sabit dereceli model tabanlı H_∞ gürbüz kontrolcü sentezi işlemleri, $S/KS/T$ karışık duyarlılık problemi çerçevesinde ele alınmıştır. Öte yandan, sabit dereceli veriye dayalı H_∞ gürbüz kontrolcü sentezi, tez çalışması kapsamında geliştirilen iki aşamalı yeni bir yöntem aracılığıyla gerçekleştirilmiştir. Tasarlanan kontrolcülerin kararlılık ve performans özellikleri, kapalı döngü transfer fonksiyonlarının frekans alanındaki tepkileri incelenerek tespit edilmiştir. Son olarak, askeri uygulamalarda kullanılan stabilize platform ile gerçekleştirilen gerçek zamanlı deneyler aracılığıyla,

tasarlanan kontrolcülerin referans takibi ve bozucu etki giderimi performansları karşılaştırılmıştır.

Anahtar Kelimeler: stabilize platform, görüş hattı stabilizasyonu, H_∞ gürbüz kontrol, model tabanlı kontrol, veriye dayalı kontrol

ACKNOWLEDGMENTS

TABLE OF CONTENT

LIST OF FIGURES

xii

LIST OF TABLES

SYMBOLS AND ABBREVIATIONS

Symbols

A_i	Amplitudes of excitation signals used in system identification tests
d_I	Input disturbance signal
d_O	Output disturbance signal
e	Error signal
G	Plant
$G_{Bi-Quad}$	Bi-quad filter
G_f	Anti-resonance filter
G_{flex}	Torsional structural dynamics
G_P	Perturbed plant
$\mathcal{G}, M$	Non-parametric model set
K	Controller
K_d	Derivative gain
K_{freq}	Number of frequency points
K_i	Integral gain
K_P	Proportional gain
K_{red}	Reduced-order controller
l_I	Multiplicative uncertainty
L	(Open) Loop transfer function
L_d	Desired loop transfer function
m	Number of system identification tests

n	Sensor (measurement) noise signal
N, T_{wz}	Closed-loop transfer function from w to z
P	Generalized plant
r	Reference (command) input signal
S	Sensitivity function
t_{delay}	Time delay
T	Complementary sensitivity function
T_f	Derivative time constant
u	Control input signal
v	Sensed outputs
w	(Weighted) Exogenous inputs
W_A	Additive uncertainty weighting function
W_I	Multiplicative uncertainty weighting function
W_P	Performance weighting function
W_u	Actuator constraint weighting function
y	Output signal
y_{ss}	Steady-state response
z	(Weighted) Exogenous outputs
$\theta, \dot{\theta}, \ddot{\theta}$	Angular position, velocity and acceleration of the platform
τ_{max}	Maximum motor torque
τ_{app}	Applied motor torque
τ_{fr}	Friction torque
ω	Frequency
γ	∞-norm of closed-loop transfer function T_{wz}
ρ	Column vector of controller parameters

ϕ	Column vector of stable and known transfer functions
σ_i	ith Hankel singular value
Π	All possible model set
$\Re$	Real part of complex number
$\Im$	Imaginary part of complex number

Abbreviations

CbT	Correlation-based Tuning
DDC	Data-Driven Control
DFT	Discrete Fourier Transform
DVF	Direct Velocity Feedback
FRF	Frequency Response Function
GM	Gain Margin
HAC	High Authority Control
IFT	Iterative Feedback Tuning
ILC	Iterative Learning Control
IRC	Integral Resonant Control
LAC	Low Authority Control
LFT	Linear Fractional Transformation
LOS	Line of Sight
LTI	Linear Time Invariant
LTR	Loop Transfer Recovery
LQG	Linear Quadratic Gaussian
LQR	Linear Quadratic Regulator
MBC	Model-Based Control

MFAC	Model-Free Adaptive Control
MIMO	Multi Input Multi Output
NP	Nominal Performance
NS	Nominal Stability
PPF	Positive Position Feedback
PID	Proportional-Integral-Derivative
PM	Phase Margin
RP	Robust Performance
RS	Robust Stability
SISO	Single Input Single Output
SPSA	Simultaneous Perturbation Stochastic Approximation
UC	Unfalsified Control
VAF	Variance Accounted For
VRFT	Virtual Reference Feedback Tuning

1. INTRODUCTION

1.1. Problem Definition

Stabilized platform is a structure that is used in many different fields like military applications, space technology and robotic systems. Examples for the applications of the stabilized platforms are shown in Figure 1.1.

Figure 1.1. Applications of stabilized platforms [1]

Although the requirements in stabilized platform control problem may vary from one field to another, a common objective is to control line of sight (LOS) which is also called as aim point of the platform.

In the literature, LOS is defined as a vector from an observer to an observed object. In LOS control problems, target tracking and LOS stabilization are the two main objectives. In target tracking problem, LOS vector should be rotated for pointing its direction to the target object. On the other hand, LOS stabilization problem is related to control of platform angular speed by eliminating external disturbances. Controlled variables of target tracking and LOS stabilization problems are the angular position and angular speed of the LOS vector, respectively. LOS control problem is illustrated in Figure 1.2. Within the scope of thesis study, only LOS stabilization problem is considered.
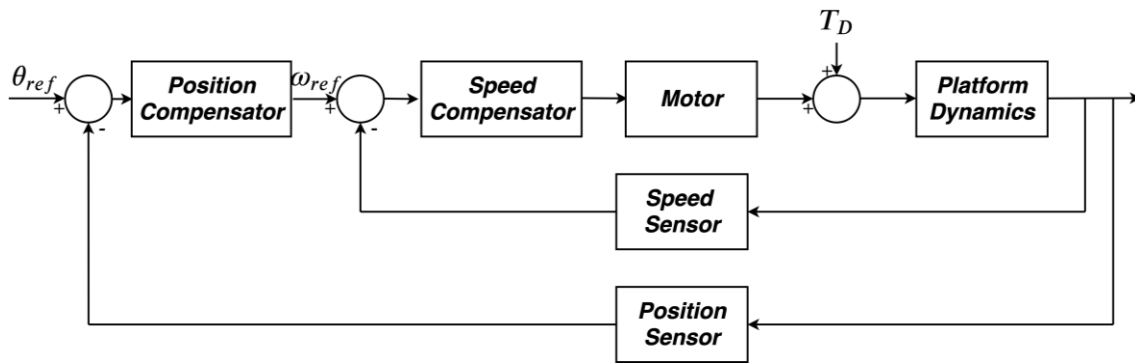
Figure 1.2. LOS control problem

1.2. Some Basic Principles in LOS Stabilization Control Problem

One of the most basic performance criteria in control problems of stabilized platform is to ensure that the platform remains stationary relative to an inertial coordinate system LOS stabilization. In this context, the basic approach to be performed is to apply counter torque, that eliminates the net torque acting on the platform. Although the stabilized platforms used today generally have a very sensitive electromechanical design, torque disturbances from different sources can affect the platform and cause undesirable reactions. On the other hand, another objective in control problems of the stabilized platform is controlling the motion of the platform according to the reference command. Therefore, gyroscopic sensors are usually integrated to the platforms to measure the inertial movement of the platform that require LOS stabilization and reference tracking.

In the single-axis stabilized platform shown in Figure 1.3, it is aimed to design a controller that provides the LOS stabilization despite of the base movement. During the mechanical design process, the suspension should be designed to minimize the friction. Also, the entire system should be balanced about axis of rotation to minimize imbalance torques. Finally, for successful mechanical design, the inertial properties and dynamics of the structure should be taken into account.

Figure 1.4 illustrates the angular speed feedback control loop used in a stabilized platform. When the reference command ω_c is set to zero, the controller's main task is to produce the torque input which is equal to the disturbance torque in opposite direction.

2
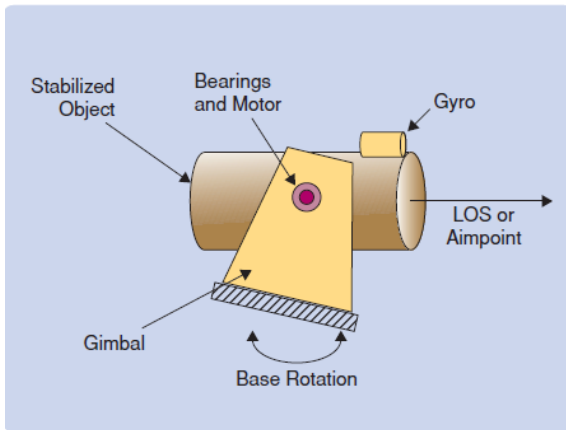
Figure 1.3. Stabilization in single-axis [1]
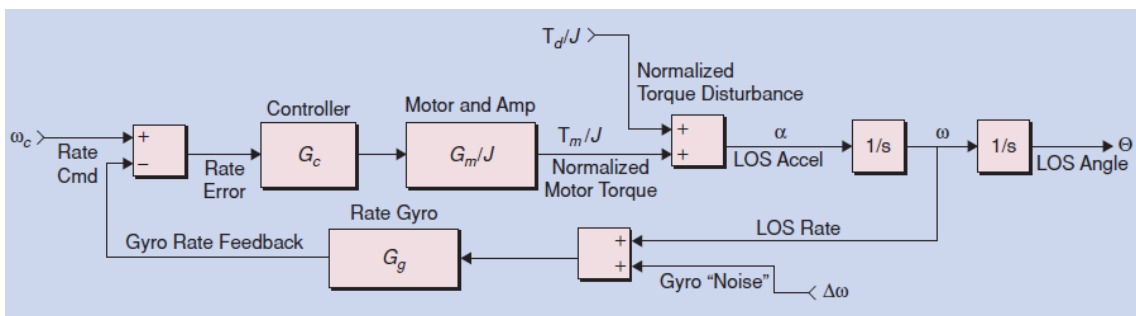
Figure 1.4. Angular speed feedback control loop for single-axis stabilized platform [1]

The bandwidth of a closed-loop control system is the main indicator for reference tracking and disturbance rejection performances of the designed controller. Figure 1.5 shows that the torque disturbances within the closed-loop system bandwidth can be successfully suppressed in an application of an angular speed feedback control.
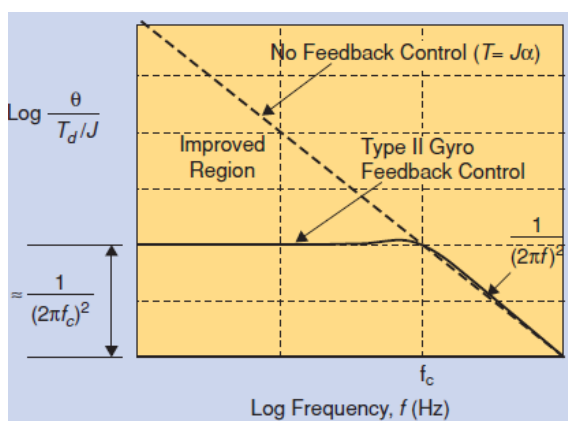
Figure 1.5. The effect of closed-loop system's bandwidth on disturbance rejection performance [1]

3

Although it is desirable to obtain the high closed-loop bandwidth, in practice, the fundamental limit for the bandwidth is determined by the dynamical characteristics of the system's components such as actuator and sensor and flexible modes of the system. Despite the fact that the PI-controller cascaded with the anti-resonance filter is widely used in real-time applications to minimize structural mode interactions, it has been shown that more complex and high-performance controllers can be synthesized by the more complex controller design algorithms.

1.3. Challenges in LOS Stabilization Control Problems

As discussed in previous section, main objective of the stabilized platform control problems is designing a controller that satisfies the precise reference tracking with high stabilization performance requirement. However, there are some challenging factors in control problems of this platforms such as:

- Low damped resonance/anti-resonance modes,
- Pole-zero flipping due to the use of non-collocated actuator/sensor pairs,
- Control/observation spillover,
- Non-linear effects,
- Variations in system parameters,
- Difficulties arise from mechanical design and hardware.

The details of the above mentioned challenges of the stabilized platform control problems are presented in this section.

The stabilized platforms may contain both bending and torsional modes as shown in Figure 1.6. In metallic structures, low structural damping and high resonant amplification is common. Increasing of the system stiffness or isolation of base motion can reduce the effect of bending modes. On the other hand, controllers should be carefully designed to reduce the effect of torsional modes which can directly affect the performance of the closed-loop system. In practice, it is generally possible to add a notch filter to the controller structure to reduce torsional flexibility by increasing closed-loop bandwidth of the system.
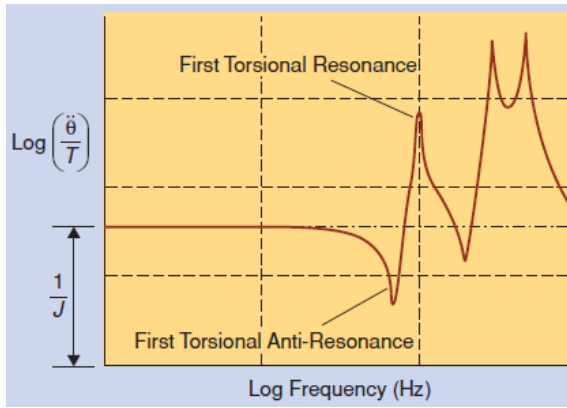
Figure 1.6. A general frequency response function of flexible mechanical system [1]

Another disturbance effect due to the flexibility is caused by the flexibility at the point where the platform connects to the main structure. In the stabilized platform applications, which relative motion should be precisely measured according to the inertial coordinate system, the base vibration have negative effects on the controller performance.

In the most of the stabilized platform control applications, the actuator and the sensor cannot be placed to the same degree of freedom, which results with a non-collocated control system [2]. In collocated control systems, the poles and the zeros of the plant are located in a sequential order in a position close to the imaginary axis. This property ensures the asymptotic stability of the closed-loop system regardless of the system parameters. In contrast to the collocated control structures, in non-collocated structures location of the poles and the zeros of the system can be affected even by small changes in system parameters. The shifting of poles and zeros of the low damping flexible modes of the system, which are located near to the imaginary axis, is called "pole-zero flipping". In non-collocated control systems, pole-zero flipping situation may result with even an unstable closed-loop system due to the small changes in system parameters. In [2], pole-zero flipping situation for non-collocated control systems which is resulted with unstable closed-loop system is visualized with the two-mass control problem as shown in Figure 1.7. In this problem, notch filter is designed to control the displacement of the second mass. The small changes in natural frequency of the flexible mode of the system results with an unstable closed-loop system.
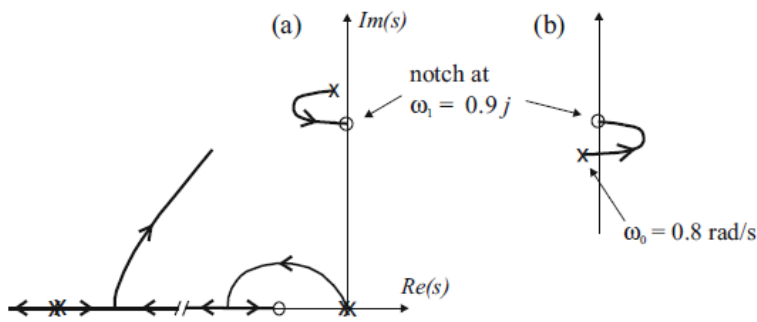
Figure 1.7. Notch filter design for the two-mass control problem in non-collocated control system [2]

Since the modeling of the mechanical systems that contain flexible modes, is finite, the frequency response function of the system can be obtained up to a certain frequency level. Moreover, to reduce the complexity of the controller synthesis procedure, the model of the plant may be simplified by reducing its order. In practice, controller can produce a signal that may excite the high frequency modes which are not modeled. As a result of this situation, the unmodeled dynamics of the system are excited and the responses in the high frequency band are measured by the sensors. When these measurements are used in the feedback loop of the control systems, the stability of the system cannot be guaranteed. This type of instability in the control system is called as control/observation spillover. To prevent the spillover phenomena, it is recommended that filter the sensor measurements with phase-locked loop pre-filter [3].

Friction, hysteresis, backlash, and flexibility in the torque transmission unit or other connections in the system can be considered as non-linear effects. In practice, it is possible to define all these non-linear effects as model uncertainty and to design a robust controller that can be operate under the defined uncertainty level. On the other hand, it is also possible to design a parallel control loops to reduce the effect of these non-linear disturbances.

The variations of the system parameters can influence the performances of the controller. Parameter uncertainties can be observed in flexible structures whose parameters are determined by the system identification tests. This leads to differences between the real system and its parametric model. In [4], the effect of variation of the system parameters on frequency response function of the system is analyzed. In this study, a two mass-spring-damper system is used to model flexible robot manipulator and it is shown that the

6

parameters that represent the stiffness (green lines) and arm inertia (blue lines), significantly influence the frequency response of the parametric model as shown in Figure 1.8. This type of analysis on flexible mechanical systems is important to determine the uncertainty level of the system.
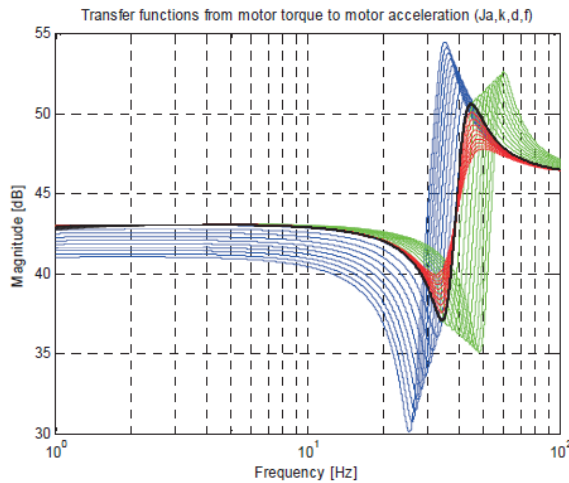
Figure 1.8. The effect of variations of model parameters on frequency response function [4]

In stabilized platform control applications, mechanical design and hardware selection can also lead some difficulties. For example, proper selection of the sensor, motor and, its driver is essential to obtain high reference tracking and stabilization performances. On the other hand, a good mechanical design can eliminate the additional friction and vibration problems.

1.4. Control Methods for Flexible Mechanical Systems

As explained in previous section, one of the main objective in control problems of stabilized platforms is to obtain good reference tracking and stabilization performances under existence of flexible modes. Therefore, throughout the literature survey, in addition to stabilized platforms, control methods for flexible mechanical systems from different fields are investigated.

In flexible mechanical systems control problems, one of the oldest idea is shaping of reference signal to reduce the vibration of the system [5]. Although there are different input shaping methods in the literature, the main difference between these methods is the robustness property of the methods. Input shaping methods are used for suppressing vibration in flexible mechanical systems by pole-zero cancellation. One popular method

7

for input shaping is convolution of impulse commands. In this method, amplitudes and applying times of impulse commands are calculated to obtain zero residual vibration [6]. In order to improve the robustness property of this method, design of impulse commands are performed with the additional constraint that the derivative of residual vibration with respect to the frequency is equal to zero at the modelling frequency [7]. This constraint results in adding a second zero on the resonance pole. In [8], it is suggested that the instead of exact pole-zero cancellation, the additional zeros are placed at the neighborhood of the resonance poles to obtain further increase in robustness property of input shaping methods. Input shaping method with convolution of impulse commands are usually used with feedback control methods in practical applications [9].

The method of shaping input signal by convolution of impulse commands is insufficient to determine the response time of the system. To overcome this problem, there are studies in the literature on the method of input shaping through the selection of response signal. By means of this method, the designer can determine the time and shape of the response within the limits of actuator. After determining response signal, the input signal is calculated by inverse dynamic methods. However, performance of this method mainly depends on the appropriate selection of response signal. In [10], response signal is defined as a polynomial function. However, this selection may result with an oscillatory motion in between and outside of the design points which are defined as displacement, velocity, and acceleration in particular time. In [11], response signal is determined as an exponential function to obtain asymptotic behavior.

In collocated control systems for lightly damped flexible mechanical systems, active damping strategy is another well-known control approach. The main objective of the active damping control strategy is to increase the negative real parts of resonance poles of the system. Active damping control strategy requires relatively low control efforts, therefore these methods are also named as Low Authority Control (LAC) [2]. Direct Velocity Feedback (DVF) control is one of the active damping control strategies where the control signal of negative feedback loop is basically calculated by multiplying the velocity measurement with an appropriate gain. In [12], DVF strategy is performed for large space structures control problems. In some situations, because of the physical nature of the flexible mechanical systems, there may arise an additional zero pair at high frequencies of the system plant, and in this situation, transfer function of the controller

should consist of more poles than the zeros. To overcome this problem, Positive Position Feedback (PPF) control method is proposed [13]. In [14], PPF controller is designed to trajectory tracking control of single-link flexible manipulator. Another active damping strategy is formulated by adding small portion of the actuator signal to the measurement signal which is called as Integral Resonant Control (IRC) [15]. This strategy resulted in an additional pair of zeros at a desired frequency, which is generally selected as lower than the first resonance mode of the flexible mechanical system.

Although above mentioned active damping methods are effective for reducing the effects of disturbances near the resonance frequencies of the flexible mechanical system, to obtain good stabilization and reference tracking performances under existence of wide-band disturbances, the poles of the plant must be substantially relocated. High Authority Control (HAC) methods are usually performed in control problems of flexible mechanical systems to improve the closed-loop performances.

Although there are numerous advanced controller design techniques, in many practical applications of control problems of flexible mechanical systems, linear proportional-integral-derivative (PID) type controllers are employed in control loops. In order to cope with the problems related to their limitations in dealing with non-linearity and uncertainty, different enhancement techniques are proposed. Some of these methods are, using cascaded multiple PID [16], gain scheduled or adaptive PID [17,18], and enlarging the PID-controller with different anti-resonance filters [19].

Besides of PID-controller design methods, pole-placement approach which is one of the most popular state-space control methods can be used in control problems of flexible mechanical systems. In the pole-placement approach, the desired locations of closed-loop poles should be selected carefully to obtain the required closed-loop performances. In [20], a state-feedback controller is calculated by pole-placement approach and overall control structure enhanced with feedforward terms and trajectory pre-filter for position control of ball screw test bed. While determining the desired closed-loop pole locations of the system, damping ratios of resonant poles are increased without changing their damped natural frequencies. In [21], the same strategy is used for determining the desired closed-loop pole locations of a non-collocated flexible manipulator control system. The performances of the designed state feedback controllers obtained by pole-placement method highly depend on the accuracy of the parametric model of the plant.

9

Linear Quadratic Gaussian control with Loop Transfer Recovery (LQG/LTR) is one efficient method for systems that have known or estimated uncertainties. Linear Quadratic Regulator (LQR) is one of the optimal control methods which has guaranteed stability properties [22]. However, to be able to perform the LQR strategy, all states of the system should be measured, which is not possible in practice. Therefore, most of the time, state feedback controller is used with a state estimator. However, introduction of a state estimator may negatively affect the robustness property of the closed-loop system. The main idea of LQG/LTR method is designing a state estimator in such a way that the obtained loop transfer function approaches the ideal LQR loop transfer function [23,24]. In [25], LQG/LTR method is performed to design a LOS control for two-axis gimbal system. According to the experimental study, stability of the closed-loop system with LQG/LTR controller is shown to be higher than the closed-loop system with Lead-PI-controller. Although LTR technique may be performed for a non-minimum phase system, the recovery of stability characteristics of the closed-loop system cannot be guaranteed. Moreover, designing a LQG/LTR controller is a complicated procedure generally resulting with a higher order complex controller.

Besides of the LQG/LTR method, H_∞ method is an another robust control method. In H_∞ control problems, controller design problem is formulated as an optimization problem with stability and performance constraints [26]. In H_∞ control problems, performances of the closed-loop system are strongly related with the selection of frequency dependent weighting functions. In [27], a genetic algorithm based method is proposed to determining the weighting functions. In [28], a comparative study is performed to analyze LOS stabilization performances of different robust controllers designed in LQG/LTR and H_∞ frameworks, and the experimental results show that the closed-loop system with H_∞ controller has better performance.

One of the biggest issues in the classical H_∞ control method is to obtain a high order controller which may lead to implementation problems in real-time systems with limited processing capability. In [29] and [30], non-smooth optimization techniques are proposed to solve H_∞ optimization problem with additional constraints related to order and structure of controller. In [31], these methods are performed to obtain lower order H_∞ controllers for stabilized platform. In [32], both full-order and fixed-order H_∞ controllers are designed for two-axis gimbal system and their disturbance rejection and reference

tracking performances are compared experimentally. According to the experimental results, although the performances of the full-order H_∞ controller is slightly better than the fixed-order H_∞ controller, a simple PI-controller, which is synthesized based on the non-smooth optimization technique in [30], can also be employed instead of a higher order complex controller in control loop.

Discussed HAC synthesis methods up to this point were model-based control methods. In other words, the performances of the closed-loop system obtained with the model-based controller, mainly depends on the accuracy of the parametric model [33]. Although data-driven control (DDC) methods, which eliminate the need for parametric plant model, are relatively new compared to the model-based control (MBC) methods, the prevalence of use increases with the developments in information science and technology. According to [34], DDC covers all available control theories and methods and controller synthesis is performed by directly using input/output data without any knowledge about the mathematical plant model.

In the literature, one categorization of DDC methods is realized according to the type of data usage. According to this categorization, simultaneous perturbation stochastic approximation (SPSA) [35], model-free adaptive control (MFAC) [36], and unfalsified control (UC) [37] are the methods classified as on-line data-base DDC methods. On the other hand, iterative feedback tuning (IFT) [38], correlation-based tuning (CbT) [39], virtual reference feedback tuning (VRFT) [40], and non-iterative data-driven model reference control [41,42] methods are the examples of off-line data-base DDC methods. Moreover, there also hybrid DDC methods like iterative learning control (ILC) [43,44] in which both on-line and off-line data are used to synthesize controller. DDC methods are also sorted into two categories according to the controller structure: DDC methods with pre-specified fixed controller structure and DDC methods with unknown controller structure.

There are limited number of experimental studies in the literature, which cover the implementation of DDC methods. In [45] and [46], frequency domain data-driven approaches are proposed to suppress vibration of SISO and MIMO systems, respectively. In these studies, mixed-sensitivity H_∞ control problem is formulated as a non-convex optimization problem by using open-loop system identification input/output data, and parameters of the controller which has fixed structure and order, are calculated by solving

the constraint non-convex optimization problem via a global optimization technique. Experimental results show that, the vibration suppression performance of the low order data-driven controllers is similar with model-based higher order H_∞ controllers, for both SISO and MIMO systems. Another non-convex optimization approach is introduced for both stable and unstable systems in [47], by using input/output data obtained from the closed-loop system identification tests performed with three different initial controllers.

Besides of the non-convex optimization approaches, in [48], frequency domain off-line data-driven method is developed to calculate the unknown parameters of linearly parameterizable controller. In this study, stability and H_∞ performance criteria are formulated as a convex feasibility problem with the help of selected line on the Nyquist plot, and the proposed approach is validated by experimental studies on a double mass-spring-damper system. On the other hand, in [49], convexification of the non-convex robust performance constraints is performed with the help of the desired loop transfer function. However, in these convex optimization approaches, the coefficients in the denominator of the specified controller transfer function cannot be included in the optimization problem and must be predetermined by the designer.

1.5. Methodology and Contributions

Within the scope of this thesis study, design methodologies of model-based and data-driven H_∞ robust controllers are proposed for LOS stabilization problem of stabilized platform. Three different robust controllers which are named as full-order model-based H_∞ controller, fixed-order model-based H_∞ controller, and fixed-order data-driven H_∞ controller are synthesized by using open-loop system identification test data.

Before designing proposed linear controllers, firstly plant model of the stabilized platform must be derived. To obtain linearized plant model, identification of the friction which is considered as the main non-linear effect on the system is performed. Then, non-parametric model set in frequency domain is calculated by using discrete Fourier transform based method. After obtaining non-parametric model set, parameters of nominal model of the plant is calculated by considering two different optimization problems that are solved by applying non-linear least squares approximation technique. Finally, multiplicative uncertainty region is determined by calculating difference between

12

the frequency response functions obtained for open-loop system identification tests performed with different excitation signals and the nominal parametric model.

After calculating nominal parametric plant model, both full-order and fixed-order H_∞ robust controllers are designed by treating model-based approaches. Synthesis of these controllers is performed by applying $S/KS/T$ mixed-sensitivity approach. Moreover, fixed-order data-driven H_∞ robust controller is synthesized by using non-parametric plant model set without need of a parametric plant model. To calculate unknown parameters of the fixed-order data-driven controller, a novel two-stage method is developed. Finally, reference tracking and disturbance rejection performances of the designed controllers are measured by real-time tests.

One major contribution of this thesis study is proposing a model-based robust method to calculate unknown parameters of the PI-controller enhanced with anti-resonance filter. Even if this controller structure is frequently used by designers [50], most of the designers calculate parameters of the controllers by heuristic approach. In this thesis study, a fixed-order model-based H_∞ controller design method is proposed to determine the unknown parameters of this controller.

In previous works, even if the controller structure is either non-linear [51,52] or linear [50,53], designers performed model-based approaches to synthesis LOS stabilization controller. Meanwhile, in this thesis study, the design of a data-driven method which is based on the direct use of input/output data obtained from open-loop system identification tests eliminates the need for a parametric plant model, and synthesis of fixed-order data-driven H_∞ controller is performed by offline optimization methods. In [48,49], researchers proposed different data-driven approaches for synthesis of fixed-order H_∞ robust controllers. However, the main disadvantage of these methods is that the coefficients in the denominator of the transfer function of the controller should be predetermined without being included in the optimization problem. Therefore, in this study, the synthesis of the fixed-order data-driven H_∞ controller has been carried out in two steps. With the help of the novel two-stage method, the unknown coefficients of the denominator of the fixed-order controller structure can also be calculated by using open-loop input/output data without the need of a parametric plant model. The proposed method has been validated using the synthesis of the controller to be used in the speed control loop of the traverse axis of a military stabilized platform.

13

Finally, the comparison of the model-based and data-driven H_∞ controllers is performed by measuring the reference tracking and disturbance rejection performances with real-time tests.

1.6. Outline of the Thesis

In Chapter 2, a general review of robust control theory is presented. Firstly, ∞-norm of signals and transfer functions are discussed. Then, the standard configuration of the feedback control system and closed-loop transfer functions are expressed. After presenting internal stability condition for feedback system, design objectives are given by considering fundamental limitation of the feedback system. Next, different weighting functions are introduced and common methodology for selection of these functions is discussed. The types of representation of uncertainty in the system are given and this chapter ends with the derivation of nominal stability, nominal performance, robust stability, and robust performance conditions for multiplicative uncertainty case.

In Chapter 3, the H_∞ robust controller design methods are discussed. First of all, a general control problem formulation for feedback control systems is given and calculation of generalized plant and closed-loop transfer function from exogenous inputs to exogenous outputs are investigated. After that, full-order and fixed-order model-based H_∞ controller synthesis methods and their solutions are introduced. Finally, fixed-order data-driven H_∞ control problem is formulated as a convex optimization problem with the help of desired open-loop transfer function.

In Chapter 4, system identification methodology which is performed to obtain both non-parametric and parametric model of stabilized platform. First, experimental test setup is introduced briefly. Then, friction model is identified to eliminate its non-linear effect on the system. After that, frequency response functions (FRFs) of the system are calculated by using open-loop system identification tests' input/output data. To obtain parametric plant model, general structure of plant model of stabilized platform is introduced and unknown parameters of this structure are calculated by applying non-linear least squares approximation technique. Chapter 4 ends with identification of the multiplicative uncertainty region for the stabilized platform.

Chapter 5 is devoted to the design of H_∞ robust controllers. After discussion of the weighting functions selection, full-order model-based H_∞ controllers are designed in

mixed-sensitivity framework. Then, PI-controller enhanced with anti-resonance filter is synthesized by performing fixed-order model-based H_∞ controller design method. Lastly, unknown parameters of the controller which has the same structure with fixed-order model-based H_∞ controller, are calculated by applying a novel two-stage data-driven method. In the first step of the proposed method, unknown parameters of the anti-resonance filter are calculated to reduce the effects of flexible modes of the stabilized platform. Then, linearly parameterized H_∞ controller is calculated by solving convex optimization problem in the second stage of the proposed method. At the end of this chapter, comparison of frequency domain performances of the designed controllers is presented.

Chapter 6 starts with the discussion about the implementations of designed H_∞ controllers. First, balanced truncation method is investigated to reduce the order of full-order model-based H_∞ controllers. After that, discretized H_∞ controllers are implemented to the stabilized platform and reference tracking and disturbance rejection performances of the designed controllers are measured by real-time tests. Chapter 6 ends with the comparison of time domain performances of the model-based and data-driven H_∞ controllers.

Chapter 7 includes summary of the thesis and discussion about some future works. At the end of the thesis study, information about the references utilized throughout the thesis study is presented.

2. REVIEW OF ROBUST CONTROL

In this chapter, the necessary information about robust control theory is presented to the reader in order to form the basis of the studies in this thesis. Within the scope of thesis study, H_∞ controllers will be designed for SISO system. Therefore, the following sections is discussed in this context.

2.1. Signal and System Norms

In control applications, the performance of a control system can be measured by the size of signal under interest. For instance, in reference tracking or disturbance rejection applications, the size of error signal indicates the performance of control system. The concept pf signal norm which must satisfy the following properties can be used as an indicator of size of any signal:

  (i) $\|u\| \geq 0$
  (ii) $\|u\| = 0$ if and only if $u(t) = 0, \forall t$
  (iii) $\|au\| = |a|\|u\|, \forall a \in \mathbb{R}$
  (iv) $\|u + v\| \leq \|u\| + \|v\|$

There are several norm definitions for signals and systems which are appropriate for different cases. For example, the least upper bound of absolute value of signal is defined as ∞-norm:

$$\|u\|_\infty = \sup_t |u(t)| \tag{1}$$

On the other hand, ∞-norm of a transfer function $G(j\omega)$ is equal to the peak value of Bode magnitude plot of $G(j\omega)$:

$$\|G(j\omega)\| = \sup_\omega |G(j\omega)| \tag{2}$$

2.2. Feedback Loop and Closed-Loop Transfer Functions

Standard configuration of a one degree of freedom feedback system is shown in Figure 2.1, where $K(s)$ and $G(s)$ are the transfer functions of controller and plant, respectively.
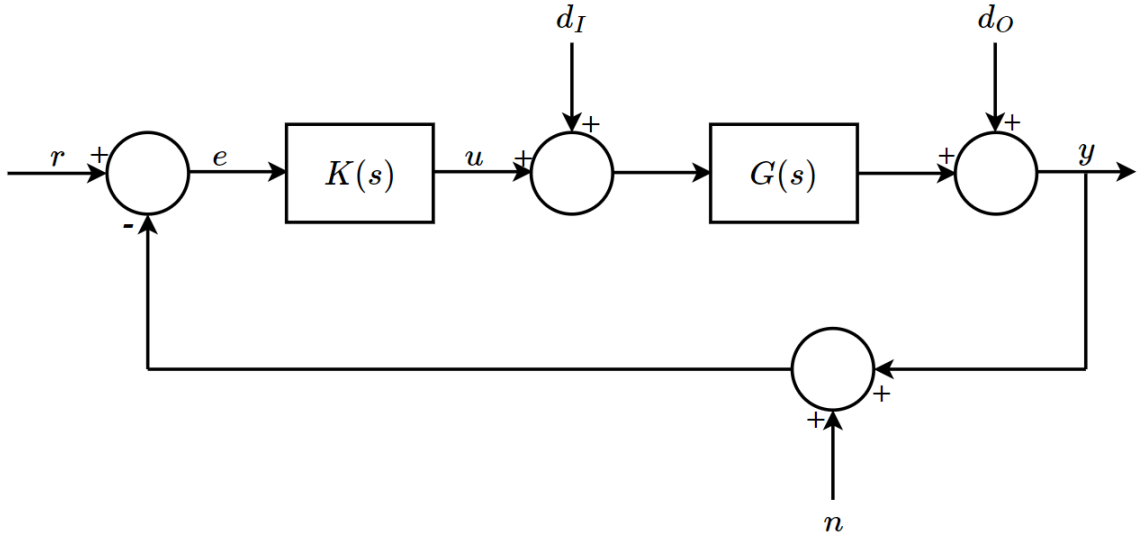
Figure 2.1. Standard configuration of feedback system

In this configuration, there are four exogenous input signals: reference (command) input signal r, input disturbance d_I, output disturbance d_O, and sensor (measurement) noise n. The other signals in the standard feedback configuration are the measured error e, the control input u and the system output y.

According to the standard configuration of feedback system shown in Figure 2.1, we define the *(open) loop transfer function, L* from the measured error to the system output as

$$L(s) = \frac{y}{e} = G(s)K(s) \tag{3}$$

the *sensitivity function, S* from the output disturbance to system output as,

$$S(s) = \frac{y}{d_O} = \left(I + G(s)K(s)\right)^{-1} = \left(I + L(s)\right)^{-1} \tag{4}$$

and the *complementary sensitivity function, T* from the reference (command) input to system output as

$$T(s) = \frac{y}{r} = I - S(s) = \left(I + G(s)K(s)\right)^{-1}G(s)K(s) = \left(I + L(s)\right)^{-1}L(s). \tag{5}$$

Using the definitions of closed-loop transfer functions, the *system output* is equal to:

$$Y(s) = S(s)D_O(s) + S(s)G(s)D_I(s) + T(s)\left(R(s) - N(s)\right) \tag{6}$$

The *measured error* is equal to:

$$E(s) = S(s)\big(R(s) - D_O(s)\big) - S(s)G(s)D_I(s) + T(s)N(s) \tag{7}$$

The *control input* is equal to:

$$U(s) = K(s)S(s)\big(R(s) - N(s) - D_O(s)\big) + T(s)D_I(s) \tag{8}$$

2.3. Internal Stability

In stability analysis of the feedback system, the signals r and n can be neglected since the transfer functions from these signals to u is equal to transfer function from d_o to u. Then the general configuration of the feedback loop in Figure 2.1 can be rearranged for stability analysis with two exogenous input such that $w_1 = d_I$ and $w_2 = d_O$ in Figure 2.2.
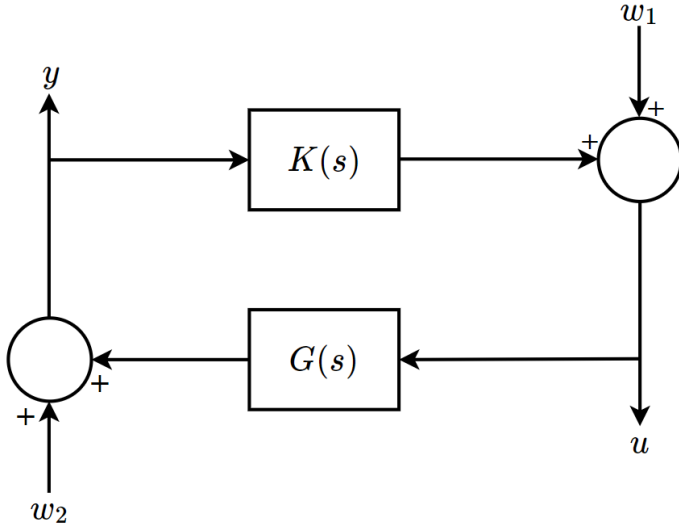
Figure 2.2. Internal stability analysis configuration of feedback system

Two outputs of the feedback system in Figure 2.2 are equal to:

$$u = (I + KG)^{-1}w_1 - K(I + GK)^{-1}w_2 \tag{9}$$

$$y = G(I + KG)^{-1}w_1 + (I + GK)^{-1}w_2 \tag{10}$$

With the assumption of no right half plane pole-zero cancellations between $G(s)$ and $K(s)$, the internal stability of the feedback system can be guaranteed by four transfer functions in Eq. 9 and Eq. 10 being all stable [26].

2.4. Design Objectives of the Feedback Control

In this section, fundamental tradeoff of the feedback control is discussed first and then design objectives of the feedback control are formulated by using the closed-loop transfer functions.

2.4.1. Fundamental Tradeoff of the Feedback Control

According to the definitions of sensitivity and complementary sensitivity functions, the following relationship between these two function can be:

$$S + T = I \tag{11}$$

For a feedback system, "perfect control" can be achieved by eliminating measured error such that $e = y - r = 0$. From Eq. 7, zero measured error requirement can also be described by following relationship:

$$e \approx 0. r - 0. d_O - 0. P. d_I + 0. n \tag{12}$$

The first three requirements in Eq. 12 named as reference tracking, output and input disturbance rejection are obtained with $S \approx 0$ or $|L| \rightarrow \infty$. On the other hand, the last requirement in Eq. 12 is related to noise cancellation and it is obtained with $T \approx 0$ or from Eq. 11 $S \approx I$ ($|L| \rightarrow 0$). This conflicting situation illustrates the fundamental tradeoff of the feedback control system. In other words, to obtain good reference tracking and disturbance rejection, high loop gain is needed, however this also leads to noise attenuation problems.

Another important signal in feedback control system is control input u. In physical systems, the control input is produced by the actuators that have physical limits. Therefore, the control input must be small to avoid saturation of the actuator. From Figure 2.1, the control input is given by $u = K(r - y - n)$ and to obtain small control input, feedback controller K and $L = GK$ must also be small.

The general design objectives in the feedback control are listed below [26]:

1. Good input and output disturbance rejection performance: Large L
2. Good reference tracking performance: Large L
3. Stabilization of unstable plant: Large L
4. Reducing the effect of measurement noise: Small L
5. Limiting magnitude of control input: Small L
6. Nominal stability: Small L (due to right half plane zeros and time delays)
7. Robust stability: Small L (due to neglected and uncertain dynamics)

The contradictory design objectives in feedback control listed above are generally related with the different frequency ranges. Therefore, one can realize a good feedback controller design by obtaining high loop gain ($|L| > 1$) at low frequencies (below the crossover

frequency) to improve the disturbance rejection and reference tracking performances, and small loop gain ($|L| < 1$) at high frequencies (above the crossover frequency) for robustness and sensor noise reduction. In the crossover region between ω_c ($|L| = 1$) and ω_{180} ($\angle L = 180°$) stability requirements should be considered. For stability, the loop gain should be less than 1 at ω_{180} and $\angle L > -180°$ at ω_c . According to these requirements, desired loop gain is shown in Figure 2.3.
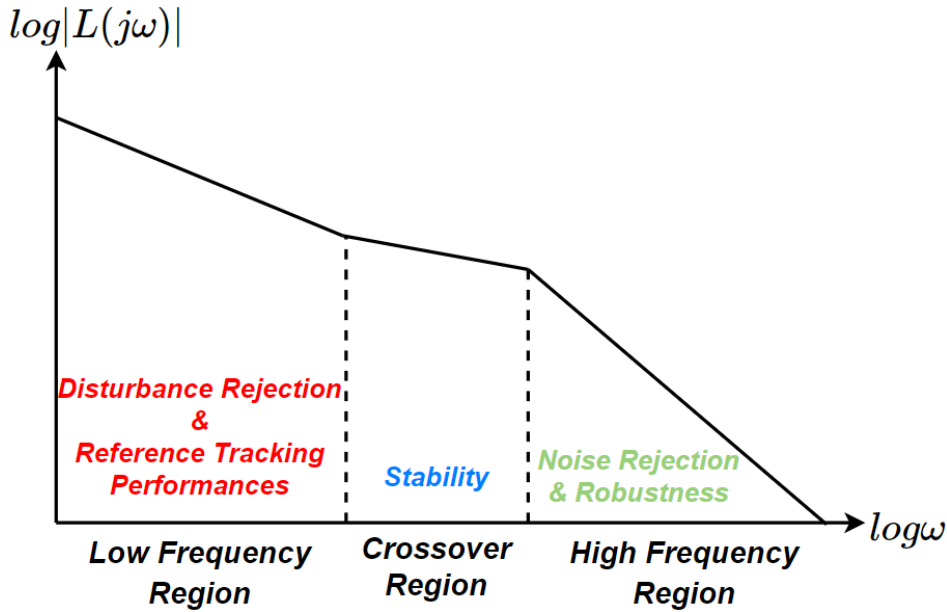
Figure 2.3. Desired loop gain $|L(j\omega)|$ for feedback control

2.4.2. Weighting Functions

In the previous section, the performance objectives are described in terms of open-loop transfer function (L). An alternative strategy to formulate performance objectives in feedback control is shaping the closed-loop transfer functions such as sensitivity (S) and complementary sensitivity (T) functions. For example, the performance criterion may be specified by defining frequency dependent bounds for sensitivity function.

$$\begin{cases} |S(j\omega)| \leq A, & \forall \omega \leq \omega_0 \\ |S(j\omega)| \leq M, & \forall \omega > \omega_0 \end{cases}$$

However, in H_∞ control problems, the performance objectives are formulated by choosing the appropriate weighting functions which reflects system requirements. For instance, preceding performance objective can be written as:

$$|W_P(j\omega)S(j\omega)| \leq 1, \quad \forall \omega$$

where

$$|W_P(j\omega)| = \begin{cases} 1/A, & \forall \omega \leq \omega_0 \\ 1/M, & \forall \omega > \omega_0 \end{cases}$$

In multivariable control systems, using weighting functions are essential for pointing out the importance of the signals and making signals with different units are comparable. Moreover, most important frequency range for minimizing error signals can be described by using weighting functions. The standard configuration of feedback control system in Figure 2.1 can be modified with weighting functions, and it is shown in Figure 2.4.
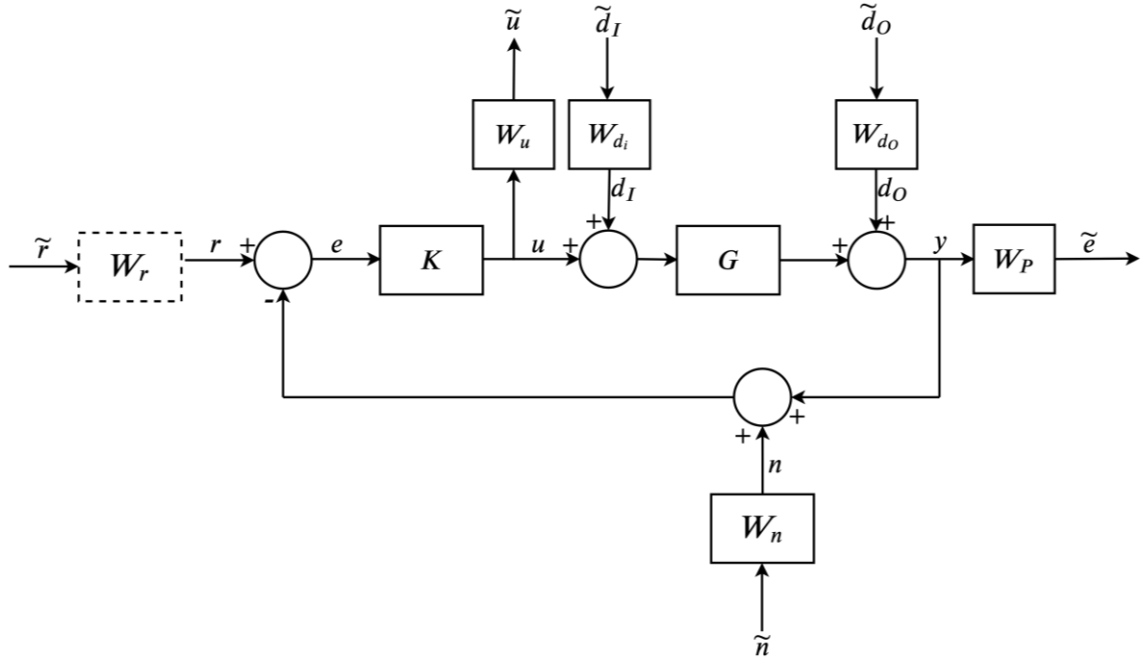
Figure 2.4. Standard feedback configuration with weighting functions

In H_∞ control, choosing the weighting functions in Figure 2.4 is a very important step for controller design process and these functions are chosen according to design objectives and knowledge of the exogenous input signals such as disturbances and sensor noise. For example, W_{d_i}, W_{d_o}, and W_n are usually determined to represent frequency contents of the input and output disturbances and measurement noise, respectively, On the other hand, W_P is selected to shape sensitivity function $(S(j\omega))$, while W_u is used to specify the physical limits of the actuator. Finally, W_r may be added the control loop to shape reference command.

As already discussed, sensitivity function is a very good indicator for both disturbance rejection and reference tracking performances of the closed-loop system. By shaping the sensitivity function, the desired performance of the closed-loop system can be achieved. There are some typical specifications for sensitivity function:

1. Peak value of $|S(j\omega)|$, M
2. Minimum bandwidth frequency, ω_B^*
3. Maximum steady-state tracking error, A
4. Slope of $S(j\omega)$ below the bandwidth frequency

If the peak value of $|S(j\omega)|$ is large, then the maximum overshoot can be large and also noise and the robustness problems may arise. Therefore, M which represents the upper bound of $1/|W_P(j\omega)|$ at high frequencies should not be very large for good controller design. On the other hand, ω_B^* may be chosen to satisfy the closed-loop bandwidth requirement of the system. In many control applications, it is desirable that the steady-state tracking error with respect to step input be equal to zero. However, in H_∞ control weighting functions cannot contain pure integrators [54]. Hence, a very small tracking error with respect to a step input may be defined by using a design parameter A which represents the upper bound of $1/|W_P(j\omega)|$ at low frequencies. Then, described performance requirements can be achieved if the following inequality is ensured:

$$|S(j\omega)| < 1/|W_P(j\omega)|, \quad \forall \omega \tag{13}$$

where,

$$W_P(s) = \frac{s/M + \omega_B^*}{s + \omega_B^* A} \tag{14}$$

In some applications, a steeper slope between the low and high frequencies for $S(j\omega)$ may be desired, and then second order weighting function in Eq. 15 may be used.

$$W_P(s) = \frac{\left(\dfrac{s}{M^{\frac{1}{2}}} + \omega_B^*\right)^2}{\left(s + \omega_B^* A^{\frac{1}{2}}\right)^2} \tag{15}$$

Magnitude of the inverse weighting function $1/|W_P(j\omega)|$ is shown in Figure 2.5. Magnitude of the inverse performance weighting function $1/|W_P(j\omega)|$ Figure 2.5.
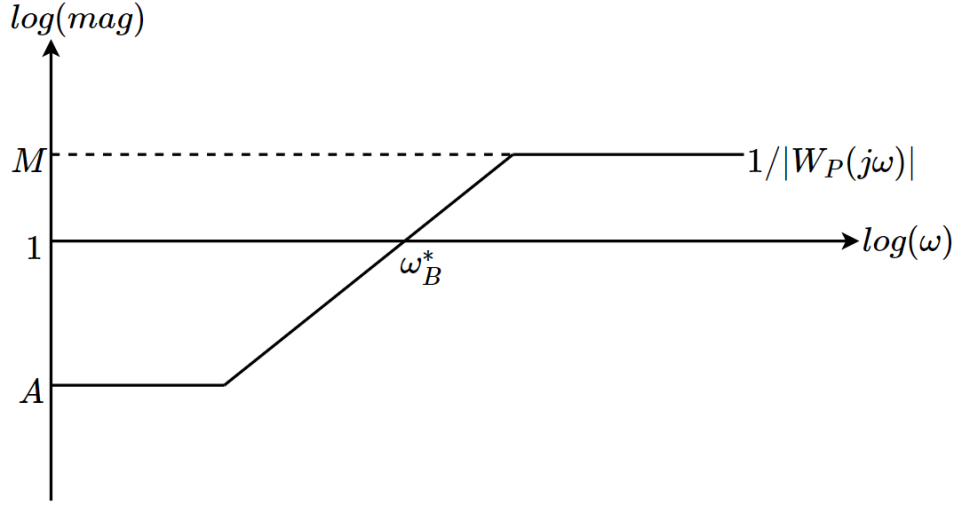
Figure 2.5. Magnitude of the inverse performance weighting function $1/|W_P(j\omega)|$

Prescribed performance objectives are satisfied if the magnitude of sensitivity function, $|S(j\omega)|$ stays below $1/|W_P(j\omega)|$ at all frequencies, i.e. $\|W_P S\|_\infty < 1$.

Actuator constraint weighting function W_u is selected by considering the control signal equation:

$$u = KS(r - d_O - n) - Td_I$$

The magnitude of $|KS|$ is limited by using weighting function W_u to avoid saturation of the actuator. Therefore, W_u may be simply selected as [26]:

$$W_{u,1}(s) = \frac{1}{\tau_{max}} \tag{16}$$

where τ_{max} represents the saturation limit value of the actuator. On the other hand, beyond the desired control bandwidth, W_u may be modified to attenuate the effects of noise and disturbance by rolling of the magnitude of $|KS|$ [54]:

$$W_{u,2}(s) = \frac{s + \omega_{bc}/\tau_{max}}{\epsilon s + \omega_{bc}} \tag{17}$$

One may obtain the faster roll of with higher order weighting function W_u in Eq. 18.

$$W_{u,2'}(s) = \frac{\left(s + \frac{\omega_{bc}}{\sqrt[k]{\tau_{max}}}\right)^k}{(\sqrt[k]{\epsilon_1}s + \omega_{bc})^k} \tag{18}$$

Magnitude of different inverse weighting function $1/|W_u(j\omega)|$ in Eq. 16 and Eq. 17 are shown in Figure 2.6.
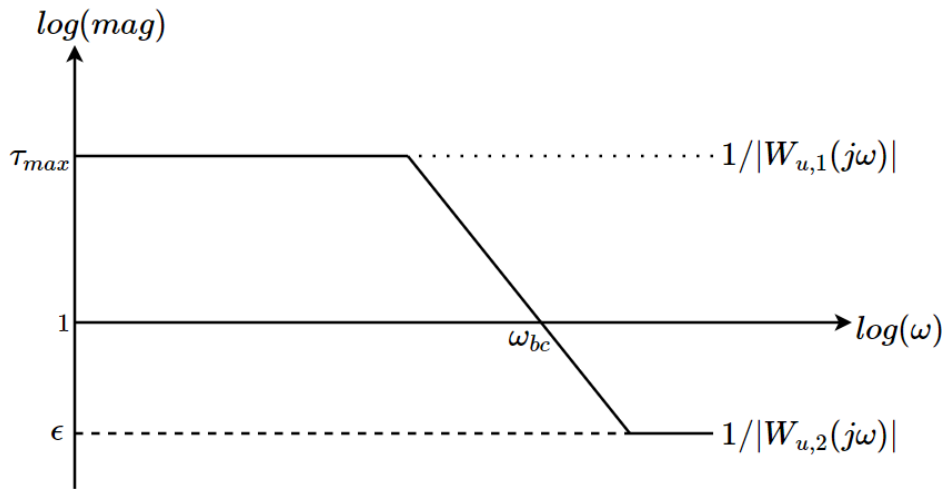
Figure 2.6. Magnitude of the inverse actuator constraints weighting function $1/|W_u(j\omega)|$

Prescribed actuator constraints are satisfied if the magnitude of $|K(j\omega)S(j\omega)|$ stays below $1/|W_u(j\omega)|$ at all frequencies, i.e. $\|W_u KS\|_\infty < 1$.

Although some standard forms of the weighting functions are given in this section, one should also note that, in H_∞ control design problems, selection of the weighting functions is a very important step which often involves many iterations and may differ from one problem to another.

2.5. Uncertainty and Robustness for SISO Systems

In this section, different representations of uncertainty are discussed and robust stability and robust performance conditions for SISO systems are analyzed.

2.5.1. Model Uncertainty

In classical and modern control design methods are based on a single model which represents the relationship between the inputs and the system responses. In reality, however, a single mathematical model cannot reflect the exact system behavior in all circumstances. Therefore, a set of mathematical models is needed to describe the dynamic behavior of the system. The key idea of the robust control methods is based on this phenomenon. In robust control methods, success of the controller is analyzed for all possible models that represent the system dynamics and to represent all possible models, model uncertainty definition that refers to the difference between the reality and mathematical model, is used. Model uncertainty may arise from different sources:

1. In linear plant models, there may be parameters that are only known approximately.

2. Parameters of the linear model may vary in time due to operating conditions or nonlinearities.

3. Obtaining the mathematical model is hard especially at high frequencies.

4. Even if the exact mathematical model of the plant is achieved, one may use a simpler model to facilitate the control design problem.

There are two approaches to represent uncertainty:

1. Structured (parametric) uncertainty (parameter bounds)
2. Unstructured uncertainty (frequency domain bounds)

Structured uncertainty can be used if the exact structure of the plant model and the real perturbations of the model parameters are known and using this type of uncertainty, unmodeled dynamics cannot be covered. Due to these reasons, structured uncertainty is usually avoided in robust control methods and representing uncertainty by defining frequency domain bounds is preferred. In unstructured uncertainty, disc-shape regions are used to represent uncertainty regions. For example, additive uncertainty definition in Eq. 19 generates perturbed plant model set in disc-shape regions around a nominal model.

$$\Pi_A: \quad G_P(s) = G(s) + W_A(s)\Delta_A(s); \quad |\Delta_A(j\omega)| \leq 1 \quad \forall \omega \tag{19}$$

where perturbed plant model set $G_P(j\omega)$ is defined in a disc-shape region that is centered at nominal model $G(j\omega)$ with disc radius $|W_A(j\omega)|$ as shown in Figure 2.7.

Another representation of disk-shape regions is multiplicative uncertainty definition in Eq. 20.

$$\Pi_I: \quad G_P = G(s)\big(1 + W_I(s)\Delta_I(s)\big); \quad |\Delta_I(j\omega)| \leq 1 \quad \forall \omega \tag{20}$$

In the multiplicative uncertainty case, both nominal model G and open-loop transfer function $L = GK$ are affected by the same uncertainty as given in Figure 2.8. Multiplicative uncertainty is often preferred in robust control problems for representing the model set, so in this thesis, robust stability and robust performance conditions are discussed with multiplicative uncertainty.
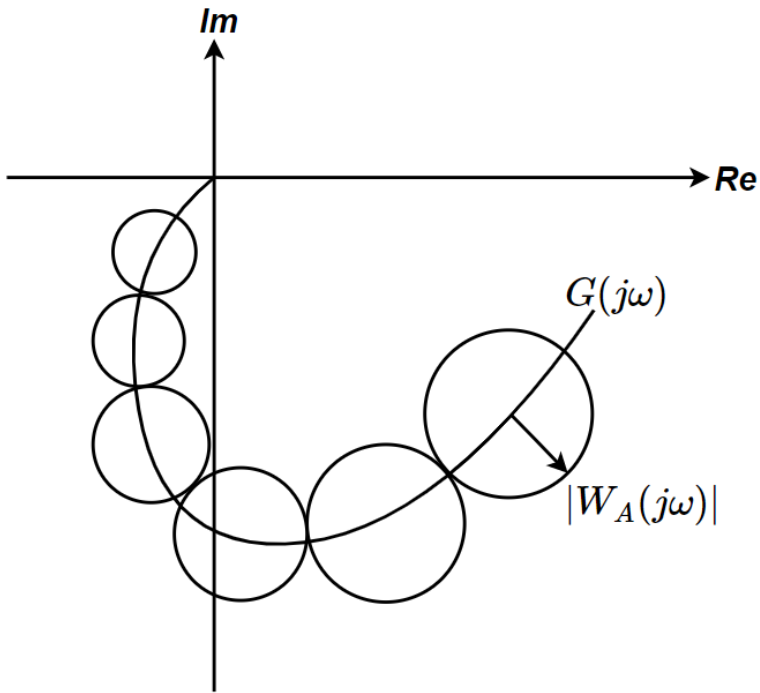
Figure 2.7. Additive uncertainty representation in Nyquist diagram
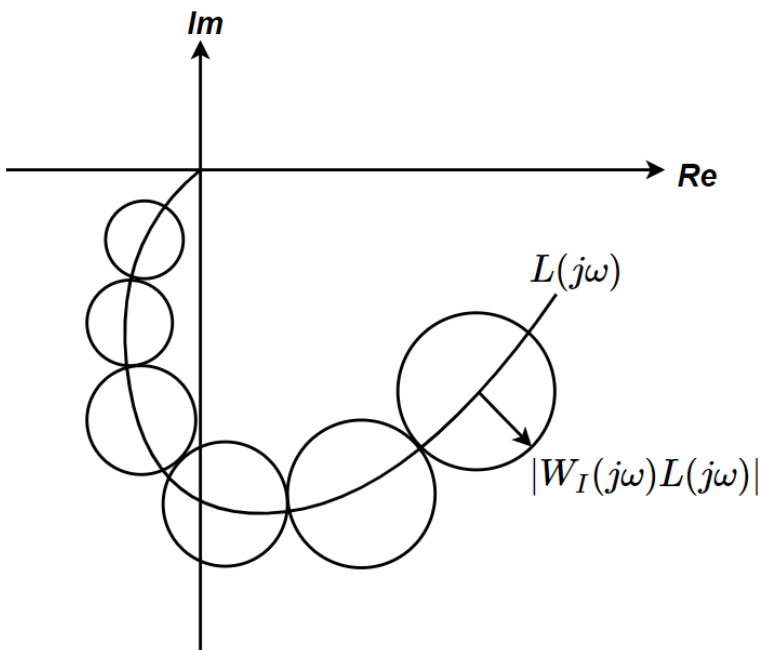
Figure 2.8. Multiplicative uncertainty representation in Nyquist diagram

2.5.2. Weighting Function for Unstructured Uncertainty

To describe all possible model set Π with the disc-shape uncertainty, the following procedure may be followed [26]:

1. Determine a nominal model $G(j\omega)$.

2. In additive uncertainty case, smallest radius of the disc (l_A) is equal to:

$$l_A(\omega) = \max_{G_P \in \Pi} |G_P(j\omega) - G(j\omega)| \tag{21}$$

Then, the weighting function $(W_A(j\omega))$ that represents the additive uncertainty must be selected to be equal or greater than the smallest radius of the disc at all frequencies.

$$|W_A(j\omega)| \geq l_A(\omega), \quad \forall \omega \tag{22}$$

3. In multiplicative uncertainty case, smallest radius of the disc $(l_I(\omega))$ is equal to:

$$l_I(\omega) = \max_{G_P \in \Pi} \left| \frac{G_P(j\omega) - G(j\omega)}{G(j\omega)} \right| \tag{23}$$

and, the multiplicative uncertainty weighting function $(W_I(j\omega))$ can be determined as:

$$|W_I(j\omega)| \geq l_I(\omega), \quad \forall \omega \tag{24}$$

2.5.3. Stability and Performance with Multiplicative Uncertainty

In robust control theory, following conditions are discussed to analyze stability and performance of the designed controller:

- **Nominal Stability (NS):** designed controller $K(s)$ stabilizes the nominal plant $G(s)$.

- **Nominal Performance (NP)**: designed controller $K(s)$ ensures the defined performance objectives for nominal plant $G(s)$.

- **Robust Stability (RS):** designed controller $K(s)$ stabilizes all perturbed plants $G_P(s)$ in the model set Π.

- **Robust Performance (RP)**: designed controller $K(s)$ ensures defined performance objectives for all perturbed plants $G_P(s)$ in the model set Π.

In the following sections, above conditions are derived under existence of multiplicative uncertainty.

2.5.3.1 Nominal Stability (NS)

Nominal stability condition is satisfied if the designed controller $K(s)$ stabilizes the nominal plant $G(s)$. Nominal stability of the closed-loop system is analyzed by using Nyquist diagram. If the open-loop transfer function $L(j\omega) = G(j\omega)K(j\omega)$ does not

encircle the point $(-1,0)$ in the Nyquist diagram for all frequencies, closed-loop system is said to have nominal stability.

2.5.3.2 Robust Stability (RS)

Robust stability condition for the closed-loop feedback system in Figure 2.9 is satisfied, if the designed controller $K(s)$ stabilizes all perturbed plants $G_P(s)$ in the model set Π.
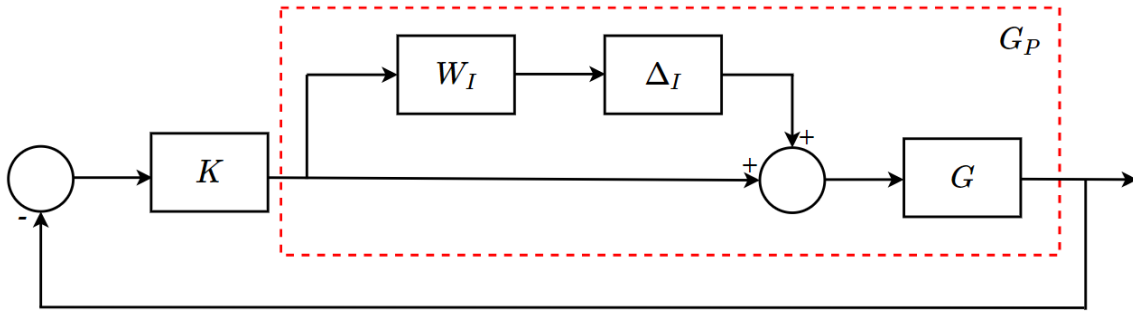
Figure 2.9. Closed-loop feedback system with multiplicative uncertainty

With multiplicative uncertainty the open-loop transfer function is defined as:

$$L_P(j\omega) = G_P(j\omega)K(j\omega) = G(1 + W_I\Delta)K = L + W_I L\Delta_I, \quad |\Delta_I(j\omega)| \le 1, \quad \forall \omega \quad (25)$$

From Eq. 25, perturbed loop transfer function L_P can be illustrated in Nyquist diagram by a disc with center L and radius $|W_I L|$ as shown in Figure 2.10. According to the Nyquist stability criterion, robust stability of the closed-loop system in Figure 2.9 is satisfied if $L_P(j\omega)$ does not encircle the point $(-1,0)$ in the Nyquist diagram for all frequencies. In other words, if the distance between the center of the disc and the point $(-1,0)$ is larger than the radius of the disc, closed-loop system is said to have robust stability.

Mathematically, robust stability condition may be expressed as following equations:

$$RS \iff |W_I(j\omega)L(j\omega)| < |1 + L(j\omega)|, \quad \forall \omega \quad (26)$$

$$RS \iff \left| \frac{W_I(j\omega)L(j\omega)}{1 + L(j\omega)} \right| < 1, \quad \forall \omega \iff |W_I(j\omega)T(j\omega)| < 1, \quad \forall \omega \quad (27)$$

$$RS \iff \|W_I(j\omega)T(j\omega)\|_\infty < 1 \quad (28)$$

By manipulating Eq. 27, robust stability condition for SISO systems may be written as:

$$RS \iff |T(j\omega)| < 1/|W_I(j\omega)| \quad (29)$$
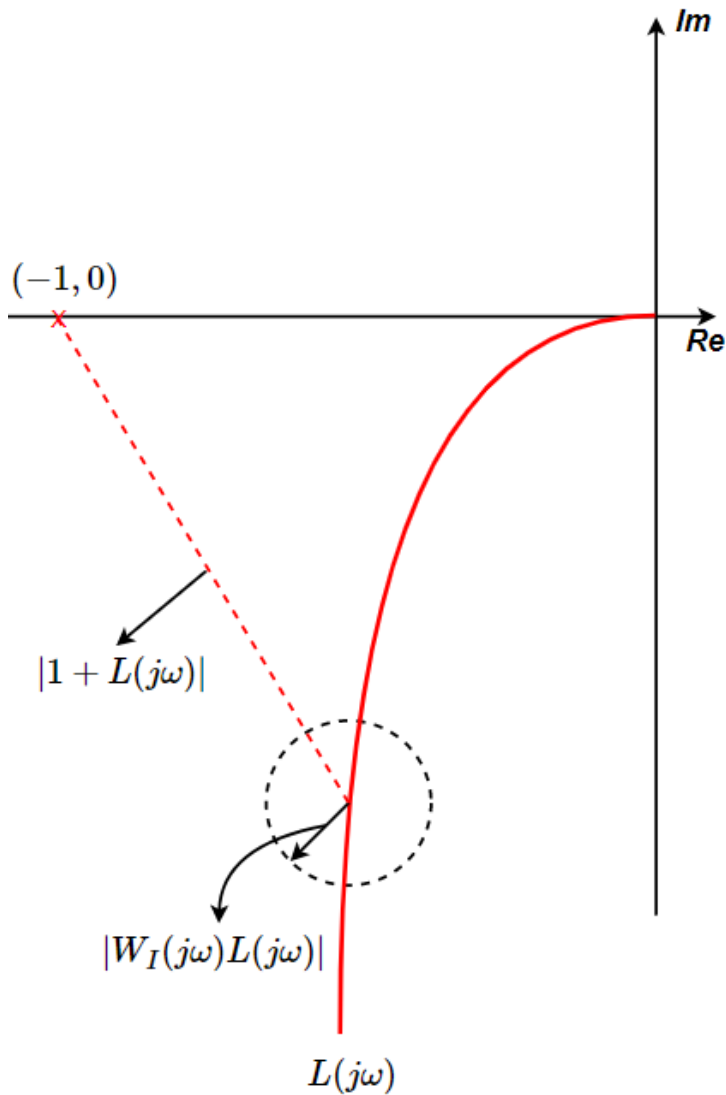
Figure 2.10. Robust stability condition in Nyquist diagram

From Eq. 29, one can easily observe that the multiplicative uncertainty weighting function W_I determines the upper bound of the complementary sensitivity function T. For robust stability of the closed-loop system in Figure 2.9, magnitude of the complementary sensitivity function should be small in the frequency region (mostly in the high frequencies) where the relative (multiplicative) uncertainty is high.

2.5.3.3 Nominal Performance (NP)

Nominal performance condition for the closed-loop feedback system in Figure 2.11 is satisfied, if the designed controller $K(s)$ ensure the performance requirements that is determined by the weighting function $W_P(s)$ for nominal plant model $G(s)$.
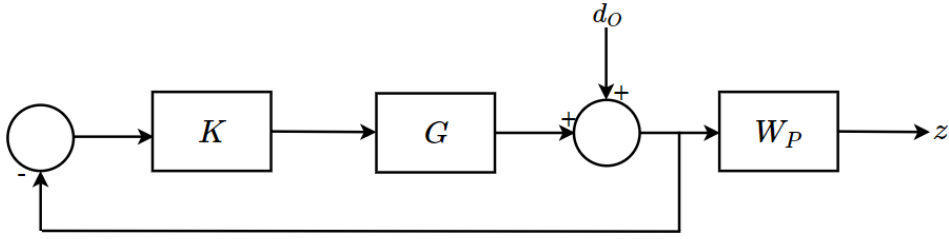
Figure 2.11. Closed-loop feedback system with the performance weighting function

In the Nyquist diagram, if the open-loop transfer function $L(j\omega)$ stay outside a disc which is centered at the point $(-1,0)$ with radius $|W_P(j\omega)|$ for all frequencies, closed-loop system is said to have nominal performance. In other words, for the nominal performance, the distance between the point $(-1,0)$ and $L(j\omega)$ should be larger than the disc radius $|W_P(j\omega)|$.

Nominal performance condition shown in Figure 2.12 may be expressed mathematically by following equations:

$$NP \iff |W_P(j\omega)| < |1 + L(j\omega)|, \quad \forall\omega \tag{30}$$

$$NP \iff \left|\frac{W_P(j\omega)}{1 + L(j\omega)}\right| < 1, \quad \forall\omega \quad \iff \quad |W_P(j\omega)S(j\omega)| < 1, \quad \forall\omega \tag{31}$$

$$NP \iff \|W_P(j\omega)S(j\omega)\|_\infty < 1 \tag{32}$$

By manipulating Eq. 31, nominal performance condition for SISO systems may be written as:

$$NP \iff |S(j\omega)| < 1/|W_P(j\omega)| \tag{33}$$

From Eq. 33, one can easily observe that the performance weighting function W_P determines the upper bound of the sensitivity function S. For nominal performance of the closed-loop system in Figure 2.11, magnitude of the sensitivity function should be small in the frequency region (mostly in the low frequencies) where the performance weighting function is high in magnitude.

2.5.3.4 Robust Performance (RP)

Robust performance condition for the closed-loop feedback system in Figure 2.13 is satisfied, if the designed controller $K(s)$ ensure the performance requirements that is determined by the weighting function $W_P(s)$ for all perturbed plants $G_P(s)$ in the model set Π.
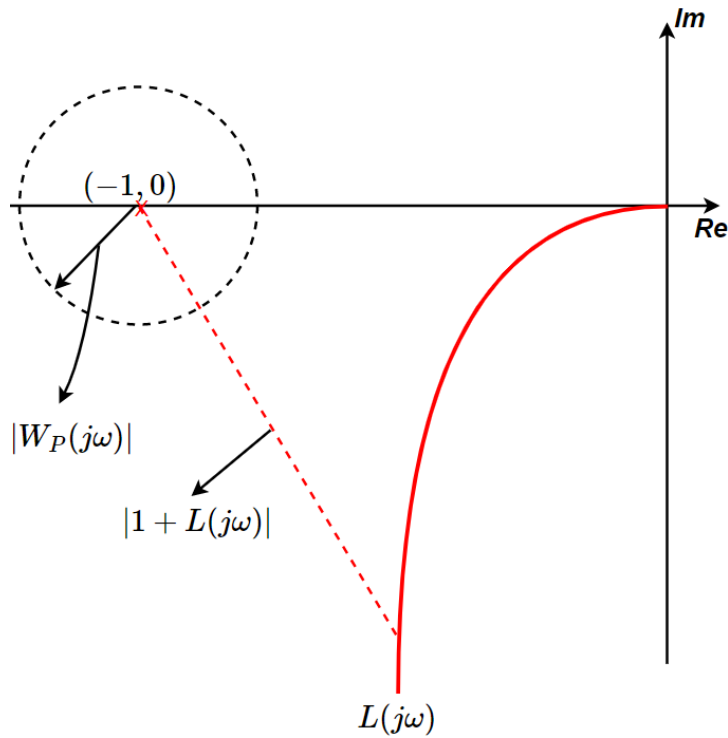
Figure 2.12. Nominal performance condition in Nyquist diagram
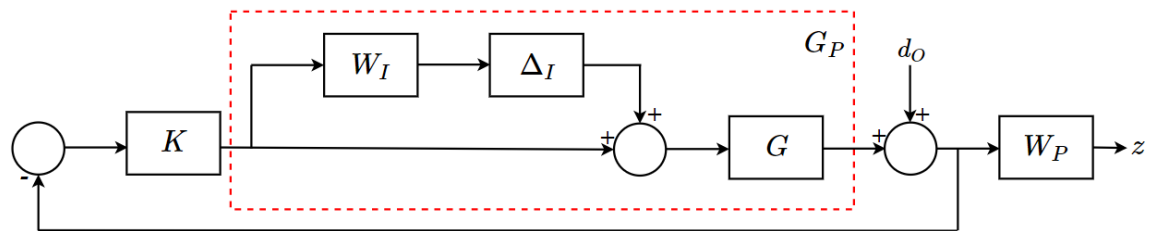
Figure 2.13. Closed-loop feedback system with multiplicative uncertainty and the performance weighting function

For robust performance, nominal performance condition which is discussed in previous section should be satisfied for all perturbed plants $G_P(s)$ in the model set Π. Therefore, all perturbed loop transfer function L_P defined by a disc with radius $|W_I L|$, should stay outside a disc which is centered at the point $(-1,0)$ with radius $|W_P(j\omega)|$ for all frequencies. In other words, if these two discs do not intersect for all frequencies, closed-loop system is said to have robust performance. If the sum of radii of these two discs is less than the distance between the point $(-1,0)$ and $L(j\omega)$, then the specified condition is guaranteed.

Robust performance condition shown in Figure 2.14 may be expressed mathematically by following equations:

$$RP \Longleftrightarrow |W_P(j\omega)| + |W_I(j\omega)L(j\omega)| < |1 + L(j\omega)|, \quad \forall \omega \tag{34}$$

$$RP \Longleftrightarrow \left|\frac{W_P(j\omega)}{1 + L(j\omega)}\right| + \left|\frac{W_I(j\omega)L(j\omega)}{1 + L(j\omega)}\right| < 1, \quad \forall \omega \tag{35}$$

$$RP \Longleftrightarrow |W_P(j\omega)S(j\omega)| + |W_I(j\omega)T(j\omega)| < 1, \quad \forall \omega \tag{36}$$
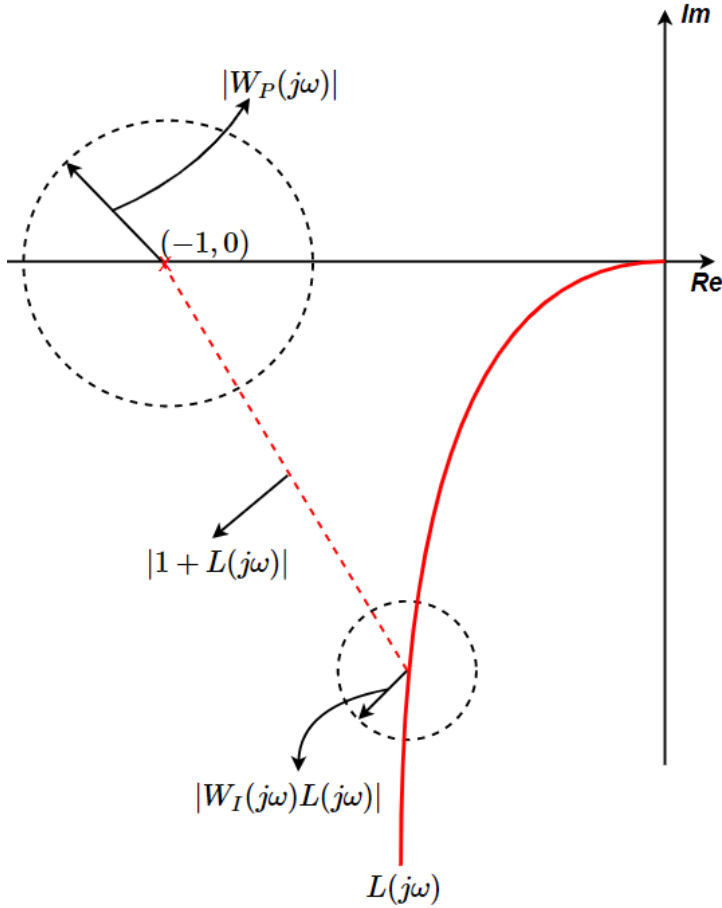
Figure 2.14. Robust performance condition in Nyquist diagram

2.5.3.5 Summary of Stability and Performance

For a SISO system with multiplicative uncertainty, nominal stability (NS), nominal performance (NP), robust stability (RP), and robust performance (RP) conditions can be summarized as:

$$NS \Longleftrightarrow Nyquist\ Stability\ Criteria \tag{37}$$

$$NP \Longleftrightarrow |W_P S| < 1, \quad \forall \omega \tag{38}$$

$$RS \Longleftrightarrow |W_I T| < 1, \quad \forall \omega \tag{39}$$

$$RP \Longleftrightarrow |W_P S| + |W_I T| < 1, \quad \forall \omega \tag{40}$$

3. MODEL-BASED AND DATA-DRIVEN H_∞ CONTROL

3.1. Obtaining A General Form for Control Configuration

In [55], a general control problem formulation method is proposed to design almost any linear controller. This formulation is based on using general control configuration that is shown in Figure 3.1.
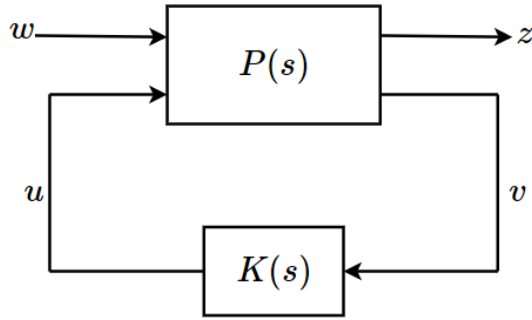
Figure 3.1. General control configuration

In Figure 3.1, the signals w, u, z, and v are named as (weighted) exogenous inputs, control signals, (weighted) exogenous outputs, and sensed outputs respectively. On the other hand, $P(s)$ and $K(s)$ represent generalized plant and controller, respectively. The controller design problem can be formulated as:

Design a controller $K(s)$ to reduce the effect of exogenous inputs w on exogenous outputs z (or minimize the closed-loop norm from w to z) by generating control signals u according to the information in v.

3.1.1. Obtaining the Generalized Plant

To obtain the generalized plant $P(s)$, signals w, u, z, and v should be identified first. Consider the feedback system shown in Figure 3.2. According to the controller design problem in Figure 3.2, the exogenous input signals w consist of reference signal, r output disturbance, d_o and measurement noise, n. In this configuration, the sensed output signal is the difference between the reference signal r and the measured output y_m. On the other hand, exogenous output z may be defined as the difference between the reference signal r and the actual output y to specify controller performance.
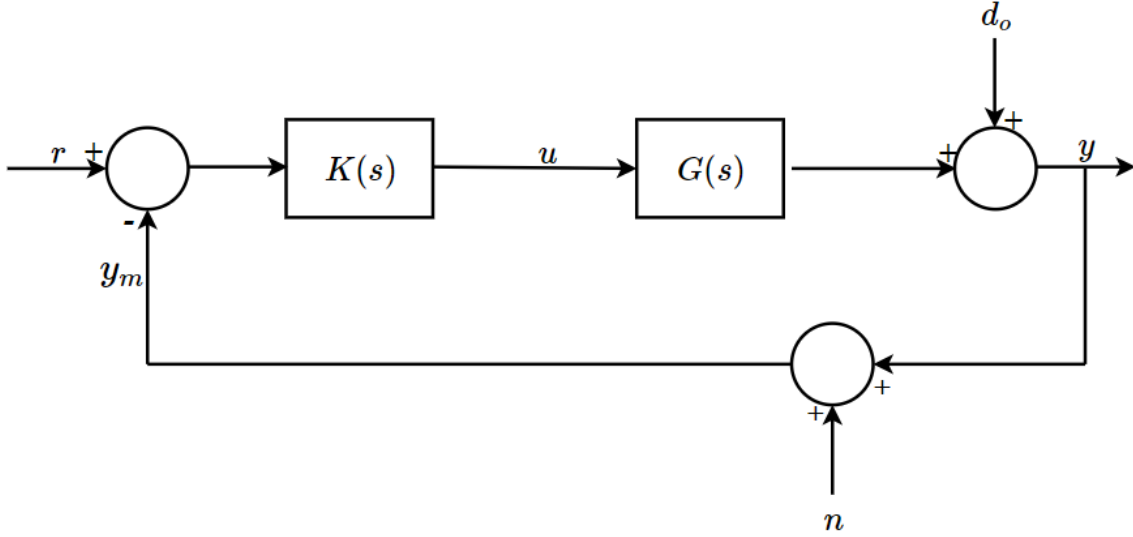
Figure 3.2. Obtaining generalized plant from feedback control configuration

$$w = \begin{bmatrix} w_1 \\ w_2 \\ w_3 \end{bmatrix} = \begin{bmatrix} r \\ d \\ n \end{bmatrix} \; ; \; z = r - y \; ; \; v = r - y_m = r - y - n \quad (41)$$

Then, the generalized plant $P(s)$ that represents the matrix from $[w \quad u]^T$ to $[z \quad v]^T$ is obtained as:

$$z = r - y = r - (Gu + d_o) = Iw_1 - Iw_2 - Gu \quad (42)$$

$$v = r - y_m = r - (Gu + d_o + n) = Iw_1 - Iw_2 - Iw_3 - G_u \quad (43)$$

$$P = \begin{bmatrix} I & -I & 0 & -G \\ I & -I & -I & -G \end{bmatrix} \quad (44)$$

3.1.2. Generalized Plant with Weighting Functions

In H_∞ control problems, controller synthesis problem is formulated with weighting functions, so the generalized plant $P(s)$ should be obtained with the addition of weighting functions. Reconsider the previous example in Figure 3.2 and assume that the frequency content of the error signal is shaped with the defined weighting function $W_P(s)$ as shown in Figure 3.3. Then, the exogenous output z in Eq. 42 is modified as:

$$z = W_P(r - y) = W_P w_1 - W_P w_2 - W_P Gu \quad (45)$$

and the generalized plant $P(s)$ is equal to:

$$P = \begin{bmatrix} W_P & -W_P & 0 & -W_P G \\ I & -I & -I & -G \end{bmatrix} \quad (46)$$
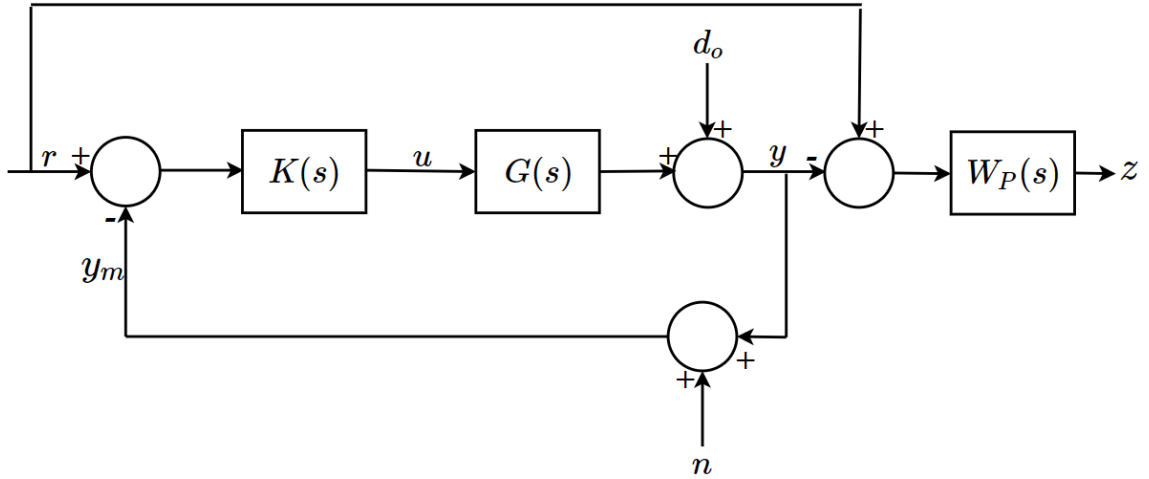
Figure 3.3. Obtaining generalized plant from feedback control configuration with weighting function

3.1.3. Obtaining Closed-loop Transfer Function

In H_∞ controller synthesis problem, the general control configuration in Figure 3.1 is used, however to analyze the performance of the closed-loop system, the structure in Figure 3.4 is preferred.
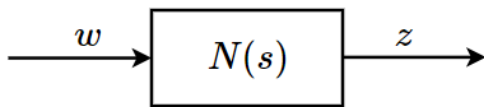
Figure 3.4. General structure for analysis of closed-loop performance

By using the general analysis structure in Figure 3.4, one can easily obtain:

$$z = Nw \tag{47}$$

To obtain the closed-loop transfer function $N(s)$ from exogenous inputs w to exogenous outputs z, partitioning of the generalized plant should be performed first as shown in the following equations:

$$z = P_{11}w + P_{12}u \; ; \quad v = P_{21}w + P_{22}u \tag{48}$$

$$P = \begin{bmatrix} P_{11} & P_{12} \\ P_{21} & P_{22} \end{bmatrix} \tag{49}$$

The closed-loop transfer function $N(s)$ can be obtained by eliminating u and v from Eq. 48 and Eq. 49 with the help of following controller equation:

$$u = Kv \tag{50}$$

N is then defined by:

$$N(s) = P_{11} + P_{12}K(I - P_{22}K)^{-1}P_{21} \triangleq F_l(P, K) \tag{51}$$

In Eq. 51, $F_l(P, K)$ denotes a lower linear fractional transformation (LFT) of P with K and in general, the design objective of the H_∞ control problem is to minimize the ∞-norm of this transfer function.

3.2. Model-Based H_∞ Control

In this section, both full-order and fixed-order model-based H_∞ controller synthesis problems are discussed.

3.2.1. Full-Order Model-Based H_∞ Control

In H_∞ control problems, the general control configuration in Figure 3.1 is used to find controller $K(s)$ that minimizes the ∞-norm of the $F_l(P, K)$. In this problem, generalized plant P is defined by state space realization:

$$P = \begin{bmatrix} A & B_1 & B_2 \\ C_1 & D_{11} & D_{12} \\ C_2 & D_{21} & D_{22} \end{bmatrix} \tag{52}$$

In [56], an algorithm is proposed to solve H_∞ control problems that is based on the state space solutions and this algorithm needs to solve two algebraic Riccatti equations. H_∞ controller that is obtained by aforementioned algorithm has the same state dimension as the generalized plant P. The assumptions given below are generally used for H_∞ (and also H_2) control problems [26]:

(A1) (A, B_2, C_2) is stabilizable and detectable.

(A2) D_{12} and D_{21} have full rank.

(A3) $\begin{bmatrix} A - j\omega I & B_2 \\ C_1 & D_{12} \end{bmatrix}$ has full column rank $\forall \omega$.

(A4) $\begin{bmatrix} A - j\omega I & B_1 \\ C_2 & D_{21} \end{bmatrix}$ has full row rank $\forall \omega$.

(A5) $D_{11} = D_{22} = 0$.

Assumption (A1) guarantees the existence of stabilizing controllers $K(s)$, and assumption (A2) is required for $K(s)$ to be proper and therefore realizable. Assumptions (A3) and (A4) provide that the controller $K(s)$ does not involve pole – zero cancellation

on the imaginary axis in complex plane which leads to instability in the closed-loop. Assumption (A5) is defined for H_2 control problems. On the other hand, in H_∞ control problems, assumption (A5) which is not a necessary condition, simplifies the problem. In some cases, additional assumptions may be used to further simplify the problem such as [26]:

(A6) $D_{12} = D_{21}^T = \begin{bmatrix} 0 \\ I \end{bmatrix}$.

(A7) $D_{12}^T C = B_1 D_{21}^T = 0$.

(A8) (A, B_1) and (A, C_1) are stabilizable and detectable, respectively.

In standard H_∞ optimal control problems, the general objective is to find all stabilizing controllers $K(s)$ that minimize ∞-norm of the transfer function from exogenous inputs w to exogenous outputs z.

$$\min_{K(s)} \|T_{wz}\|_\infty \tag{53}$$

In most of H_∞ control problems, the objective of the control problem is defined as to find a sub-optimal H_∞ controller instead of obtaining the optimal one. Finding a sub-optimal H_∞ controller is computationally simpler and this controller is close to the optimal H_∞ controller in the sense of ∞-norm. Let the ∞-norm of the transfer function in Eq. 53 be equal to γ_{min} with the optimal H_∞ controller. Then the H_∞ sub-optimal control problem is defined as finding all stabilizing controllers $K(s)$ such that:

$$\|T_{wz}\|_\infty < \gamma \tag{54}$$

where $\gamma > \gamma_{min}$. In [56], an efficient iterative algorithm is proposed to solve the sub-optimal H_∞ control problem in Eq. 54.

General H_∞ Algorithm: With the assumptions (A1) to (A8), there exist a sub-optimal H_∞ controller which satisfies the Eq. 54, if and only if following conditions are satisfied [26]:

   (i) $X_\infty \geq 0$ is a solution to the algebraic Ricatti equation:

$$A^T X_\infty + X_\infty A + C_1^T C_1 + X_\infty (\gamma^{-2} B_1 B_1^T - B_2 B_2^T) X_\infty = 0 \tag{55}$$

   such that $Re\ \lambda_i [A + (\gamma^{-2} B_1 B_1^T - B_2 B_2^T) X_\infty] < 0, \forall_i$.

   (ii) $Y_\infty \geq 0$ is a solution to the algebraic Ricatti equation:

$$AY_\infty + Y_\infty A^T + B_1 B_1^T + Y_\infty (\gamma^{-2} C_1^T C_1 - C_2^T C_2) Y_\infty = 0 \tag{56}$$

such that $Re\ \lambda_i [A + Y_\infty (\gamma^{-2} C_1^T C_1 - C_2^T C_2)] < 0, \forall_i.$

(iii) $\rho(X_\infty Y_\infty) < \gamma^2.$

Then, the sub-optimal H_∞ controller $K(s)$ is obtained such that:

$$K(s) = -Z_\infty L_\infty (sI - A_\infty)^{-1} F_\infty \tag{57}$$

where

$$F_\infty = -B_2^T X_\infty, \quad Z_\infty = (I - \gamma^{-2} Y_\infty X_\infty)^{-1}, \quad L_\infty = -Y_\infty C_2^T$$

$$A_\infty = A + \gamma^{-2} B_1 B_1^T X_\infty + B_2 F_\infty + Z_\infty L_\infty C_2 \tag{58}$$

The controller in Eq. 57 can also be written as combination of the state estimator (observer) and state feedback:

$$\dot{\hat{x}} = A\hat{x} + B_1 \gamma^{-2} B_1^T X_\infty \hat{x} + B_2 u + Z_\infty L_\infty (C_2 \hat{x} - y) \tag{59}$$

$$u = F_\infty \hat{x} \tag{60}$$

$\boldsymbol{\gamma}$ **– Iteration:** ∞-norm of the transfer function from exogenous inputs w to exogenous outputs z can be reduced by performing bisection algorithm on γ [26].

3.2.1.1 Mixed-Sensitivity Framework

In mixed-sensitivity H_∞ control problems, sensitivity function S is shaped with one or two other closed-loop transfer functions such as complementary sensitivity function T or KS. As explained in Chapter 2, all three closed-loop transfer functions are needed to be shaped for different purposes. For both regulation and reference tracking problems, magnitude of the sensitivity function S should be small at low frequencies for good disturbance rejection and command tracking performance, respectively. On the other hand, shaping of the complementary sensitivity function T is required for preventing robust stability and noise amplification problems. Moreover, to avoid actuator saturation problems KS should be shaped. Mixed-sensitivity configuration for regulation problem is defined by using the block diagram in Figure 3.5. In mixed-sensitivity problem, generalized plant is defined by following equation:

$$P = \begin{bmatrix} W_P & W_e G \\ 0 & -W_u \\ 0 & -W_I G \\ -I & -G \end{bmatrix} \tag{61}$$

Then the cost function of the mixed-sensitivity H_∞ control problem is equal to:

$$\|T_{wz}\|_\infty = \left\| \begin{bmatrix} W_P S \\ W_u KS \\ W_I T \end{bmatrix} \right\|_\infty \tag{62}$$
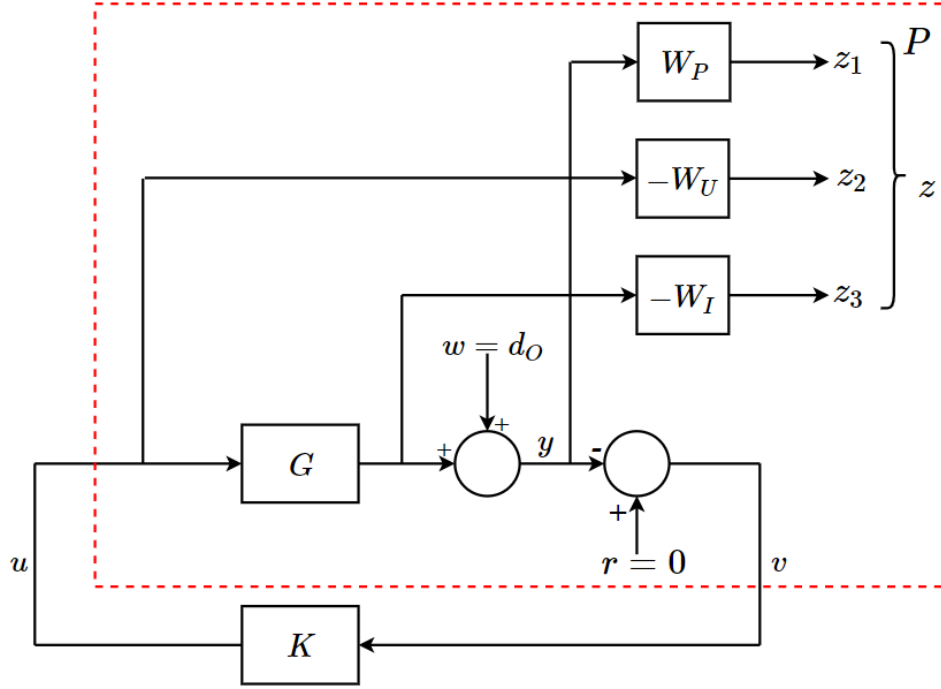
Figure 3.5. $S/KS/T$ mixed-sensitivity problem

3.2.2. Fixed-Order Model-Based H_∞ Control

In this thesis study, fixed-order model-based H_∞ controller synthesis is performed by using non-smooth optimization techniques in [30]. In fixed-order model-based H_∞ controller design problem, classical H_∞ problem is solved under additional constraints which are related to the structure of controller. The controller synthesis problem is given by

$$\min_{K \in \mathcal{K}} \|T_{wz}\|_\infty \tag{63}$$

where $K \in \mathcal{K}$ represents the controller structure constraints. If the controller K is structured with parameter θ, then the closed-loop transfer function from exogenous inputs w to exogenous outputs z can be written as a function of controller as shown in Eq. 64.

$$T_{wz}(P, K(\theta)) = \begin{bmatrix} A(K(\theta)) & B(K(\theta)) \\ C(K(\theta)) & D(K(\theta)) \end{bmatrix} \tag{64}$$

Then, objective function of fixed-order model-based H_∞ controller synthesis problem becomes a non-smooth, non-convex function as shown in Eq. 65.

$$f(\theta) := \left\| T_{wz}\big(P, K(\theta)\big) \right\|$$
$$= \max_{\omega \in \mathbb{R}} \bar{\sigma}\left(C\big(K(\theta)\big) \big(j\omega I - A(K(\theta))\big)^{-1} B\big(K(\theta)\big) + D\big(K(\theta)\big) \right) \tag{65}$$

where $\bar{\sigma}$ represents the maximum singular value of the function. The non-convex optimization problem in Eq. 65 is solved by using non-smooth optimization techniques and the details of the solution method can be found in [30].

3.3. Fixed-Order Data-Driven H_∞ Control

In this section, fixed-order data-driven H_∞ control theory is discussed. Although there are different approaches are proposed for data-driven H_∞ controller synthesis problems in the literature, in this thesis study, the method discussed in [49] is followed.

3.3.1. H_∞ Control Problem Formulation

In this section, class of models and controllers that are used in fixed-order data-driven control problems are introduced. Moreover, the design specification that is used as linear or convex constraints of the optimization problems is derived.

3.3.1.1 Non-Parametric Model Set

In fixed-order data-driven control problems, set $\mathcal{G}$ that involves m non-parametric models with (unstructured) multiplicative uncertainty is used. This model set can be defined by using multiplicative uncertainty weighting functions W_{Ii} discussed in Chapter 2 as shown in Eq. 66.

$$\mathcal{G} = \{G_i(j\omega)[1 + W_{Ii}(j\omega)\Delta] \ ; \ i = 1,2,\dots,m\} \tag{66}$$

Non-parametric model set $\mathcal{G}$ can be obtained from either parametric model or frequency domain data.

3.3.1.2 Linearly Parameterized Controllers

Linearly parameterized controllers are defined as follows:

$$K(s,\rho) = \rho^T \phi(s) \tag{67}$$

where ρ and $\phi(s)$ are column vectors that includes controller parameters and stable and known transfer functions with bounded infinity norms, respectively

$$\rho^T = [\rho_1 \quad \rho_2 \quad \cdots \quad \rho_n] \tag{68}$$

$$\phi^T(s) = [\phi_0(s) \quad \phi_1(s) \quad \dots \quad \phi_{n-1}(s)] \tag{69}$$

where n is the number of controller parameters and $\phi_i(s)$ may be chosen as orthonormal basis functions like Laguerre functions, Kautz functions or generalized orthonormal functions [57]. Generalized form of orthonormal functions are given as:

$$\phi_i(s) = \frac{\sqrt{2\Re\{\xi_i\}}}{s + \xi_i}\phi_{i-1}(s) \; ; \; i = 1,2,\dots,n-1$$

$$\phi_i(s) = \prod_{k=1}^{i}\frac{s - \bar{\xi}_k}{s + \xi_k} \; ; \; \phi_0(s) = 1 \tag{70}$$

where $\bar{\xi}_k$ and ξ_k are complex conjugate pairs. One of the special form of generalized orthonormal functions is Laguerre basis defined as:

$$\phi_0(s) = 1 \; ; \; \phi_i(s) = \frac{\sqrt{2\xi}(s - \xi)^{i-1}}{(s + \xi)^i} \; ; \; i = 1,2,\dots,n-1 \tag{71}$$

with $\xi > 0$. It can be proven that, by increasing the number of controller parameters with the appropriate choice of ξ, Laguerre basis can approximate any finite order stable transfer function [57].

Besides of orthonormal functions that are mentioned above, PID controllers can also be written in the linearly parameterized form as:

$$K(s,\rho) = \rho^T\phi(s) = [K_P \quad K_i \quad K_d]\left[1 \quad \frac{1}{s} \quad \frac{s}{1 + T_f s}\right]^T \tag{72}$$

where derivative time constant T_f is assumed to be known.

By using linearly parameterized controllers, loop transfer function L can be defined as a linear function of controller parameters as shown in the following equation and this property helps formulating fixed-structure H_∞ controller synthesis problem as a convex optimization problem.

$$L(j\omega,\rho) = K(j\omega,\rho)G(j\omega) = \rho^T\phi(j\omega)G(j\omega) \tag{73}$$

3.3.1.3 Design Specifications

In fixed-order data-driven H_∞ control problem, robust performance criterion which is shown in Eq. 40 is considered and finite number of linear or convex constraints are

produced with the help of Nyquist diagram. These constraints guarantee that the closed-loop system with designed controller satisfies the robust performance criterion.

3.3.2. Fixed-Order Data-Driven H_∞ Controller Design

3.3.2.1 Constraints of Control Problem

Multiplying the robust performance criterion in Eq. 40 by the distance between the point $(-1,0)$ and $L(j\omega, \rho)$ gives:

$$|W_P(j\omega)| + |W_I(j\omega)L(j\omega, \rho)| < |1 + L(j\omega, \rho)|, \quad \forall \omega \tag{74}$$

One may remember that, if the two discs which are centered at $(-1,0)$ and $L(j\omega, \rho)$ with a radius of $|W_P(j\omega)|$ and $|W_I(j\omega)L(j\omega, \rho)|$, do not intersect for all frequencies in the Nyquist diagram, closed-loop system is said to have robust performance [26]. These non-convex robust performance constraints can be redefined by considering a straight line d^* which is orthogonal to the line between the point $(-1,0)$ and $L(j\omega, \rho)$ and tangent to the circle with radius $|W_P(j\omega)|$. The line d^* divides the Nyquist diagram into two regions and, if the loop transfer function $L(j\omega, \rho)$ stays in the region that does not contain the critical point $(-1,0)$ for all frequencies, the nominal performance condition is satisfied as shown in Figure 3.6.

However, d^* is a function of the controller parameters ρ, therefore this condition cannot be specified as a convex function. For representing robust performance criterion as convex or linear constraints, desired loop transfer function $L_d(j\omega)$ which has a known frequency response function is defined. Then, a new line d which is tangent to the same circle as d^* but orthogonal to the line between the point $(-1,0)$ and $L_d(j\omega)$, is formed to formulate robust performance criterion under convex or linear constraints. The closed-loop system is said to have nominal performance, if the actual loop transfer function $L(j\omega, \rho)$ is at the right hand side of the line d, for all frequencies in the Nyquist diagram, and the desired loop transfer function $L_d(j\omega)$ is close to the actual one as shown in Figure 3.7.

As shown in Figure 3.7, the equation of the line $d(\omega)$ is independent of the controller parameters and is defined as:

$$|W_P(j\omega)[1 + L_d(j\omega)]| - [1 + \Re\{L_d(j\omega)\}][1 + x] - \Im\{L_d(j\omega)\}y = 0 \tag{75}$$

where x and y represent the real and imaginary parts of a point on the complex plane.
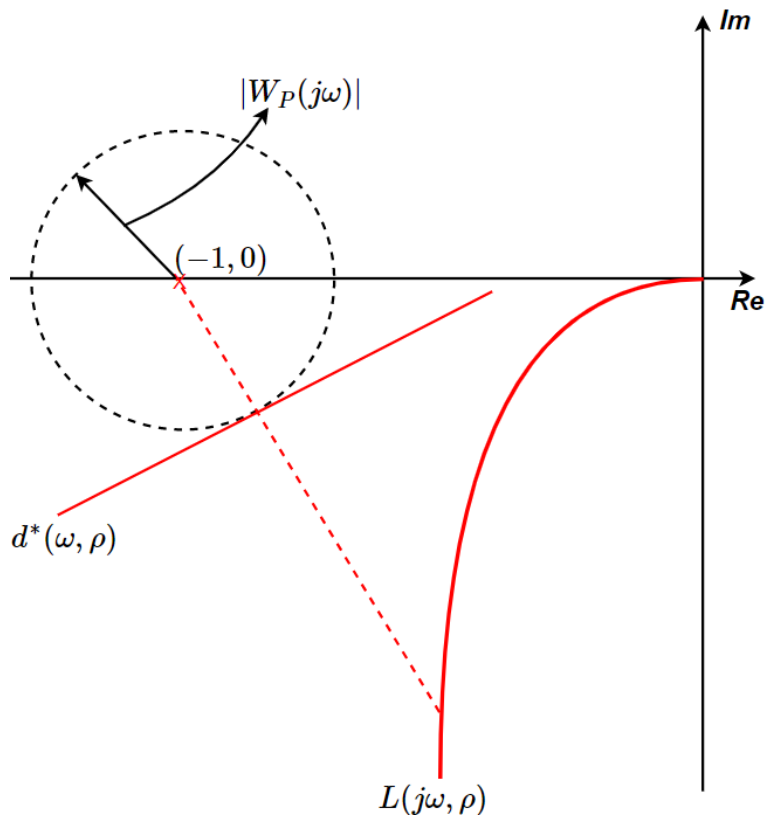
Figure 3.6. Modified nominal performance condition in Nyquist diagram
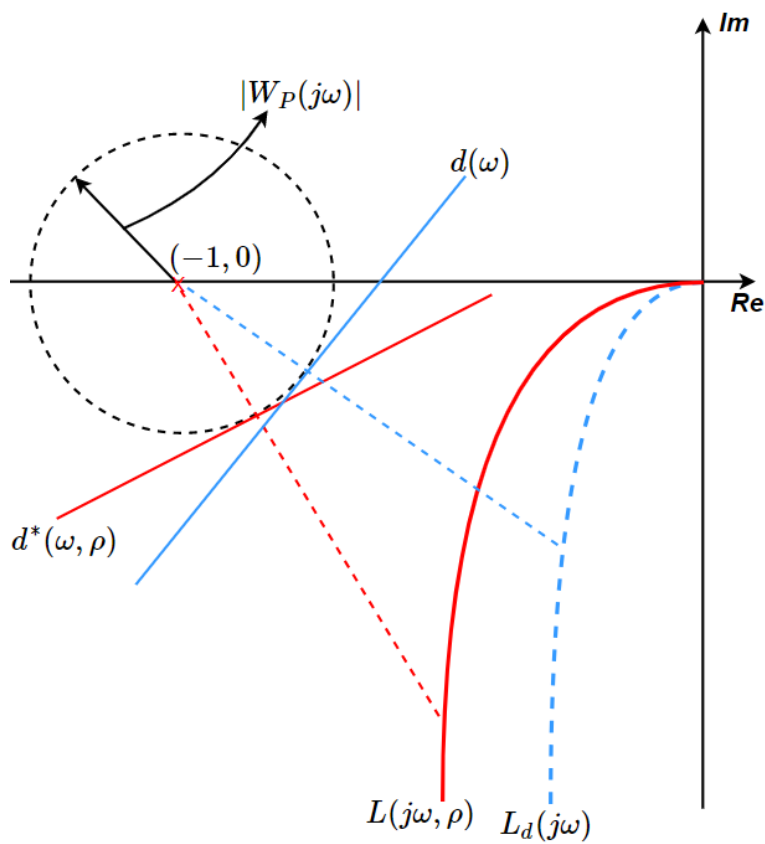
Figure 3.7. Linear constraints for nominal performance condition in Nyquist diagram

The linear constraints for nominal performance criterion can be represented as:

$$|W_P(j\omega)[1 + L_d(j\omega)]| - [1 + \Re\{L_d(j\omega)\}][1 + \Re\{L(j\omega,\rho)\}] -$$
$$\Im\{L_d(j\omega)\}\Im\{L(j\omega,\rho)\} < 0, \quad \forall\omega \tag{76}$$

Above equation guarantees that the loop transfer function $L(j\omega,\rho)$ remains at the region which does not include the point $(-1,0)$ in Nyquist plot for all frequencies. Above equation may be simplified by using following relationships:

$$\Re\{L_d(j\omega)\} = \frac{1}{2}[L_d(j\omega) + L_d(-j\omega)]$$

$$\Im\{L_d(j\omega)\} = \frac{1}{2}[L_d(j\omega) - L_d(-j\omega)] \tag{77}$$

Then, substituting Eq. 77 into the Eq. 76 yields:

$$|W_P(j\omega)[1 + L_d(j\omega)]| - \Re\{[1 + L_d(-j\omega)][1 + L(j\omega,\rho)]\} < 0, \quad \forall\omega \tag{78}$$

To satisfy robust performance criterion, condition in Eq. 78 should be satisfied for all models which is represented by a multiplicative uncertainty region. By approximating disc shaped uncertainty region by a polygon with $q > 2$ vertices, robust performance condition in Eq. 40 may be expressed as linear constraints [49]. If all vertices of the polygon stay in the right side of the line $d(\omega)$, then the robust performance condition is satisfied:

$$|W_P(j\omega)[1 + L_d(j\omega)]| - Re\{[1 + L_d(-j\omega)][1 + L_n(j\omega,\rho)]\} < 0,$$
$$\forall\omega \; \& \; n = 1, \dots, q \tag{79}$$

where $L_n(j\omega,\rho) = K(j\omega,\rho)G_n(j\omega)$ and

$$G_n(j\omega) = G(j\omega)\left[1 + \frac{|W_I(j\omega)|}{\cos\left(\frac{\pi}{q}\right)} e^{\frac{j2\pi n}{q}}\right] \tag{80}$$

Another alternative for representing robust performance criterion is using uncertainty circle with radius $|W_I(j\omega)L(j\omega,\rho)|$ directly to define all possible models. This alternative results with following convex constraints [49]:

$$|W_P(j\omega)[1 + L_d(j\omega)]| + |W_I(j\omega)L(j\omega,\rho)[1 + L_d(j\omega)]|$$
$$- \Re\{[1 + L_d(-j\omega)][1 + L(j\omega,\rho)]\} < 0, \quad \forall\omega \tag{81}$$

These two alternatives of representation of the robust performance constraint are shown in Figure 3.8. Although the number of linear constraints are q times more than number of convex constraints, using convex constraints complicates the optimization problem.
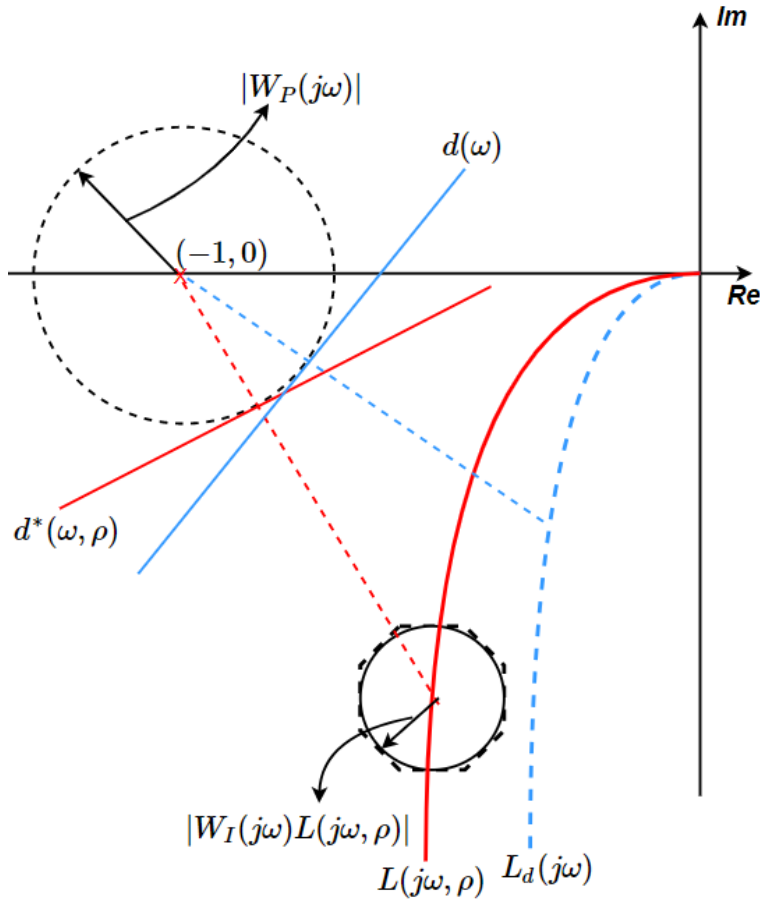
Figure 3.8. Linear or convex constraints for robust performance condition in Nyquist diagram

3.3.2.2 Objective Function of Control Problem

In fixed-order data-driven H_∞ controller synthesis problem, robust performance condition is represented as either linear or convex constraints with the help of the defined desired loop transfer function $L_d(j\omega)$. However, to guarantee the robust performance condition for the actual closed-loop system, desired loop transfer function $L_d(j\omega)$ should be the good approximation of the actual one $L(j\omega, \rho)$. Therefore, the objective function of the optimization problem is defined as minimizing the difference between these two loop transfer functions as shown in following equation:

$$\min\|L(j\omega,\rho) - L_d(j\omega)\|_2^2 = \min\|\rho^T \phi(j\omega)G(j\omega) - L_d(j\omega)\|_2^2 \tag{82}$$

If the optimization problem which is defined by the objective function in Eq. 82 is solved under linear constraints in Eq. 79 or convex constraints in Eq. 81, robust performance constraint in Eq. 40 is satisfied. Moreover, to improve the fixed-order data-driven H_∞ controller performance, ∞-norm of the transfer function from exogenous inputs w to exogenous outputs z can be reduced by performing bisection algorithm on γ [26].

3.3.3. Choice of Desired Loop Transfer Function

The proper choice of desired loop transfer function $L_d(j\omega)$ should be "close" to actual loop transfer function $L(j\omega, \rho)$ to satisfy the robust performance criterion by the obtained closed-loop system. Therefore, following suggestions should be applied while determining the desired loop transfer function $L_d(j\omega)$.

- The solution of the full-order model-based H_∞ controller problem is based on stable pole-zero cancelation of the plant by the designed controller. Thus, desired loop transfer function $L_d(j\omega)$, should contain the unstable poles of the plant. Similarly, desired loop transfer function $L_d(j\omega)$, should also contain the right half-plane zeros.

- The number of integrators in the desired loop transfer function should be equal to total number of integrators of plant and controller. For example, if a PID-controller is designed for a plant that also contains another integrator, the number of the integrator in desired loop transfer function should be equal to two.

- The characteristic polynomial of the closed-loop system with the desired loop transfer function should satisfy Routh-Hurwitz stability criterion. Therefore, parameters of the desired loop transfer function should be selected by considering closed-loop stability.

- For improving the performance of the closed-loop system, desired loop transfer function can be selected iteratively. For example, if the initial controller $K_0(j\omega)$ is designed with the initial choice of $L_d^{(1)}(j\omega)$, then the new desired loop transfer function can be selected based on $K_0(j\omega)$ as $L_d^{(2)}(j\omega) = G(j\omega)K_0(j\omega)$.

4. SYSTEM IDENTIFICATION

In this chapter, the system used in experimental studies is introduced. Then, the system identification method which is performed to obtain both non-parametric and parametric plant models is discussed.

4.1. Experimental Setup

In this part of the study, H_∞ controller synthesis methods explained in Chapter 3 are implemented on a military two-axis stabilized platform named as "System A". Note that, results for an additional experimental study with another stabilized platform named as "System B" are presented in the Appendix.

In general, two-axes stabilized platforms are defined as platforms which can be moved and stabilized in both traverse and elevation axes which are shown in Figure 4.1.
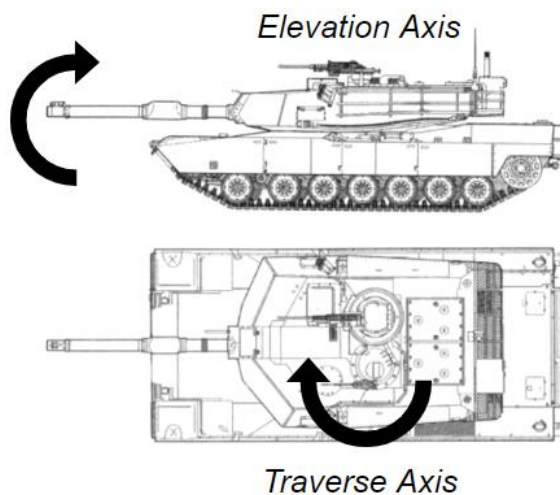
Figure 4.1. Traverse and elevation axes of stabilized platform

In these platforms, one brushless DC motor is used as an actuator for each axis. These motors have a resolver which is used to provide commutation as well as to generate motor position and speed information. Although torque transmission structure used in two-axis stabilized platforms may vary from one platform to another, the torque transfer process is carried out by means of the gearbox on the traverse axis of the system used in this thesis study. The position information required for guiding the axes is provided by encoders which are placed to different axes. Finally, relative angular velocities of the axes with respect to the ground that are required for stabilization are measured by a two-axis gyroscope generally mounted on the elevation axis. The control software running within the motor drive unit continuously calculates the amount of current to be supplied to the

motors by using sensor data in the feedback loop. Signal flow for the closed-loop system of the traverse axis angular speed control is shown in Figure 4.2.
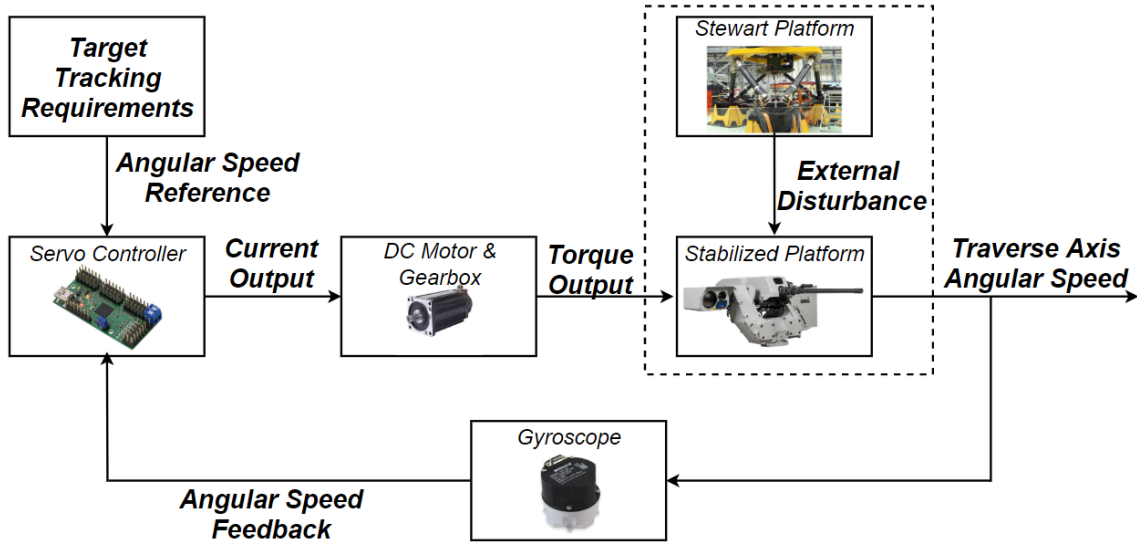
Figure 4.2. Signal flow for the closed-loop system of experimental test setup

4.2. System Identification Method

In this section, the traverse axis of the two-axis stabilized platform (System A) is analyzed and plant model from motor torque input to the angular velocity output of the traverse axis is identified to synthesize different the H_∞ controllers discussed in Chapter 3. In this section, identification of the friction model which is the main non-linear effect on the system is introduced. Then, proposed system identification method in frequency domain to obtain non-parametric and parametric plant models is discussed.

4.2.1. Friction Model

To identify a LTI model of the traverse axis of the two-axis stabilized platform, non-linear effects should be identified first. In traverse axis, the main nonlinear effect originates from friction between the moving parts which are mechanically in contact with each other. By considering Newton's second law, friction torque applied to the system can be calculated from:

$$J\ddot{\theta} = \tau_{app} - \tau_{fr} \tag{83}$$

If the system moves with constant velocity $(\ddot{\theta} = 0)$, the friction torque (τ_{fr}) is equal to applied motor torque (τ_{app}). To make use of this fact, reference tracking tests are performed in both counter clockwise and clockwise direction with different velocity

commands and motor torque input is detected in constant velocity region. In following figures, variation of applied motor torque relative to the axis position are shown for different velocity commands.
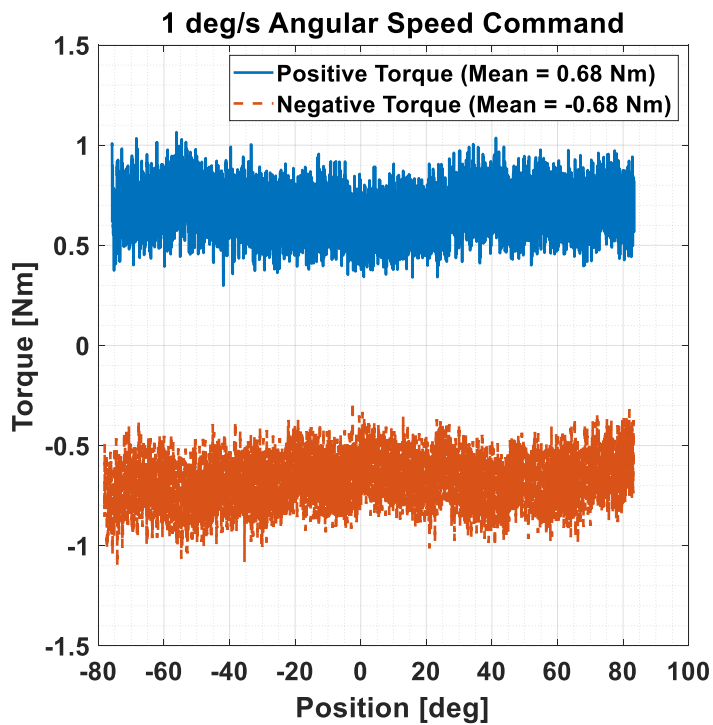
Figure 4.3. Friction identification test (1 deg/s angular speed command)
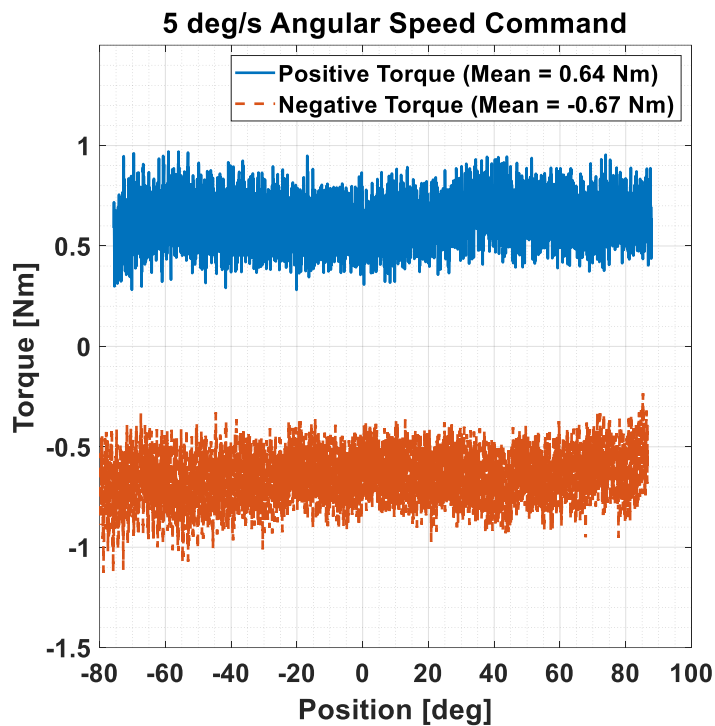
Figure 4.4. Friction identification test (5 deg/s angular speed command)

As shown in Figure 4.3 and Figure 4.4, the magnitude of the friction torque varies negligibly with respect to the velocity of the platform and direction of motion. Therefore, friction model used in thesis study is considered as Coulomb friction model and parameter of the model $(\bar{\tau}_{fr})$ is calculated by taking average of the obtained data from different tests. The friction torque is calculated by using following equation:

$$\tau_{fr} = \bar{\tau}_{fr}sign(\dot{\theta}) \tag{84}$$

4.2.2. Linear Platform Model

To obtain linear model of the system, open-loop system identification tests were performed. In these tests, sinusoidal motor torque input signals with different amplitudes were applied to the system. Excitation signals used in open-loop system identification tests are defined as follows:

$$\tau_{app,i} = A_i \cos(\omega_k t) \quad ; \quad i = 1, \dots, 4 \;\; \& \;\; \omega_k = 1, 1.5, \dots, 150 \; Hz. \tag{85}$$

where amplitudes of the excitation signals (A_i) have a relationship such that $A_1 < A_2 < A_3 < A_4$. In order to obtain linear model of the system from net torque to angular velocity of the traverse axis, friction torque was subtracted from applied torque as shown in Figure 4.5.
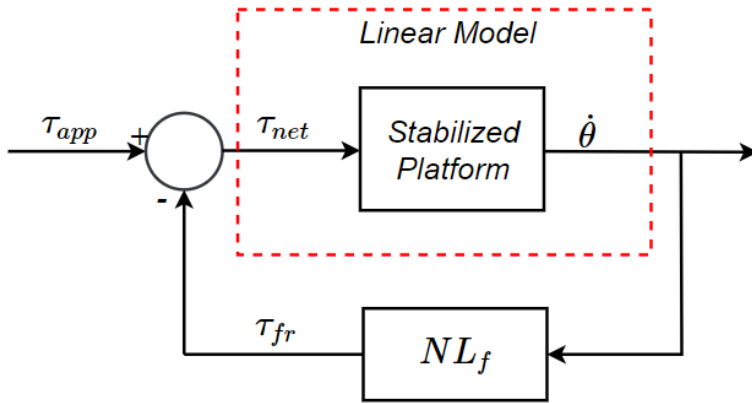
Figure 4.5. Subtraction of non-linear friction effect to obtain linear model of the system

In this thesis study, both non-parametric and parametric models were identified to describe the dynamical behavior of the system. To obtain these models, frequency domain system identification method was performed.

4.2.2.1 Non-Parametric Model Set

In non-parametric modelling approach, behavior of the system is described by using input/output data obtained from system identification tests. In this thesis study, frequency domain approach is used and non-parametric model of the system is determined by using frequency response function (FRF) of the system.

Measurement of the FRF is a fundamental and crucial step in control applications. For stable systems, FRF can be measured by performing open-loop system identification tests. In these tests, input signal in a specific frequency band of interest is applied to the system directly and both input and output signals are recorded in the time domain. When a stable plant is excited with a sinusoidal input at a certain frequency ($u(t) = \cos(\omega t)$), steady-state response of the plant is at the same frequency as the input signal and has a certain phase difference.

$$y_{ss}(t) = |G(j\omega)| \cos\big(\omega t + \arg(G(j\omega))\big) \tag{86}$$

In the above equation, $G(j\omega)$ represents the frequency response function of the stable system. To obtain the complex value $G(j\omega)$, open-loop system identification tests' time domain input/output data should be converted to the frequency domain by using Discrete Fourier Transform (DFT). The DFT relation between the time and frequency domain data is defined as follows [58]:

$$U(k) = \frac{1}{\sqrt{N}} \sum_{n=0}^{N-1} u(nT_s) e^{-\frac{j2\pi kn}{N}}$$

$$Y(k) = \frac{1}{\sqrt{N}} \sum_{n=0}^{N-1} y(nT_s) e^{-\frac{j2\pi kn}{N}} \tag{87}$$

where N is the number of samples and T_s is the sampling time of the system. According to this definition, the representation of the frequency response function of the plant at frequency f_k is expressed by following equation:

$$G(j\omega_k) = \frac{Y(k)}{U(k)} \tag{88}$$

When the excitation signal applied in the open – loop system identification tests covers the frequency range required to represent dynamic behavior of the system, non-parametric plant model is obtained in the frequency domain. The set of non-parametric plant models

which is calculated by m system identification tests performed at K_{freq} frequency points is shown by following expression:

$$M \triangleq \{G_i(j\omega_k)|i = 1,2,\dots,m; \quad k = 1,2,\dots,K_{freq}\} \tag{89}$$

In this thesis study, four different open-loop system identification tests were performed with different amplitudes of excitation signal (A_i). Linear non-parametric model set was obtained from net motor torque to angular velocity of the traverse axis as shown in Figure 4.6.
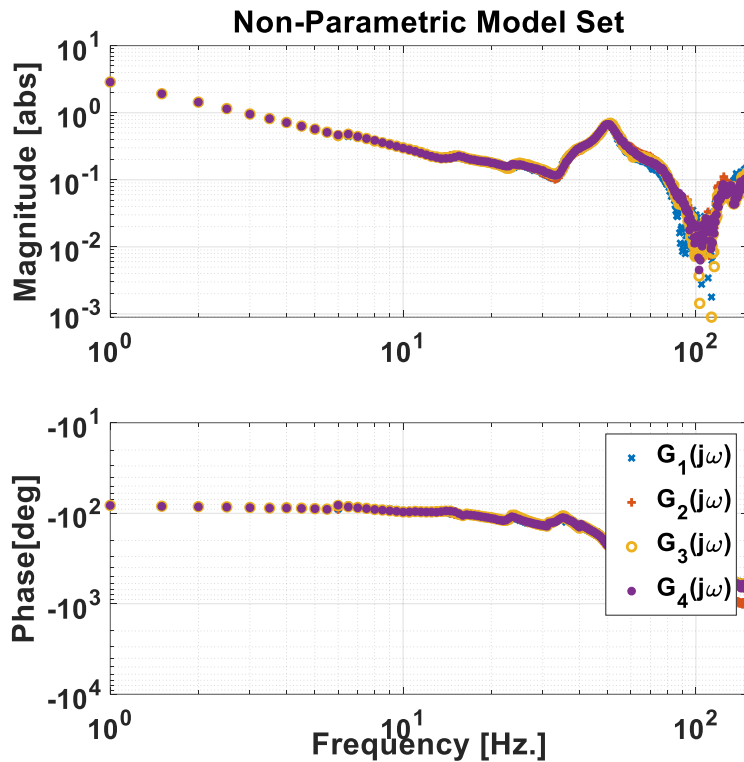
Figure 4.6. Non-parametric model set for traverse axis of the stabilized platform

4.2.2.2 Parametric Model

A parametric plant model should be obtained to implement model-based controller design methods. In parametric modelling approach, behavior of the system is characterized by model parameters. Parameters of the mathematical model of the plant were obtained by performing parameter estimation techniques using mean frequency response function of the system which is shown in Figure 4.7.

According to the mean frequency response function of the system in Figure 4.7, behavior of the system can be considered similar to behavior of the flexible mechanical systems. For flexible mechanical systems, general structure of the plant model from motor torque

input to body angular velocity contains rigid body dynamics and torsional structural dynamics as shown in Figure 4.8 [1].
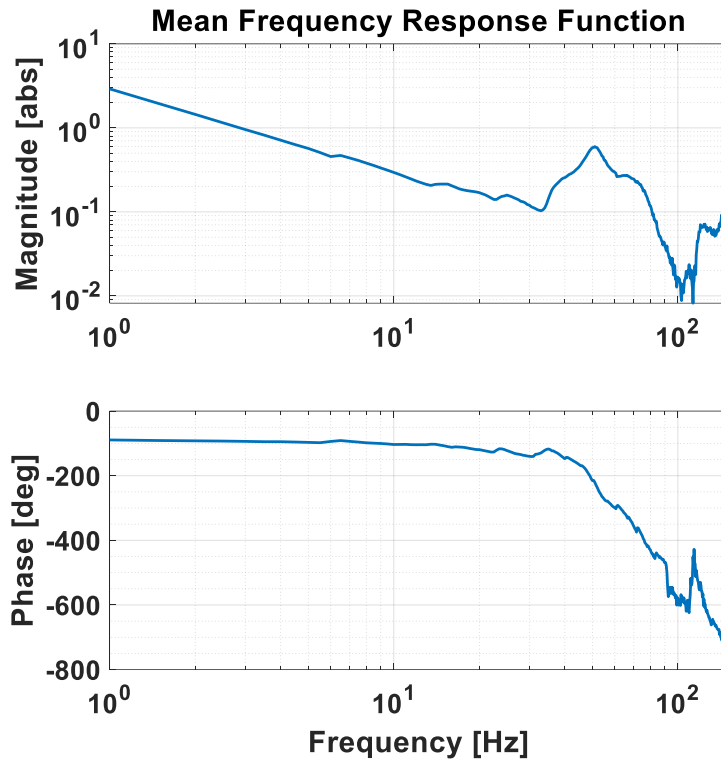
Figure 4.7. Mean frequency response function for traverse axis of the stabilized platform
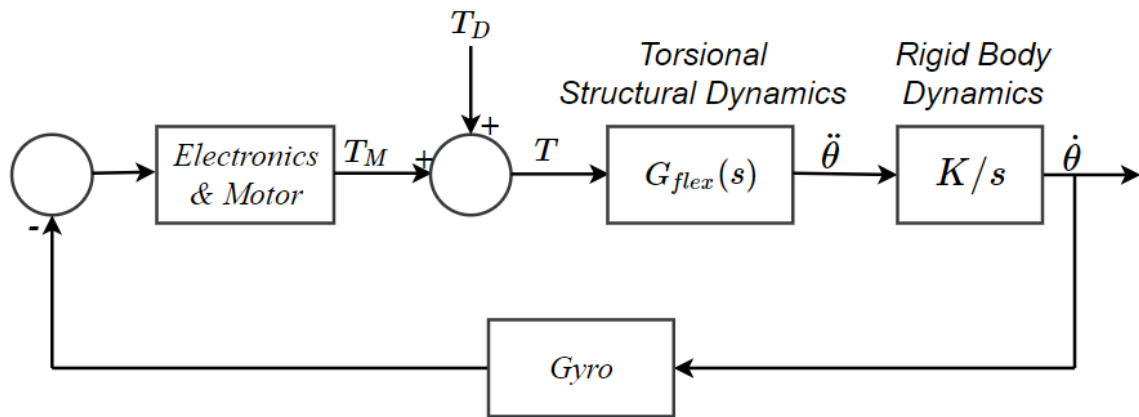
Figure 4.8. General structure of flexible mechanical system's plant model

According to Figure 4.8, plant model can be formed by the term that represents rigid body dynamics of the system and a transfer function that represents the flexibility of the system dynamics. Moreover, time delay can also be added to the plant model due to existence of the electronic components. General structure of the plant model in Laplace domain is given below:

$$G(s) = \frac{K}{s} G_{flex}(s) e^{-s t_{delay}} \tag{90}$$

Model parameters in the above equation were identified separately by using frequency domain data. The term that represents rigid body dynamics of the system was calculated as $K = 18.2555$ from magnitude of the frequency response function in low frequency range.

In the second step of the identification of parametric model, the term that represents the torsional structural dynamics of the system was determined. This term should contain the flexible modes of the system. Therefore, each resonance and anti-resonance pair that arise in frequency response function of the system, was represented by a second order transfer function that include two imaginary poles and two imaginary zeros. To represent the torsional structural dynamics of the system, multiple cascaded bi-quad filters were used [50] and the parameters of the bi-quad filters can be calculated by using non-linear least squares approximation technique. General form of the bi-quad filter is shown in following equation:

$$G_{Bi-Quad}(s) = \frac{\omega_{nD}^2 (s^2 + 2\xi_N \omega_{nN} s + \omega_{nN}^2)}{\omega_{nN}^2 (s^2 + 2\xi_D \omega_{nD} s + \omega_{nD}^2)} \tag{91}$$

By using non-linear least squares approximation technique, four cascaded bi-quad filters were fitted to frequency response function that does not contain the rigid body (K/s) term.

$$G_{flex} = G_{bi-quad,1} G_{bi-quad,2} G_{bi-quad,3} G_{bi-quad,4} \tag{92}$$

Initial guesses and calculated values for bi-quad filter parameters are shown in Table 4.1 and Table 4.2, respectively.

Table 4.1. Initial guesses for identification of bi-quad filter parameters

	Numerator		Denominator	
	$\omega_n/2\pi \; [Hz.]$	ξ	$\omega_n/2\pi \; [Hz.]$	ξ
Bi – quad 1	33	0.5	36	0.5
Bi – quad 2	42	0.5	51	0.5
Bi – quad 3	61	0.5	68	0.5
Bi – quad 4	103	0.5	120.5	0.5

Table 4.2. Calculated values for bi-quad filter parameters

	Numerator		Denominator	
	$\omega_n/2\pi \ [Hz.]$	ξ	$\omega_n/2\pi \ [Hz.]$	ξ
Bi – quad 1	36.4625	0.1086	38	0.0812
Bi – quad 2	47.717	0.5242	50.864	0.0748
Bi – quad 3	64.6621	0.3869	72.0794	0.1084
Bi – quad 4	101.4478	0.0465	150	0.2374

Frequency response functions of parametric model of torsional structural dynamics and the real system without rigid body dynamics are compared in Figure 4.9.
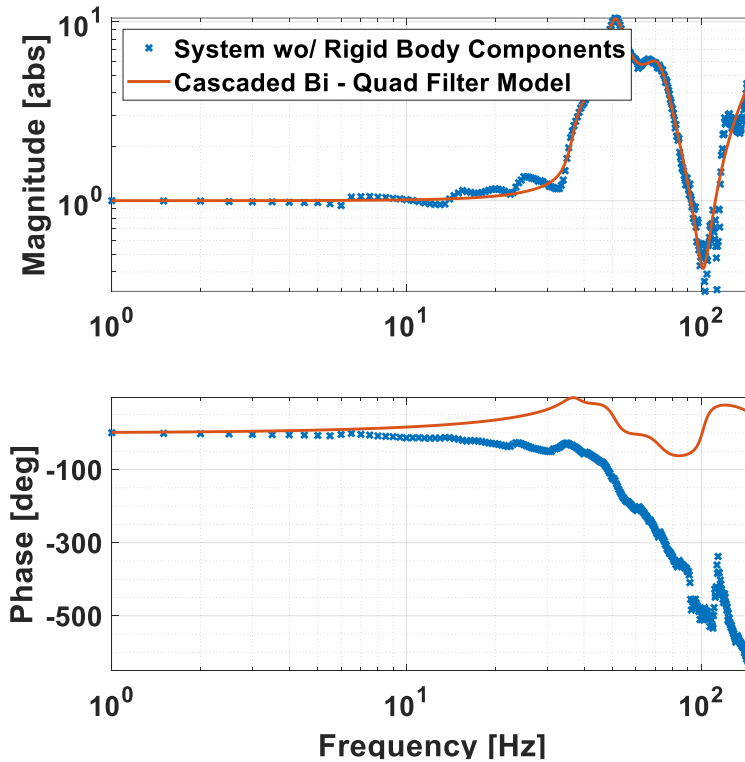
Figure 4.9. Identification of torsional structural dynamics

The final term of the parametric model in Eq. 90 is the delay term $(e^{-st_{delay}})$ and it should be added to the plant model to compensate the phase difference shown in Figure 4.9. To calculate time delay value (t_{delay}), non-linear least squares technique was performed and the difference between the phase responses of the real system and the

parametric plant model was minimized. The time delay value was calculated as $t_{delay} = 10.3606$ miliseconds.

The frequency response of parametric plant model which consists of the terms that represent the rigid body dynamics, the torsional structural dynamics, and the time delay is shown in Figure 4.10.
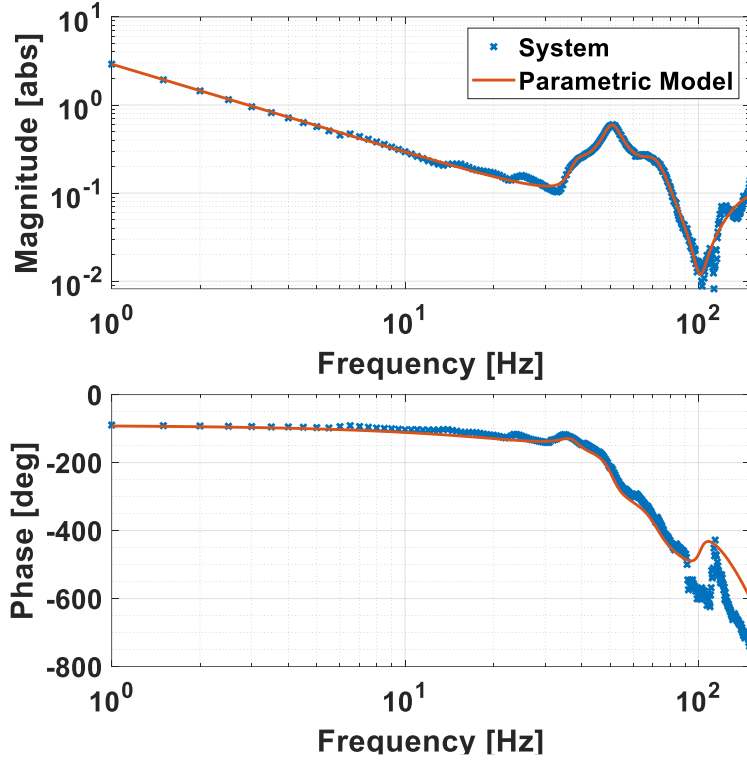
Figure 4.10. Mean FRF of the system and FRF of the parametric model

To evaluate the success of the system identification method, the percentage "Variance Accounted For (VAF)" between the system and the parametric model time responses that is defined in Eq. 93, for four different open-loop system identification tests were calculated as shown in Table 4.3.

$$VAF_i = \left(1 - \frac{var(y_i - \hat{y}_i)}{var(y_i)}\right).100\% \tag{93}$$

where y_i and $\hat{y}_i$ represent the time responses of real system and parametric model, respectively.

When the VAF value between the two signals is equal to 1, then these two signals are identical. As shown in Table 4.3, VAF values between the time responses of the real system and parametric model are close to 1 and this means that, these two signals are

almost same. Therefore, it can be said that the identified parametric model successfully represents the real system dynamics.

Table 4.3. Percentage VAF between the system and the parametric model time responses

	Test 1	Test 2	Test 3	Test 4
VAF_i	97.89%	97.65%	97.65%	97.18%
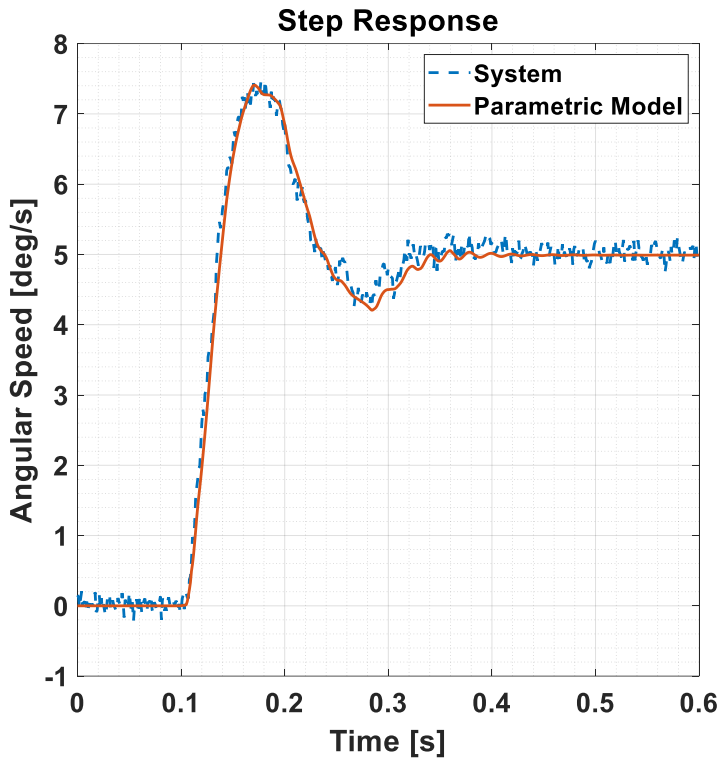
Figure 4.11. Step responses of the real system and the identified parametric model

Another evaluation for the success of the system identification method was performed by comparing the step responses of the real system and the parametric model as shown in Figure 4.11. According to the Figure 4.11, there is a high similarity between the step responses of the real system and the identified parametric model.

4.2.3. Identification of Multiplicative Uncertainty

Identification of the parametric model was performed by using mean frequency response function of the system as discussed previous section. The multiplicative uncertainty arises from the differences between the average frequency response function and the frequency response functions corresponding to the torque inputs with different amplitudes, and from

errors caused by parametric modelling. Multiplicative uncertainty at the frequency ω_k is identified by using following equation:

$$l_I(\omega_k) = \left| \frac{G_i(j\omega_k) - G(j\omega_k)}{G(j\omega_k)} \right| \quad ; \quad i = 1, \dots, 4 \tag{94}$$

Using Eq. 94, four different uncertainty points are obtained at each frequency value. Multiplicative uncertainty between frequency response data and identified parametric model is shown in Figure 4.12.
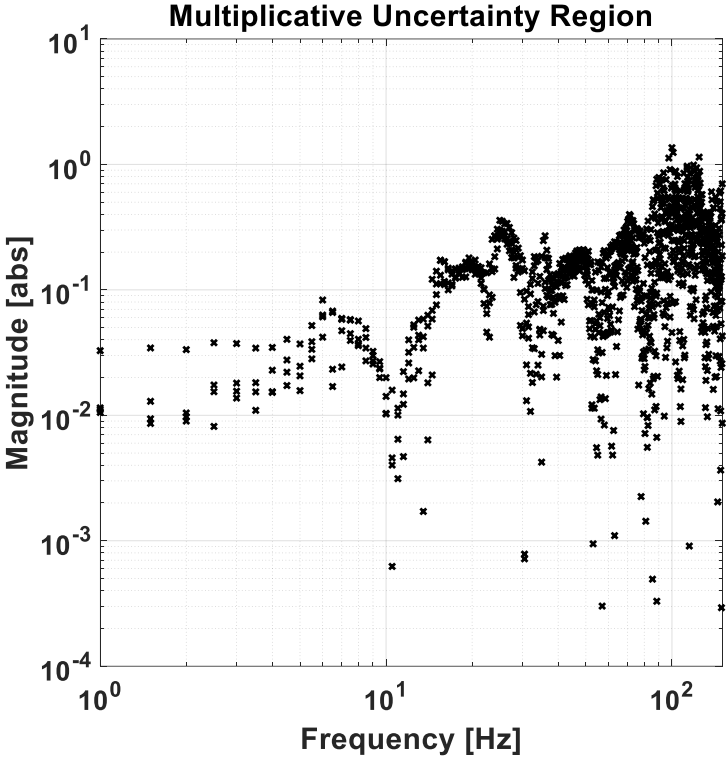
Figure 4.12. Multiplicative uncertainty between system frequency response function and identified parametric model

5. DESIGN OF H_∞ CONTROLLERS

In this chapter full-order and fixed-order model-based H_∞ controllers were synthesized with the methods that are discussed in Chapter 3. While designing model-based H_∞ controllers, $S/KS/T$ mixed-sensitivity framework was used.

After synthesis of model-based H_∞ controllers, fixed-order data-driven H_∞ controller was designed with a novel two-stage controller design method. With the help of this method, transfer functions that have unknown parameters in their denominators can be added to the structure of the controller that is synthesized by the optimization methods.

5.1. Weighting Functions Selection

In model-based H_∞ controller synthesis, $S/KS/T$ mixed-sensitivity framework which is shown in Figure 3.5, was used. In this framework, three weighting functions should be included to the structure of the generalized plant.

The multiplicative uncertainty weighting function was adapted to the structure of the generalized plant to represent the multiplicative uncertainty that arises due to nonlinearity, parametric modelling error, and unmodeled dynamics. To represent all possible plants in non-parametric model set, multiplicative uncertainty weighting function $\left(W_I(j\omega)\right)$ should cover the multiplicative uncertainty region which is shown in Figure 4.12. Therefore, following relationship should be considered while determining the multiplicative uncertainty weighting function:

$$|W_I(j\omega_k)| \geq \max\left|\frac{G_i(j\omega_k) - G(j\omega_k)}{G(j\omega_k)}\right| \quad ; \quad i = 1, \dots, 4, \ \forall \omega_k \tag{95}$$

To determine the multiplicative uncertainty weighting function $\left(W_I(j\omega)\right)$, "*ucover*" function in MATLAB Robust Control Toolbox was used and first order weighting function that provides the Eq. 95 was obtained as:

$$W_I(j\omega) = \frac{19.41 + 2.047j\omega}{708.2 + j\omega} \tag{96}$$

In $S/KS/T$ mixed-sensitivity control problem, magnitude of $|KS|$ is limited by using weighting function W_u to avoid saturation of the actuator. Therefore, W_u was determined as:

$$W_u(j\omega) = \frac{1}{\tau_{max}} \tag{97}$$

where τ_{max} is the maximum torque that can be generated by the motor that was placed to the traverse axis of the two-axis stabilized platform. For traverse axis of the System A, maximum motor torque is equal to $22\ Nm$.

Multiplicative Uncertainty Weighting Function
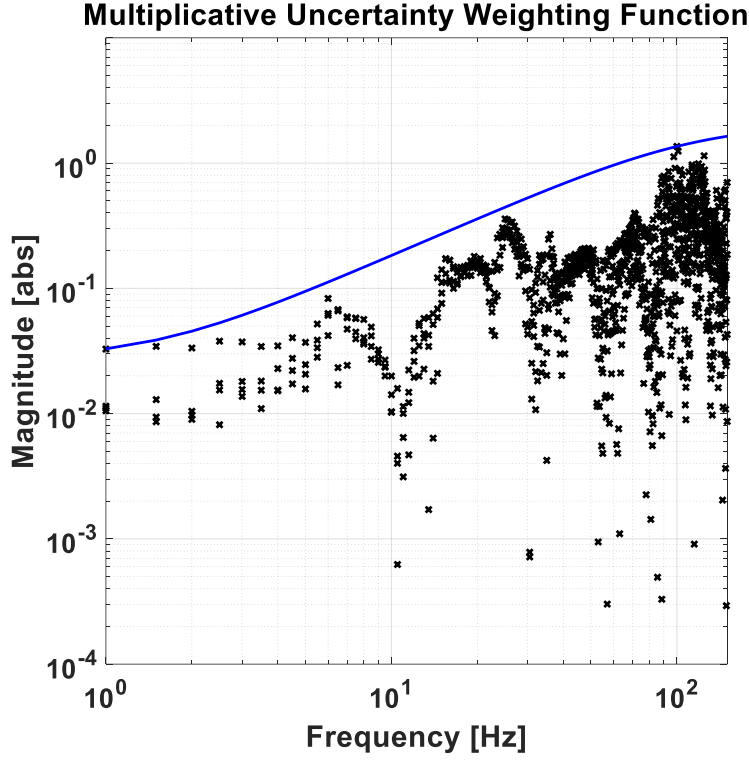
Figure 5.1. Multiplicative uncertainty region and weighting function

The last weighting function that was added to the structure of the generalized plant is the performance weighting function $\left(W_P(j\omega)\right)$. In $S/KS/T$ mixed-sensitivity control problem, magnitude of the sensitivity function ($|S|$) is limited by using the weighting function W_P. As discussed in Chapter 2, performance weighting function was determined according to closed-loop performance requirements as:

$$W_P(j\omega) = \frac{\left(\dfrac{j\omega}{M^{\frac{1}{2}}} + \omega_B^*\right)^2}{\left(j\omega + \omega_B^* A^{\frac{1}{2}}\right)^2} \quad ; \quad M = 3, \omega_B^* = 2\pi5, A = 10^{-6} \tag{98}$$

5.2. Full-Order Model-Based H_∞ Controller Design

In this section, two different full-order model-based H_∞ controllers are designed with different performance weighting functions.

Full-order model-based H_∞ controller was designed in $S/KS/T$ mixed-sensitivity framework. As discussed in Chapter 3, main objective in $S/KS/T$ mixed-sensitivity controller synthesis problem is calculating the sub − optimal H_∞ controller that satisfies the following inequality:

$$\left\| \begin{bmatrix} W_P S \\ W_u KS \\ W_I T \end{bmatrix} \right\|_\infty < \gamma \tag{99}$$

where γ is close to optimal value γ_{min}. The block diagram representation of the controller synthesis problem is shown in Figure 5.2.
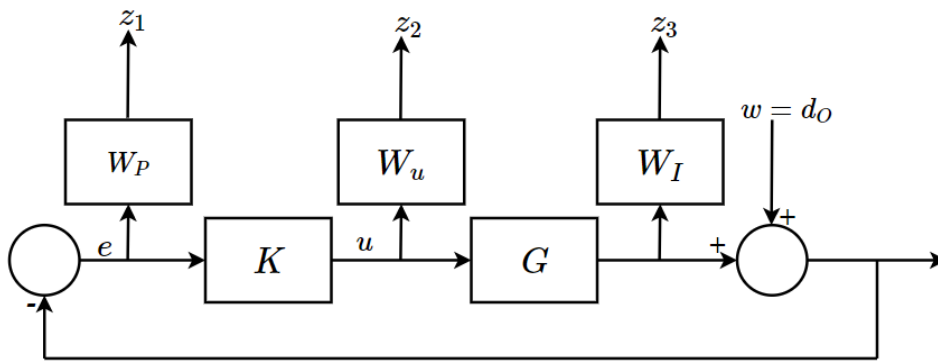
Figure 5.2. Block diagram representation of full-order model-based H_∞ controller design problem

Generalized plant was obtained according to the block diagram representation of the controller synthesis problem shown in Figure 5.2 by using "*sysic*" function in MATLAB Robust Control Toolbox. Then, another MATLAB Robust Control Toolbox function "*hinfsyn*" was performed to calculate full-order model-based H_∞ controller. Since "*hinfsyn*" function cannot be used for plant models with time delays, first order Pade approximation was used to approximate time delay in the identified plant model:

$$e^{-st_{delay}} = \frac{-t_{delay}s + 2}{t_{delay}s + 2} \tag{100}$$

Total order of the weighting functions and order of the parametric model are equal to 3 and 10 (one extra order from Pade approximation), respectively. Therefore, generalized plant and calculated H_∞ controller having order of 13.

5.2.1. Design 1

Firstly, the full-order model-based H_∞ controller is designed with performance weighting function in Eq. 98. At the end of the full-order model-based H_∞ controller design procedure, γ value is calculated as 0.7245, and stability and performance properties for the obtained closed-loop system are shown in Figure 5.3 and Figure 5.4.

Figure 5.3. Nominal stability condition for closed-loop system with full-order model-based H_∞ controller (Design 1)

According to Nyquist stability criterion, closed-loop system with full-order model-based H_∞ controller ensures nominal stability condition as shown in Figure 5.3. Moreover, gain and phase margins of the closed-loop system are calculated as $9.45\ dB$ and $48.8°$ respectively. On the other hand, Figure 5.4 shows that nominal performance, robust stability, and robust performance properties which are defined in Eq. 38, Eq. 39, and Eq. 40 are satisfied.

As shown in Figure 5.5, magnitude of $|KS|$ stays below the maximum motor torque limit. Therefore, actuator constraint which is defined by the weighting function $W_u(j\omega)$ is also fulfilled.

Figure 5.4. Nominal performance, robust stability, and robust performance conditions for closed-loop system with full-order model-based H_∞ controller (Design 1)

Figure 5.5. Actuator constraint for closed-loop system with full-order model-based H_∞ controller (Design 1)

5.2.2. Design 2

Another full-order model-based H_∞ controller is designed with a different performance weighting function defined in Eq. 101.

$$W_P(j\omega) = \frac{\left(\dfrac{j\omega}{M^{\frac{1}{2}}} + \omega_B^*\right)^2}{\left(j\omega + \omega_B^* A^{\frac{1}{2}}\right)^2} \quad ; \quad M = 3, \omega_B^* = 2\pi(2.5), A = 10^{-6} \tag{101}$$

In second design of the full-order model-based H_∞ controller, γ value is calculated as 0.5073, and stability and performance conditions for the obtained closed-loop system are shown in Figure 5.6 and Figure 5.7.
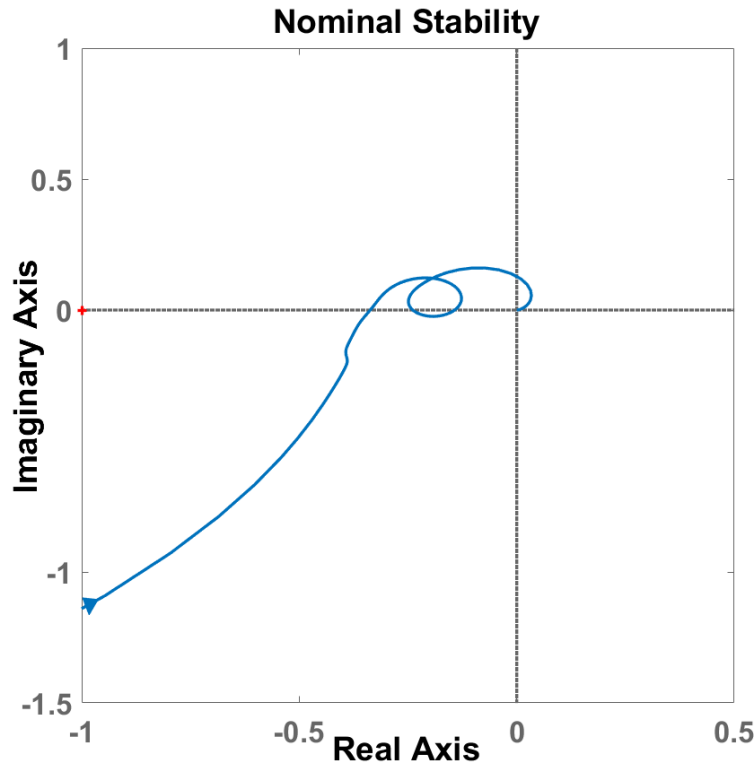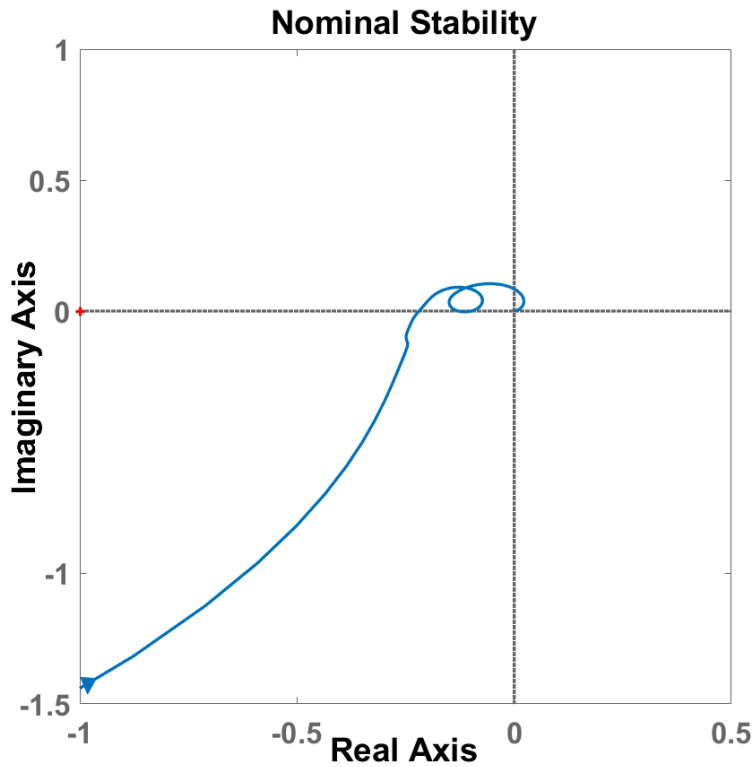

Figure 5.6. Nominal stability condition for closed-loop system with full-order model-based H_∞ controller (Design 2)

According to Nyquist stability criterion, closed-loop system with full-order model-based H_∞ controller ensures nominal stability condition as shown in Figure 5.6. Moreover, gain and phase margins of the closed-loop system are calculated as $13.2\ dB$ and $58.6°$ respectively. On the other hand, Figure 5.7 shows that nominal performance, robust stability, and robust performance conditions which are defined in Eq. 38, Eq. 39, and Eq. 40 are satisfied.

Figure 5.7. Nominal performance, robust stability, and robust performance conditions for closed-loop system with full-order model-based H_∞ controller (Design 2)

Figure 5.8. Actuator constraint for closed-loop system with full-order model-based H_∞ controller (Design 2)

As shown in Figure 5.8, magnitude of $|KS|$ stays below the maximum motor torque limit. Therefore, actuator constraint which is defined by the weighting function $W_u(j\omega)$ is also fulfilled.
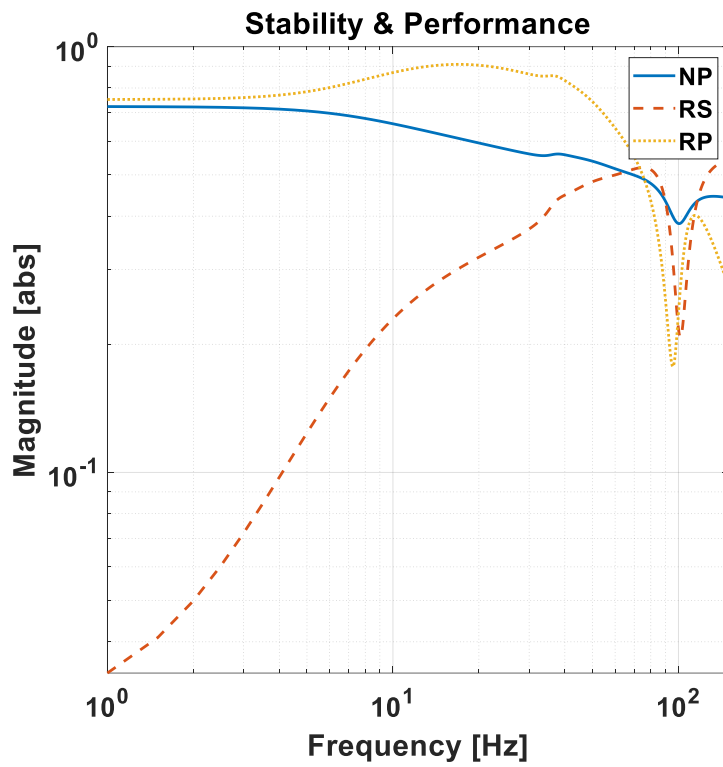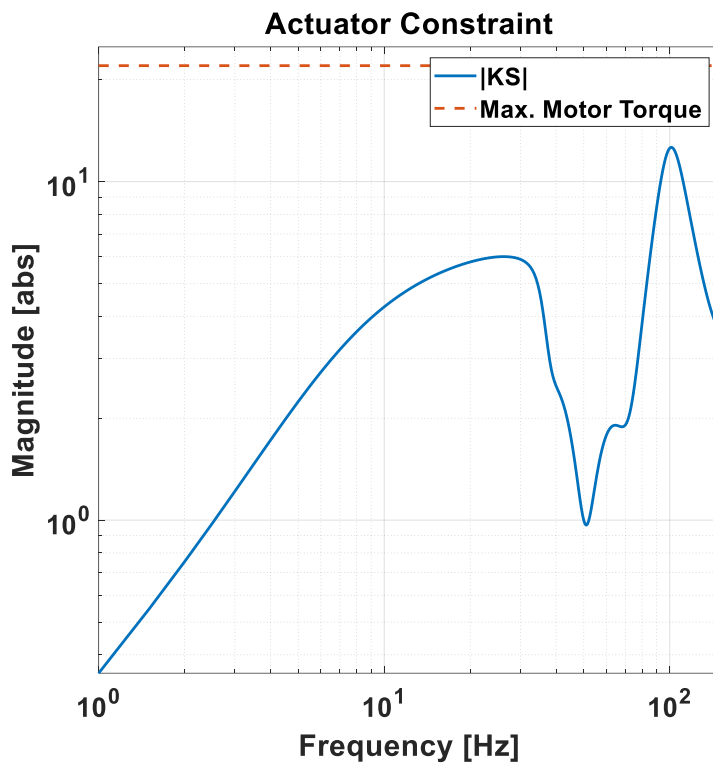
5.3. Fixed-Order Model-Based H_∞ Controller Design

Fixed-order model-based H_∞ controller was also designed in $S/KS/T$ mixed-sensitivity framework. However, the structure of the controller is predetermined and the objective of the controller synthesis problem is modified as finding controller parameters that satisfies the inequality in Eq. 99.

In this thesis study, structure of the fixed-order model-based H_∞ controller was determined to include an anti-resonance filter and a PI-controller. Although different type of anti-resonance filters can be used to reduce the effect of the flexible modes of the mechanical systems [59], an asymmetric notch filter were added to the control structure. Transfer function of the asymmetric notch filter is shown in Eq. 102:

$$G_f(s) = R_f^2 \frac{s^2 + 2\xi_f \omega_{n,f} s + \omega_{n,f}^2}{\left(s + R_f \omega_{n,f}\right)^2} \tag{102}$$

The high frequency response of the asymmetric notch filter is controlled by the parameter R_f. On the other hand, the parameters $\omega_{n,f}$ and ξ_f determine natural frequency and damping ratio of the asymmetric notch filter, respectively. The block diagram representation of the fixed-order model-based H_∞ controller synthesis problem is shown in Figure 5.9.
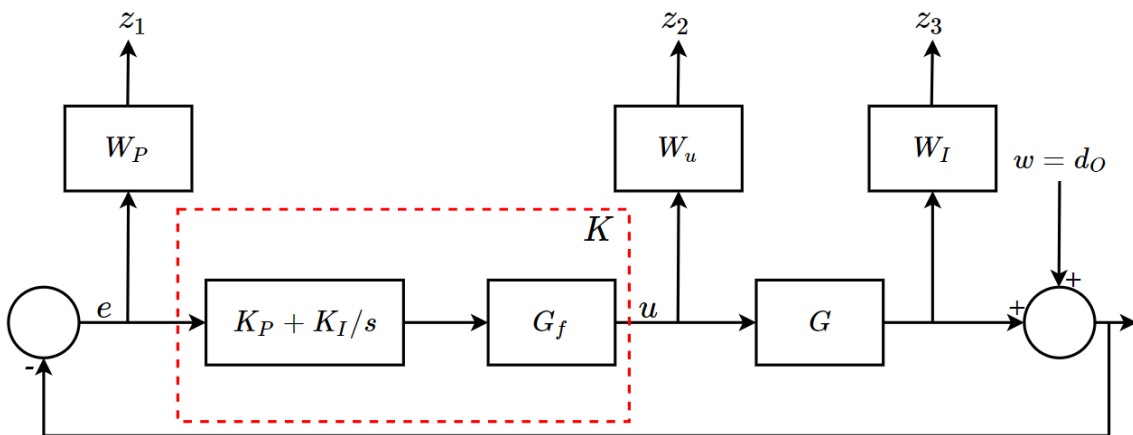
Figure 5.9. Block diagram representation of fixed-order model-based H_∞ controller design problem

To design fixed-order model-based H_∞ controller, MATLAB Robust Control Toolbox function "*hinfstruct*" was used. In this function, unknown controller parameters $(K_p, K_I, R_f, \omega_{n,f}, \xi_f)$ are defined as tunable parameters and "*hinfstruct*" tries to minimize infinity norm of closed-loop transfer function from exogenous inputs w to exogenous outputs z which is a function of unknown controller parameters. Calculated controller parameters are shown in Table 5.1.

Table 5.1. Fixed-order model-based H_∞ controller parameters

K_P	K_I	R_f	$\omega_{n,f}/2\pi\ [Hz.]$	ξ_f
3.0882	49.8233	0.4902	81.6704	0.5

At the end of the fixed-order model-based H_∞ controller design procedure, γ value is calculated as 1.0822, and stability and performance conditions for the obtained closed-loop system are shown in Figure 5.10 and Figure 5.11.
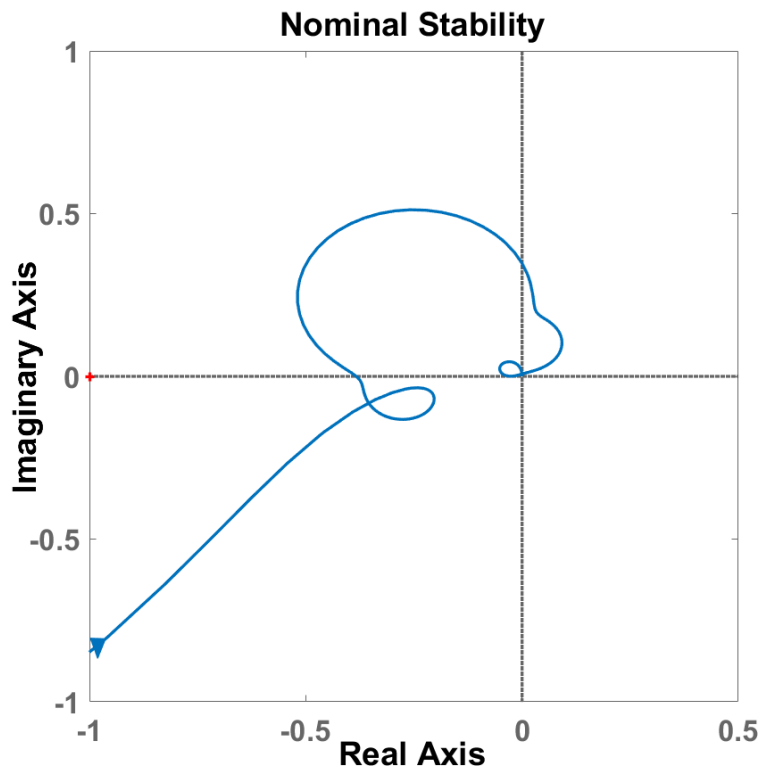
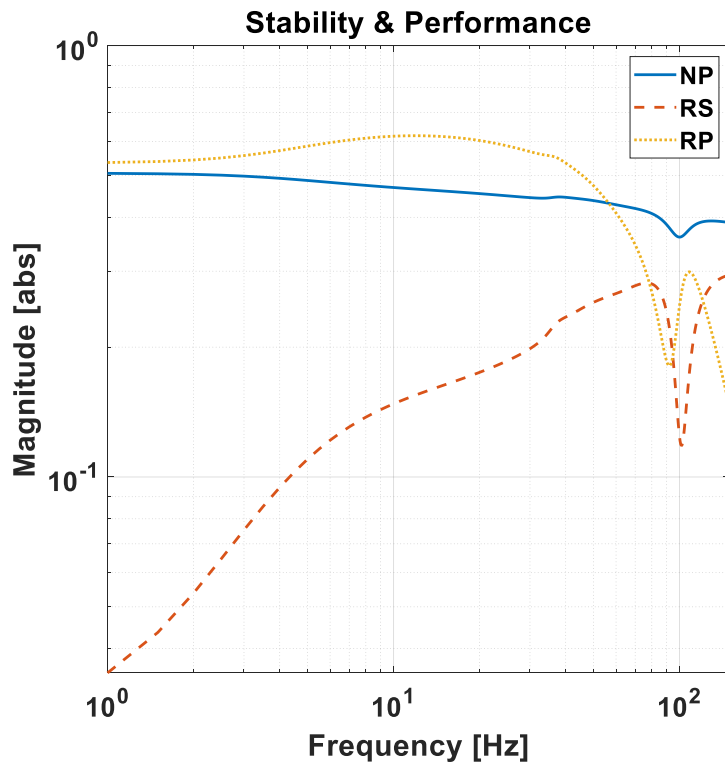Figure 5.10. Nominal stability condition for closed-loop system with fixed-order model-based H_∞ controller
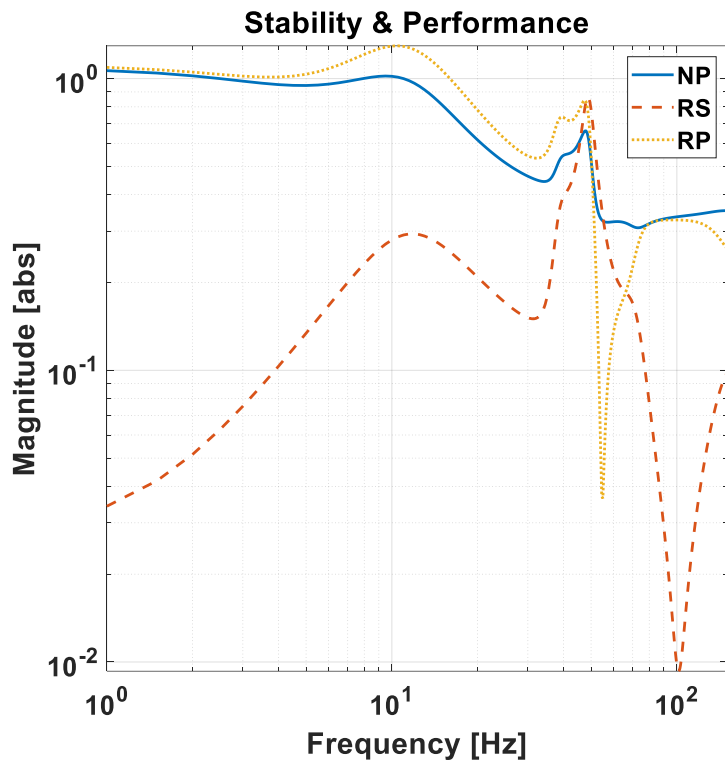
Figure 5.11. Nominal performance, robust stability, and robust performance conditions for closed-loop system with fixed-order model-based H_∞ controller
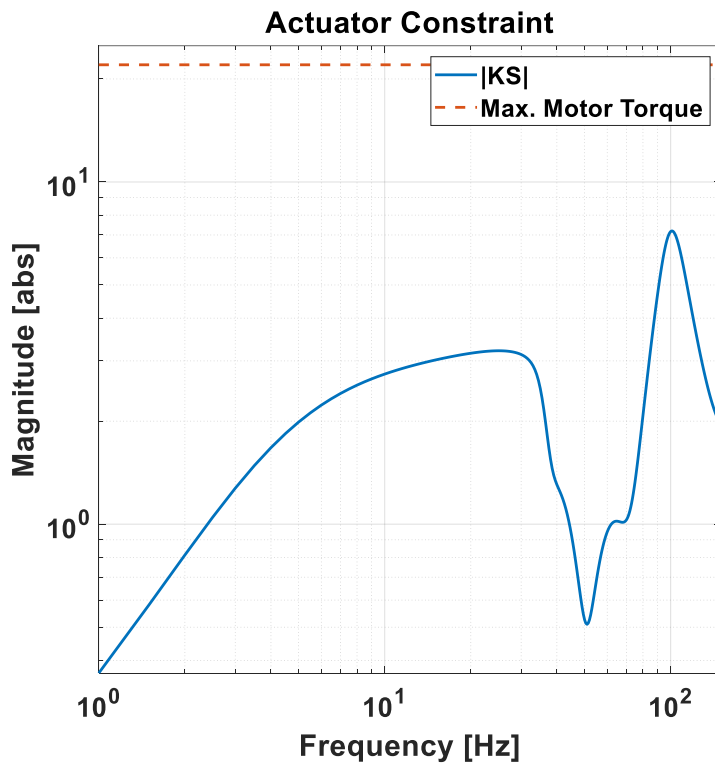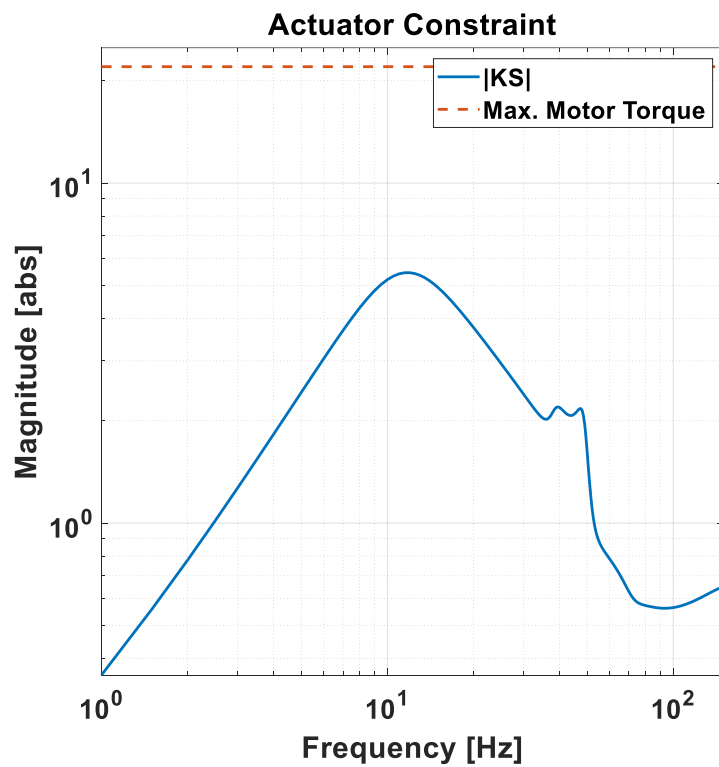

Figure 5.12. Actuator constraint for closed-loop system with fixed-order model-based H_∞ controller

According to Nyquist stability criterion, closed-loop system with fixed-order model-based H_∞ controller ensures nominal stability condition as shown in Figure 5.10. Moreover, gain and phase margins of the closed-loop system are calculated as $8.33\ dB$ and $37.1°$ respectively.

Although robust stability condition which is defined in Eq. 39 is satisfied by the fixed-order model-based H_∞ controller, Figure 5.11 shows that nominal performance and robust performance conditions which are defined in Eq. 38 and Eq. 40 cannot be guaranteed.

As shown in Figure 5.12, magnitude of $|KS|$ stays below the maximum motor torque limit. Therefore, actuator constraint which is defined by the weighting function $W_u(j\omega)$ is fulfilled.

5.4. A Novel Two-Step Method for Fixed-Order Data-Driven H_∞ Controller Design

Fixed-order data-driven H_∞ controller synthesis was performed by using S/KS mixed-sensitivity framework. The main objective in S/KS mixed-sensitivity controller synthesis problem is calculating the sub-optimal H_∞ controller that satisfies the following inequality:

$$\left\| \begin{bmatrix} W_P S \\ W_u KS \end{bmatrix} \right\|_\infty < \gamma \tag{103}$$

where γ is close to optimal value γ_{min}. The block diagram representation of the controller synthesis problem is shown in Figure 5.13.

Figure 5.13. Block diagram representation of fixed-order data-driven H_∞ controller synthesis problem

In this thesis study, the H_∞ controller synthesis problem defined by Eq. 103 has been reduced to Eq. 104 in order to obtain linear constraints for controller synthesis problem.

$$|W_P(j\omega)S(j\omega)| + |W_u(j\omega)K(j\omega)S(j\omega)| < 1, \quad \forall\omega \tag{104}$$

The term $|W_u(j\omega)K(j\omega)S(j\omega)|$ in Eq. 104 can be expressed as

$$|W_u(j\omega)K(j\omega)S(j\omega)| = |W_u'(j\omega)T(j\omega)| \tag{105}$$

where

$$W_u'(j\omega) = \frac{W_u(j\omega)}{G(j\omega)} \tag{106}$$

Thus, the constraints of the fixed-order data-driven H_∞ controller synthesis problem is reformulated as the robust performance criterion with different multiplicative uncertainty weighting function in Eq. 106.

$$|W_P(j\omega)S(j\omega)| + |W_u'(j\omega)T(j\omega)| < 1, \quad \forall\omega \tag{107}$$
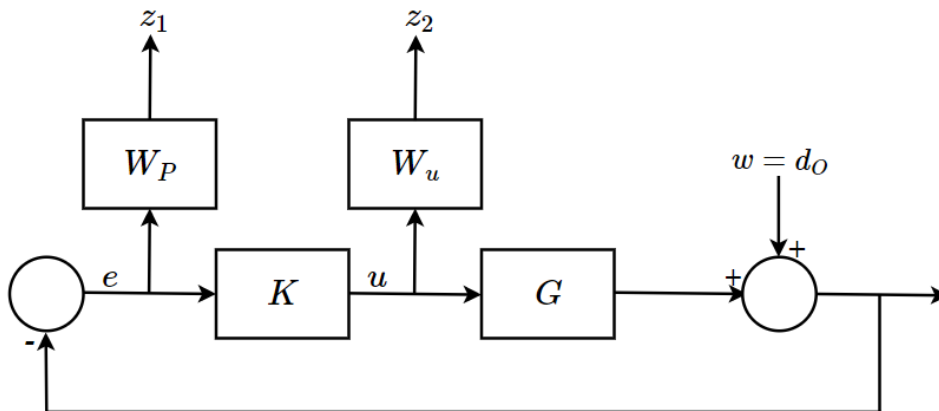
In this thesis study, the fixed-order data-driven H_∞ controller has the same structure with the fixed-order model-based H_∞ controller. Due to the existence of unknown parameters in denominator of the controller structure, the fixed-order data-driven controller synthesis method discussed in Chapter 3 cannot be performed directly. Therefore, in this thesis study, a new two-stage controller synthesis method is proposed to calculate unknown parameters of the fixed-order data-driven H_∞ controller.

In the first step of the proposed method, unknown parameters of the asymmetric notch filter are calculated according to an optimization problem whose objective function is formulated as reducing the effect of flexible modes of the stabilized platform. Then, linearly parameterized H_∞ controller is calculated by solving an optimization problem under linearized H_∞ constraints obtained with the help of Nyquist diagram as discussed in Chapter 3, in the second stage of the proposed method.

5.4.1. Anti-Resonance Filter Design for Flexible Mechanical Systems

For flexible mechanical systems, general structure of the plant model from motor torque input to body angular velocity is shown in Figure 4.8. General structure of the plant model in frequency domain is given below:

$$G(j\omega) = \frac{K}{j\omega}G_{flex}(j\omega)e^{-j\omega t_{delay}} \tag{108}$$

In order to increase the stabilization and command tracking performances of the flexible mechanical systems, the effect of flexible modes of the system should be minimized. Therefore, the anti-resonance filter represented by the transfer function in Eq. 109 is added to the structure of the fixed-order controller.

$$G_f(j\omega) = \frac{N_f(j\omega)}{D_f(j\omega)} \tag{109}$$

Flexible modes of the stabilized platform is included to the system parametric model as $G_{flex}(j\omega)$ in Eq. 108. Accordingly, when the anti-resonance filter added to the control loop converges to $G_{flex}^{-1}(j\omega)$, the effect of flexible modes of the platform are minimized. Using the non-parametric plant model, the terms $N_f(j\omega)$ and $D_f(j\omega)$ of the anti-resonance filter can be determined by solving optimization problem whose objective function is shown in Eq. 110.

$$\min \left\| |G_f(j\omega_k)| |G(j\omega_k)| - \frac{K}{\omega_k} \right\|_2^2 \quad ; \quad \forall \omega_k \tag{110}$$
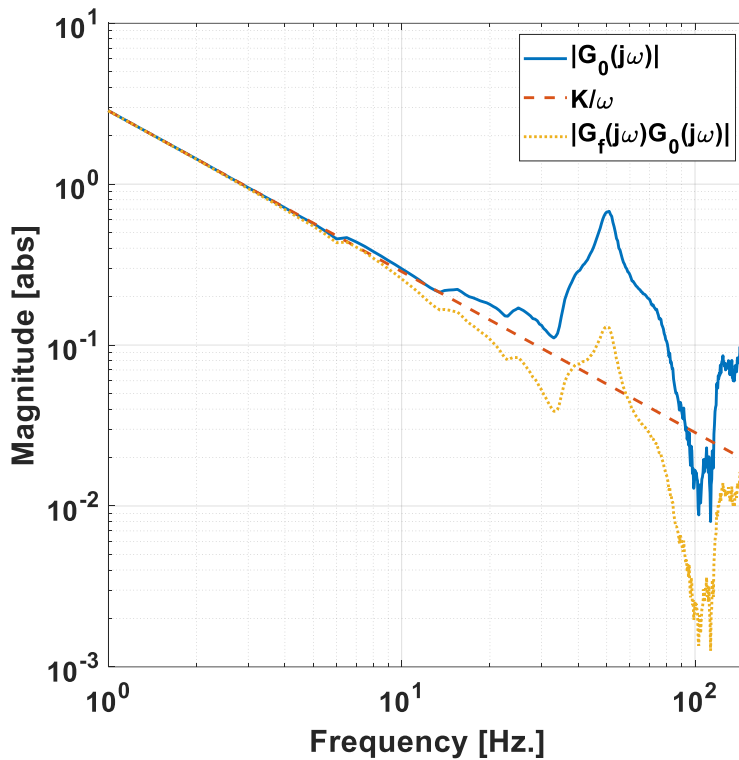

Figure 5.14. Loop transfer function obtained with asymmetric notch filter and nominal plant model

Using the nominal non-parametric plant model calculated by taking average of the FRFs obtained from the open-loop system identification tests, the coefficients of the asymmetric notch filter are determined by solving the optimization problem in Eq. 110. The loop transfer function generated when the notch filter obtained by the solution of this optimization problem is added to the control loop is shown in Figure 5.14.

5.4.2. Linearly Parameterized Data-Driven H_∞ Controller Synthesis

In the second stage of the fixed-order H_∞ controller synthesis, the parameters of the PI controller that is used with the asymmetric notch filter are calculated. The structure of the linearly parameterized H_∞ controller is shown in Eq. 111.

$$K(s,\rho) = \rho^T \phi(s) = [K_P \quad K_I] \left[G_f(s) \quad \frac{G_f(s)}{s} \right] \tag{111}$$

According to the H_∞ controller synthesis problem in Eq. 107, the unknown controller parameters in Eq. 111, K_P and K_I are calculated by solving the optimization problem given below:

$$\min \| \rho^T \phi(j\omega_k) G_i(j\omega_k) - L_d(j\omega_k) \|_2^2 \quad ; \quad i = 1, \dots, 4 \ \& \ \forall \omega_k \tag{112}$$

under a finite number of linear constraints

$$|W_P(j\omega_k)[1 + L_d(j\omega_k)]| - \Re\{[1 + L_d(-j\omega_k)][1 + L_n(j\omega_k, \rho)]\} < 0 \quad ; \quad \forall \omega_k \tag{113}$$

where $L_n(j\omega_k, \rho) = K(j\omega_k, \rho) G_n(j\omega_k)$ and

$$G_n(j\omega_k) = G_i(j\omega_k) \left[1 + \frac{|W'_u(j\omega_k)|}{\cos\left(\frac{\pi}{q}\right)} e^{\frac{j2\pi n}{q}} \right] \quad ; \quad n = 1, \dots, q \tag{114}$$

The general structure of the flexible mechanical system's plant model in Eq. 108 and the controller in Eq. 111 contain integrators. Therefore, desired loop transfer function is determined as:

$$L_d(s) = K_L \frac{s + z}{s^2} \tag{115}$$

A stable zero at $(-z, 0)$ is added to the transfer function of $L_d(s)$ to ensure Routh Hurwitz stability criterion. The characteristic equation for the closed-loop system with given loop transfer function in Eq. 115 is equals to: $s^2 + K_L s + K_L z$. According to Routh Hurwitz stability criterion, closed-loop system is stable when $K_L > 0$ and $z > 0$. These

parameters are chosen as $K_L = 50$ and $z = 30$ according to the nominal performance criteria and optimization problem defined in Eq. 112 is solved under linear constraints to calculate controller parameters. Calculated controller parameters are shown in Table 5.2.

Table 5.2. Fixed-order model-based H_∞ controller parameters

K_P	K_I	R_f	$\omega_{n,f}/2\pi$ [Hz.]	ξ_f
3.7803	59.1238	0.4325	61.4002	0.5

With calculated fixed-order data-driven H_∞ controller, γ_{max} value is calculated as 0.9172 and Nyquist diagram for obtained loop transfer function are shown in Figure 5.15.

According to Nyquist stability criterion, closed-loop system with fixed-order data-driven H_∞ controller ensures nominal stability condition as shown in Figure 5.15. Moreover, gain and phase margins of the closed-loop system are calculated as 8.73 dB and 38.5° respectively. Moreover, the $\gamma_{max} = 0.9172$ value indicates that both nominal stability condition and actuator constraint are satisfied for the four non-parametric models with the obtained fixed-order data-driven H_∞ controller.
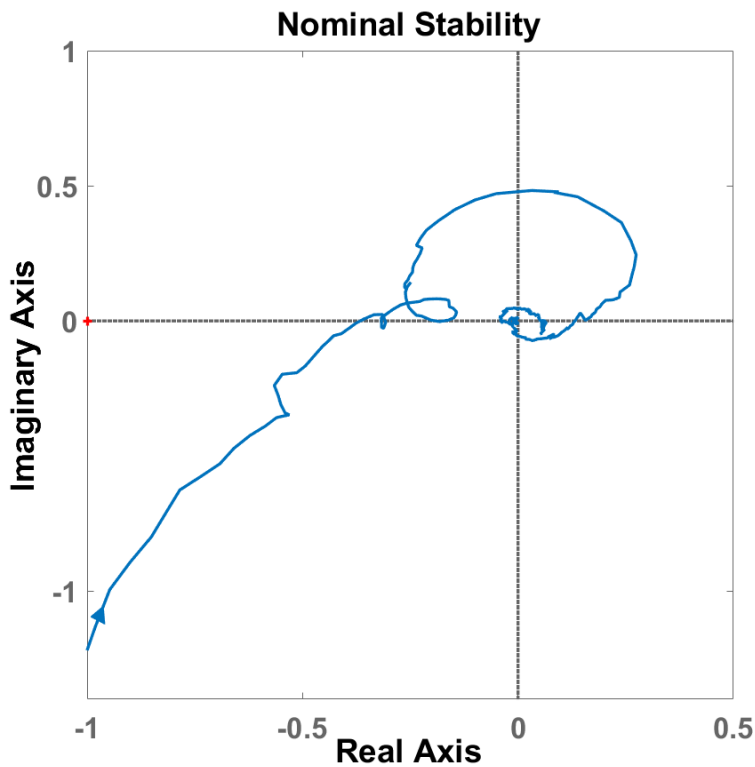
Figure 5.15. Nominal stability condition for closed-loop system with fixed-order data-driven H_∞ controller

For the nominal non-parametric model, magnitude of $|S|$ and $|KS|$ are shown in Figure 5.16 and Figure 5.17, respectively. As shown in Figure 5.16, the nominal sensitivity function approaches the desired sensitivity function which is defined in Eq. 116 and the magnitude of $|S|$ stays below the magnitude of $|W_P^{-1}|$. Therefore, nominal performance condition which is defined in Eq. 38 is satisfied by the fixed-order data-driven H_∞ controller.

$$S_d(s) = \frac{1}{1 + L_d} = \frac{s^2}{s^2 + K_L s + K_L z}. \tag{116}$$

As shown in Figure 5.17, magnitude of $|KS|$ stays below the maximum motor torque limit. Therefore, actuator constraint which is defined by the weighting function $W_u(j\omega)$ is also fulfilled.
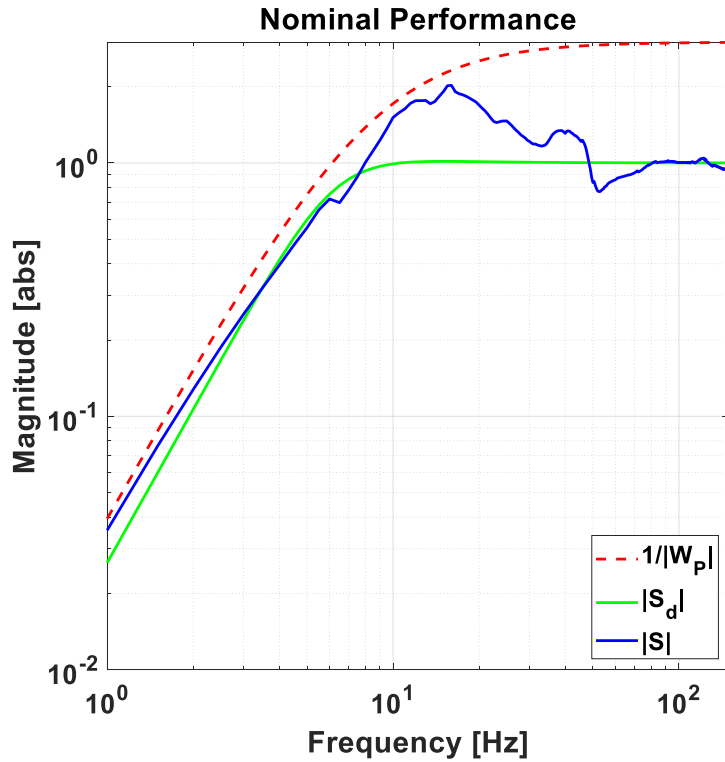
Figure 5.16. Nominal performance condition for closed-loop system with fixed-order data-driven H_∞ controller
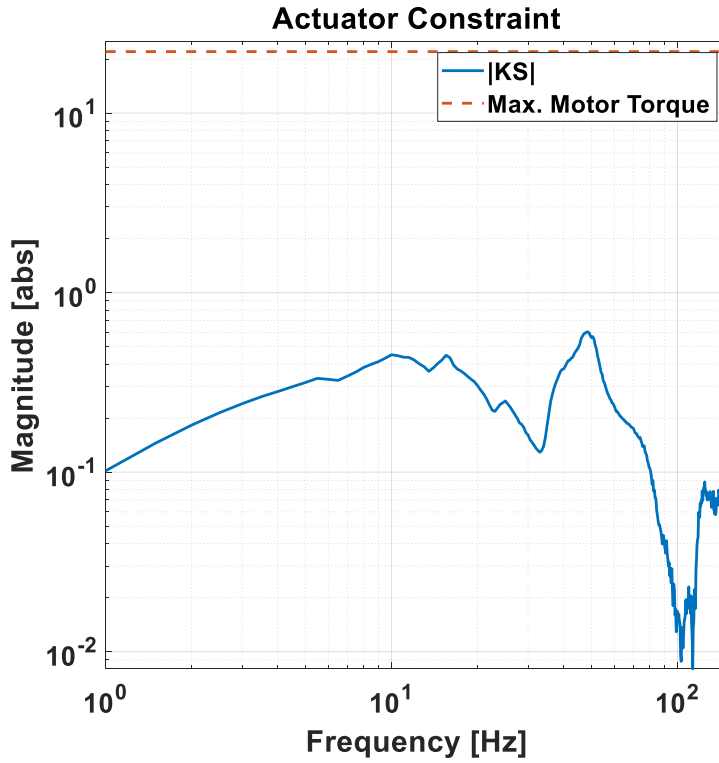
Figure 5.17. Actuator constraint for-closed-loop system with fixed-order data-driven H_∞ controller

5.5. Comparison of Controllers in Frequency Domain

In this chapter, three different H_∞ controller synthesis method are performed to design the speed controller of the traverse axis of the stabilized platform. The obtained frequency domain results for the closed-loop systems with these three controllers are summarized in Table 5.3.

Comparison of frequency response of the closed-loop transfer functions are shown in Figure 5.18, Figure 5.19, and Figure 5.20. In these figures, closed-loop transfer functions are obtained by using nominal non-parametric model.

According to Figure 5.18, in the low frequency region in between $1\,Hz$ and $5\,Hz$, full-order model-based H_∞ controller in Design 2 has the worst disturbance rejection and reference tracking performances. On the other hand, in the high frequency region, performances of the controllers are seen to be similar. Although all four controllers satisfy robust stability condition which is defined by multiplicative uncertainty weighting function $W_I(j\omega)$ as shown in Figure 5.19, robust stability margin of closed-loop system which is obtained with full-order model-based H_∞ controller in Design 1 is low in the high frequency region. Similarly, actuator constraint is fulfilled by the designed H_∞

controllers as shown in Figure 5.20, however, in the high frequency region the magnitudes of the closed-loop transfer function $|K(j\omega)S(j\omega)|$ obtained with the full-order model-based H_∞ controllers is close to maximum motor torque limit.

Table 5.3. Obtained frequency domain results for designed controllers

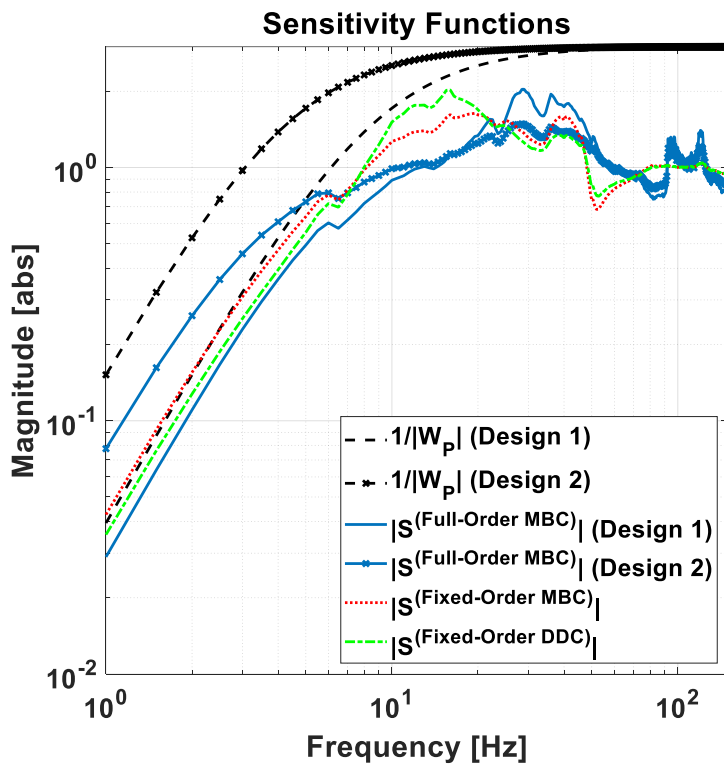|	Order	GM [dB]	PM [°]	NS	NP	RS	RP	γ
Full-Order Model-Based H_∞ Controller (Design 1)	13	9.45	48.8	✓	✓	✓	✓	0.7245
Full-Order Model-Based H_∞ Controller (Design 2)	13	13.2	58.6	✓	✓	✓	✓	0.5073
Fixed-Order Model-Based H_∞ Controller	3	8.33	37.1	✓	✗	✓	✗	1.0822
Fixed-Order Data-Driven H_∞ Controller	3	8.73	38.5	✓	✓	✓	✓	0.9173

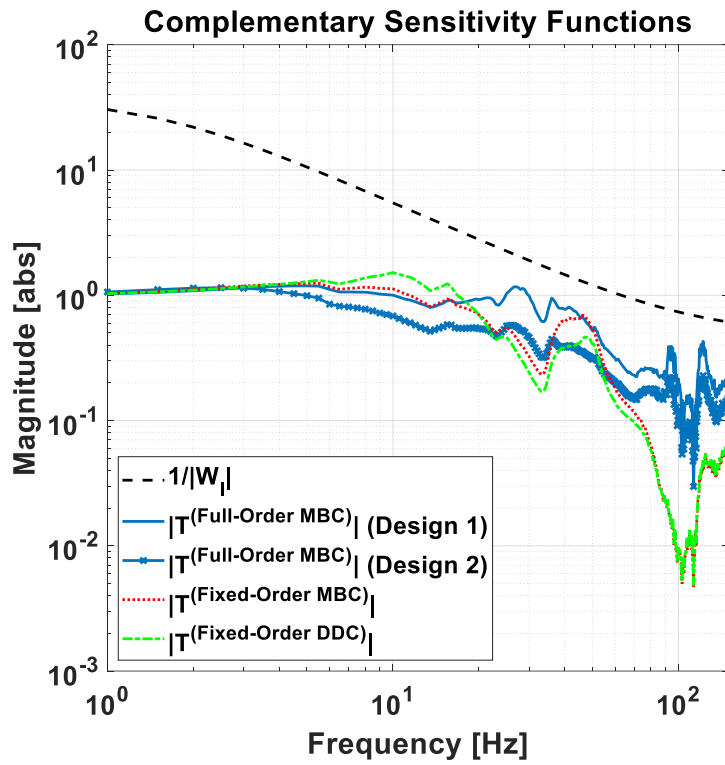Figure 5.18. Comparison of sensitivity functions

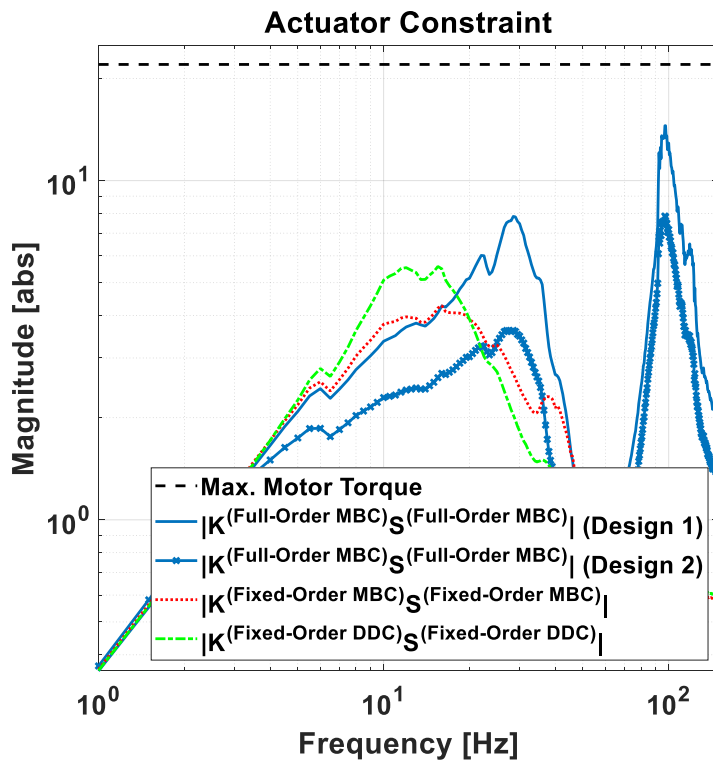Figure 5.19. Comparison of complementary sensitivity functions

Figure 5.20. Comparison of closed-loop transfer functions related to actuator constraint

6. IMPLEMENTATION OF THE H_∞ CONTROLLERS AND EXPERIMENTAL RESULTS

In this chapter, discussion about the implementation of the designed H_∞ controllers are presented. First of all, since the full-order model-based H_∞ controllers have high order, reduced-order model-based H_∞ controllers are calculated by using balanced truncation method. Then, discretization of the designed controllers is performed to implement these controllers in real-time tests. Finally, the experimental results of reference tracking and disturbance rejection tests are presented.

6.1. Implementation

In this section, controller order reduction is discussed first. Then, discretization method of the controllers is presented.

6.1.1. Order Reduction for Full-Order Model-Based H_∞ Controller

The full-order model-based H_∞ controller design method discussed in Chapter 3 generally results with high order complex controllers. For instance, in this thesis study, the order of above mentioned controllers is equal to 13. Because of the process cost and reliability issues, the lower order controllers are always preferred. Therefore, controller reduction technique which is named as balanced truncation method [60] is performed to reduce the order of the controllers.

In balanced truncation method, the main objective is to calculate reduced-order controller which keeps the important dynamics of the original full-order controller and the cost function is defined in Eq. 117

$$\|K - K_{red}\|_\infty \tag{117}$$

where K_{red} represents the reduced-order controller. In this thesis study, the balanced realization of the full-order model-based H_∞ controller is performed by using "*balancmr*" function in MATLAB Robust Control Toolbox. This function computes the balanced realization of the controller via square root method and this method guarantees that the error between the two controllers satisfies the following condition [61]:

$$\|K - K_{red}\|_\infty < 2 \sum_{i=r+1}^{n} \sigma_i \tag{118}$$

where σ_i is the ith Hankel singular value of the controller and r is the order of the reduced-order controller. In this model, one should select r such that $\sigma_r \gg \sigma_{r+1}$.

6.1.1.1 Reduced-Order Controller for Design 1

To determine the order of the reduced-order model-based H_∞ controller, Hankel singular values of the full-order controller in Design 1 are calculated as shown in Figure 6.1.
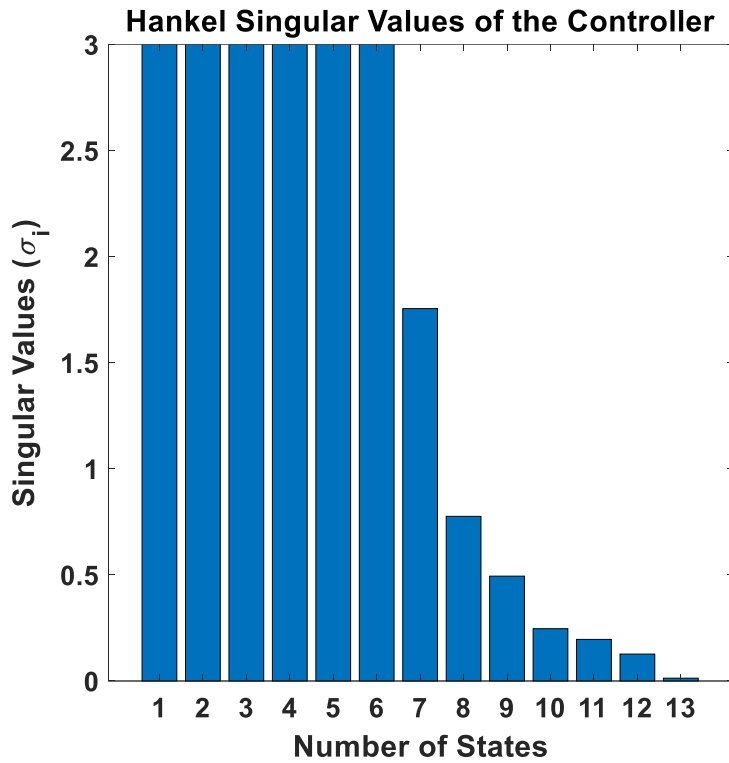
Figure 6.1. Hankel singular values of full-order model-based H_∞ controllers (Design 1)

According to the Figure 6.1, order of the reduced-order model-based H_∞ controllers is selected as 11 and the last two states are truncated. The frequency response of the full-order and reduced-order controllers are shown in Figure 6.2. According to Figure 6.2, frequency responses of these two controllers are similar.

Stability and performance conditions for the obtained closed-loop system are shown in Figure 6.3 and Figure 6.4. According to Nyquist stability criterion, closed-loop system with reduced-order model-based H_∞ controller ensures nominal stability condition as shown in Figure 6.3. Moreover, gain and phase margins of the closed-loop system are calculated as 9.52 dB and 44.6° respectively. On the other hand, Figure 6.4 shows that nominal performance, robust stability, and robust performance conditions which are defined in Eq. 38, Eq. 39, and Eq. 40 are satisfied.

Figure 6.2. Frequency response of full-order and reduced-order model-based H_∞ controllers (Design 1)

Figure 6.3. Nominal stability condition for closed-loop system with reduced-order model-based H_∞ controller (Design 1)

Figure 6.4. Nominal performance, robust stability, and robust performance conditions for closed-loop system with reduced-order model-based H_∞ controller (Design 1)

Figure 6.5. Actuator constraint for closed-loop system with reduced-order model-based H_∞ controller (Design 1)

As shown in Figure 6.5, magnitude of $|KS|$ stays below the maximum motor torque limit. Therefore, actuator constraint which is defined by the weighting function $W_u(j\omega)$ is also fulfilled.

6.1.1.2 Reduced-Order Controller for Design 2

For order reduction, similar procedure as given in previous section is performed for the full-order model-based H_∞ controller in Design 2. Hankel singular values of this controller are shown in Figure 6.6.
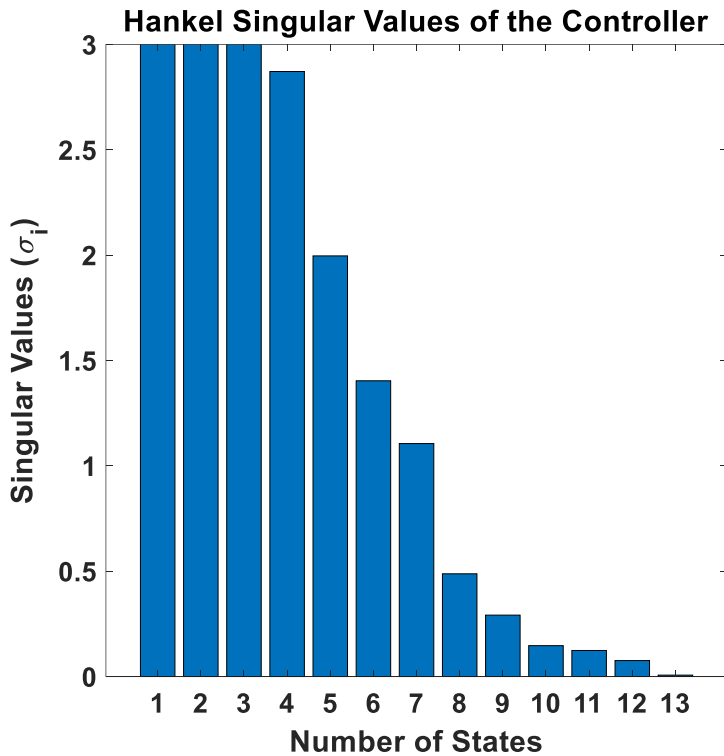
Figure 6.6. Hankel singular values of full-order model-based H_∞ controllers (Design 2)

According to the Figure 6.6, order of the reduced-order model-based H_∞ controllers is selected as 9 and the last four states are truncated. The frequency response of the full-order and reduced-order controllers are shown in Figure 6.7.

Stability and performance conditions for the obtained closed-loop system are shown in Figure 6.8 and Figure 6.9. Although reduced-order controller is slightly different than full-order controller according to the frequency responses of these two controllers in Figure 6.7, stability and performance conditions are fulfilled by the closed-loop system obtained with reduced-order controller as shown in Figure 6.8 and Figure 6.9.
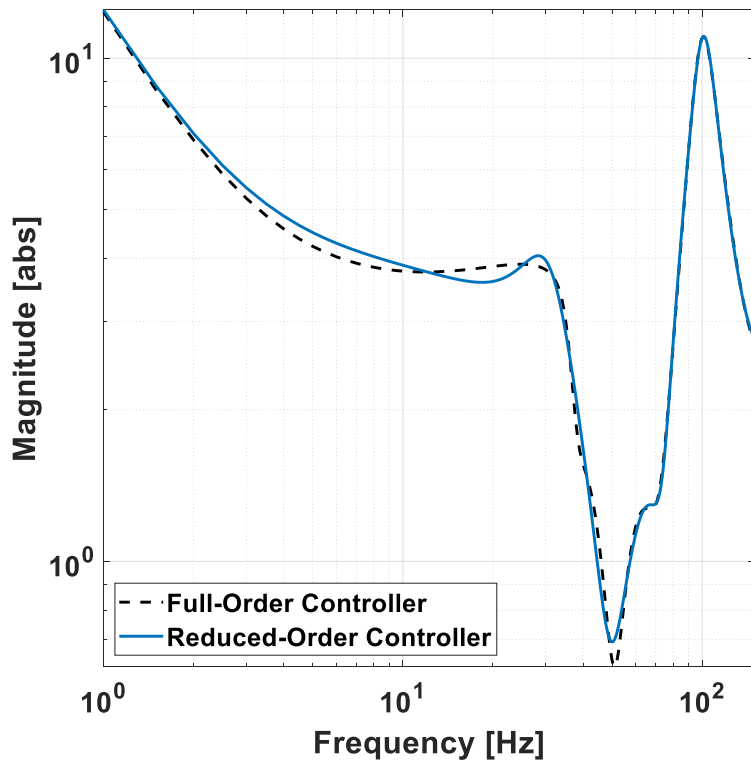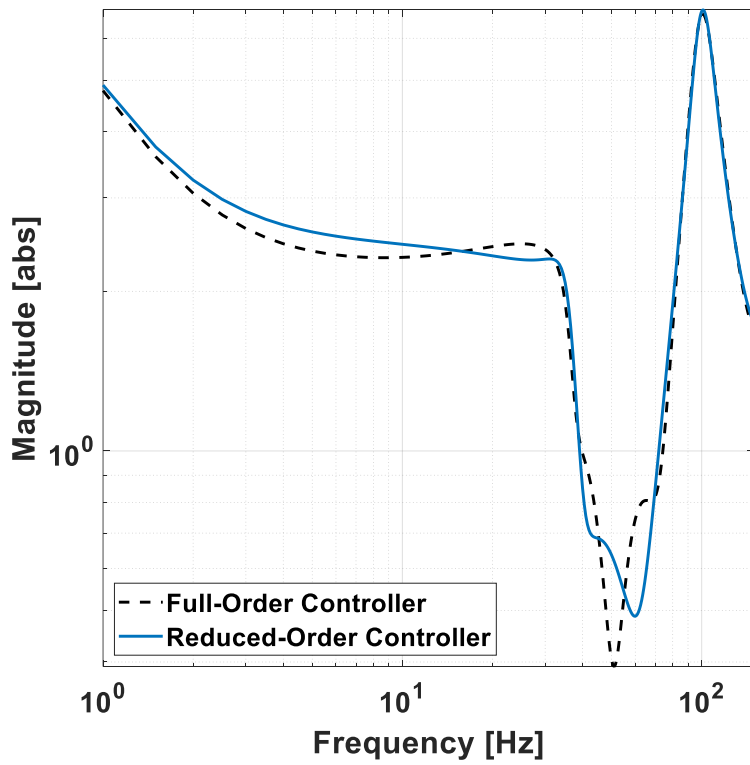
Figure 6.7. Frequency response of full-order and reduced-order model-based H_∞ controllers (Design 2)
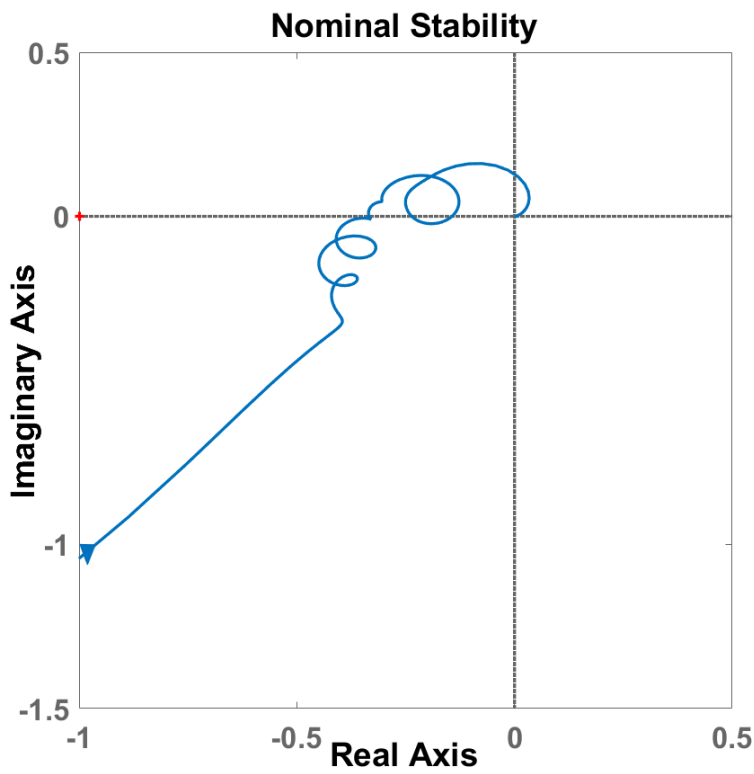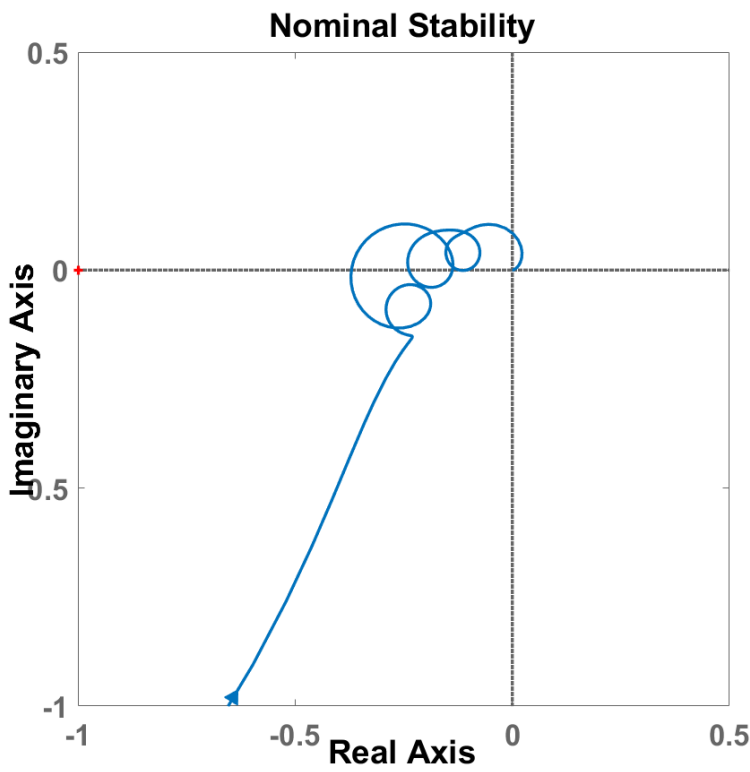

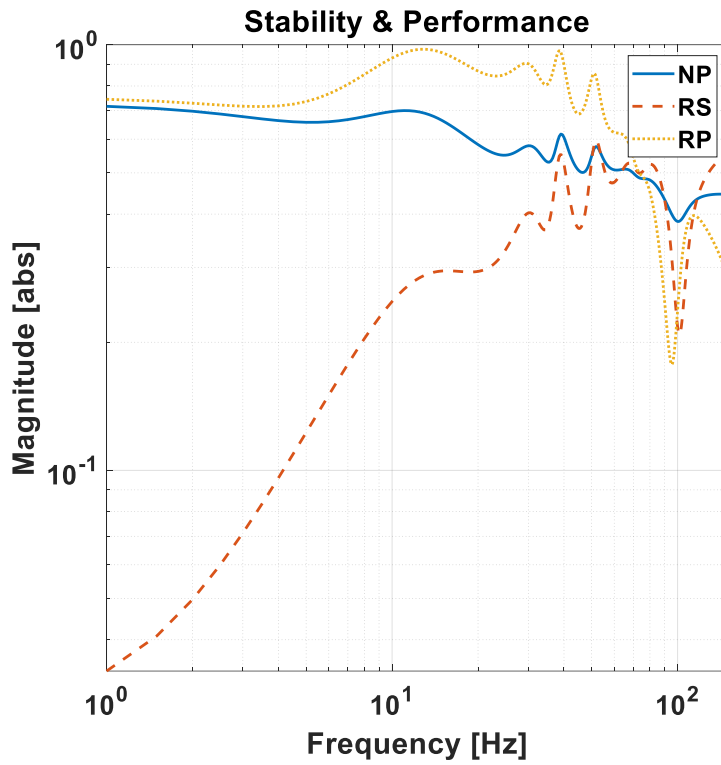Figure 6.8. Nominal stability condition for closed-loop system with reduced-order model-based H_∞ controller (Design 2)
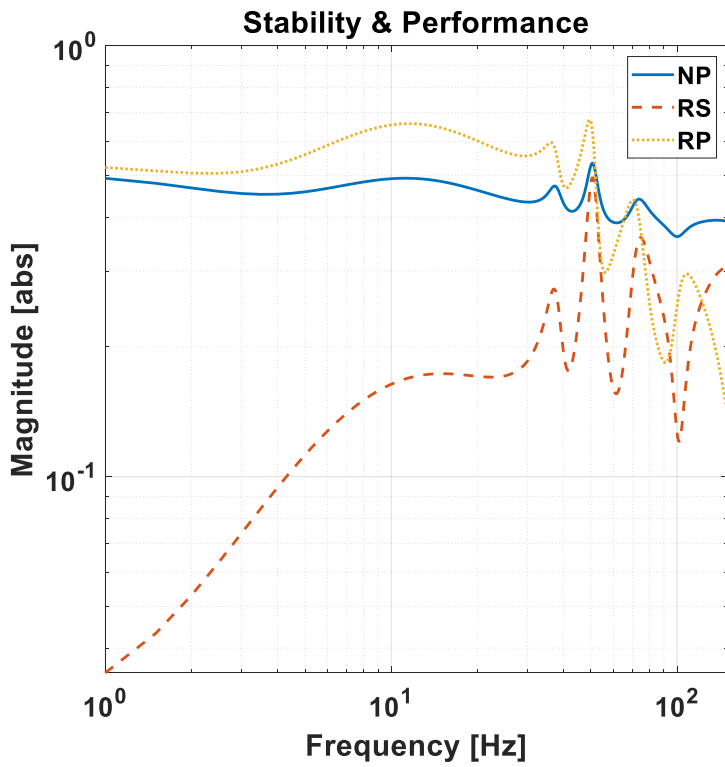
Figure 6.9. Nominal performance, robust stability, and robust performance conditions for closed-loop system with reduced-order model-based H_∞ controller (Design 2)
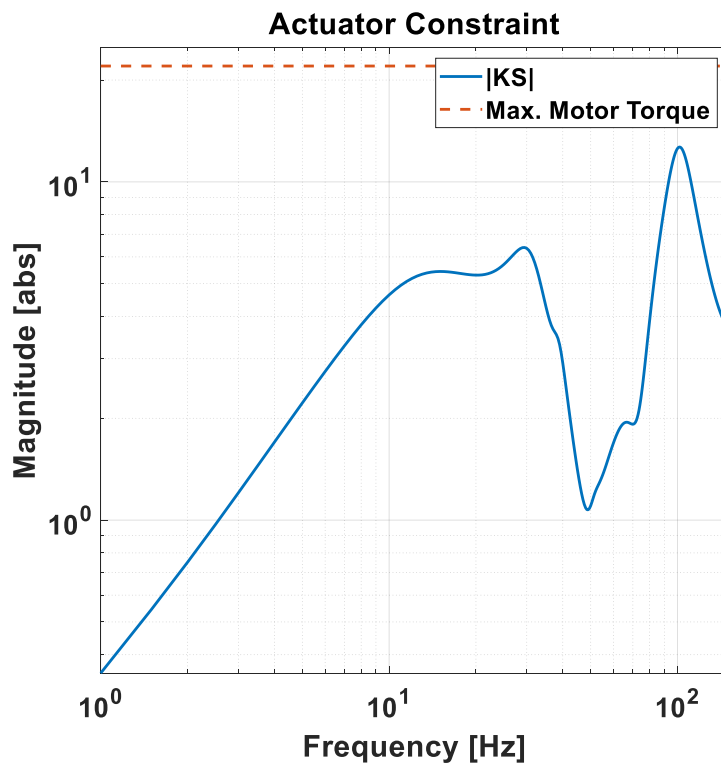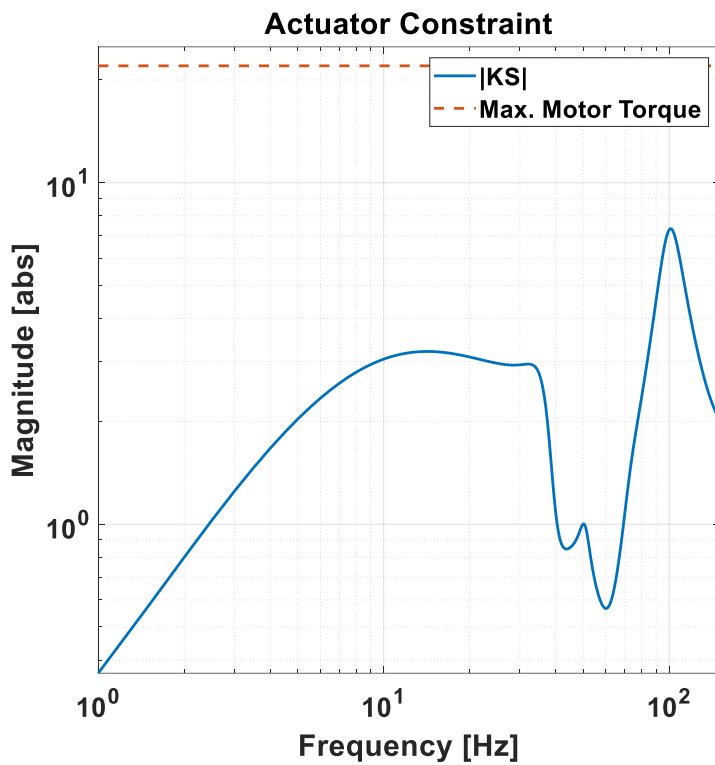

Figure 6.10. Actuator constraint for closed-loop system with reduced-order model-based H_∞ controller (Design 2)

The gain and phase margins of the closed-loop system are calculated as $8.63\ dB$ and $56.2°$ respectively. As shown in Figure 6.10, magnitude of $|KS|$ stays below the maximum motor torque limit. Therefore, actuator constraint which is defined by the weighting function $W_u(j\omega)$ is also satisfied.

6.1.2. Discretization of the Controllers with Tustin Approximation

To discretize the continuous H_∞ controllers, a common discretization technique called as Tustin or bilinear approximation is used in this thesis study. In this approximation technique, the discretization $K_d(z)$ of a continuous controller $K(s)$ is:

$$K_d(z) = K(s) \ ; \ \ s = \frac{2}{T_s}\frac{z-1}{z+1} \tag{119}$$

In this thesis study, discretization of the continuous controllers is performed by using "*c2d*" function in MATLAB Control System Toolbox.

6.2. Experimental Results

In this section, time domain performances of the H_∞ controllers are presented. The reference tracking and stabilization performances of the synthesized data-driven and model-based H_∞ controllers have been measured by real-time tests.

The square wave responses of the closed-loop systems are measured to determine reference tracking performances of the designed controllers. Meanwhile, the stabilization performances of the synthesized controllers have been examined by real-time tests with disturbance input. A motion simulator- a Stewart platform- is used to create external disturbance input. The change of traverse axis position of the stabilized platform under the disturbance input is calculated to examine stabilization performances of the designed controllers.

6.2.1. Reduced-Order Model-Based H_∞ Controller

Although two different reduced-order model-based H_∞ controllers were calculated in previous section and were shown to theoretically satisfy stability and performance conditions, real-time tests with reduced-order model-based H_∞ controller in Design 1 resulted with unstable response. Possible reasons of this situation is listed below:

- The one of the possible reason is considered as the implementation problems. As discussed in Chapter 1, a high order controller may lead to implementation problems in real-time systems due to its limited processing capability.

- Another possible reason is considered as the spillover phenomena discussed in Chapter 1. The frequency response function of the stabilized platform was obtained up to a certain frequency level. Also, to reduce the complexity of the model-based controller design procedure, the order of the plant model was not selected as too high. Therefore, reduced-order model-based H_∞ controller in Design 1 may produce a signal that may excite the high frequency modes which are not modeled. Then, the unmodeled dynamics of the system may be excited. The responses in the high frequency band used in the feedback loop of the control systems may cause the unstable response.

- Lastly, pole-zero flipping phenomena discussed in Chapter 1 may be another possible reason of the unstable response. In full-order model-based H_∞ controller synthesis problems, pole-zero cancellation between plant and controller generally occurs [26]. Then, pole-zero flipping may occur due to the modelling error and it may lead to unstable closed-loop system.

In this section, experimental results obtained with reduced-order model-based H_∞ controller in Design 2 are presented. The experimental reference tracking and stabilization performances of the reduced-order model-based H_∞ controller are shown in Figure 6.11 and Figure 6.12, respectively.
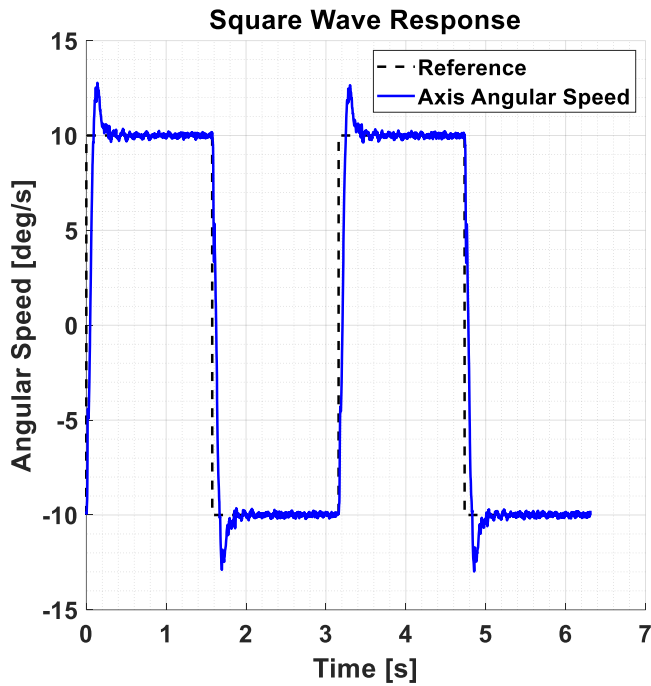
Figure 6.11. Reference tracking performance of the reduced-order model-based H_∞ controller
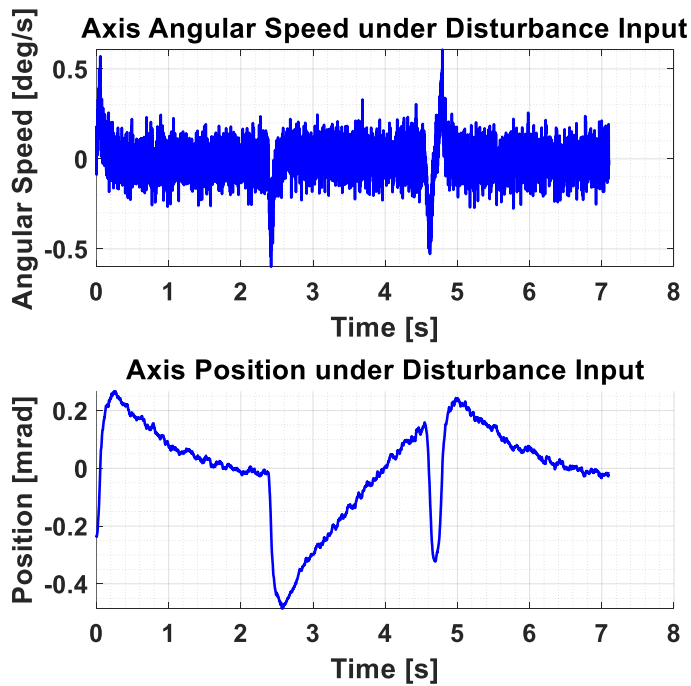
Figure 6.12. Stabilization performance of the reduced-order model-based H_∞ controller

6.2.2. Fixed-Order Model-Based H_∞ Controller

The experimental reference tracking and stabilization performances of the fixed-order model-based H_∞ controller are shown in Figure 6.13 and Figure 6.14, respectively.
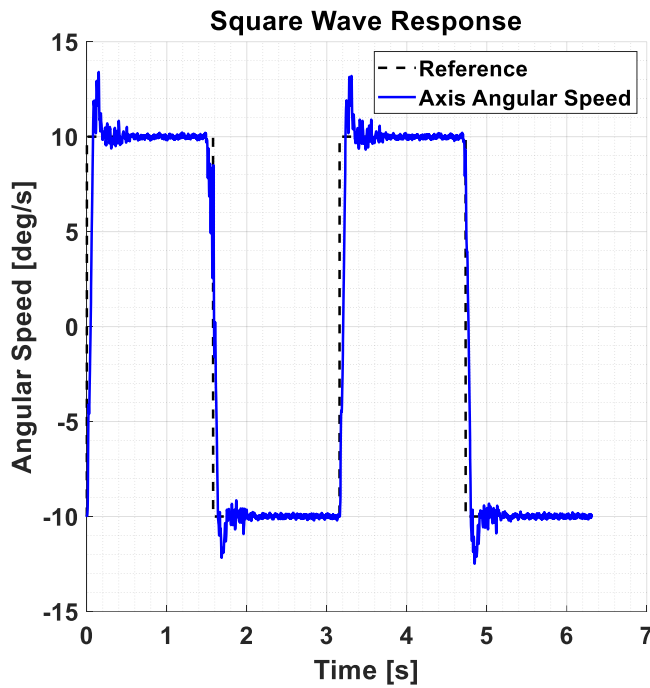
Figure 6.13. Reference tracking performance of the fixed-order model-based H_∞ controller
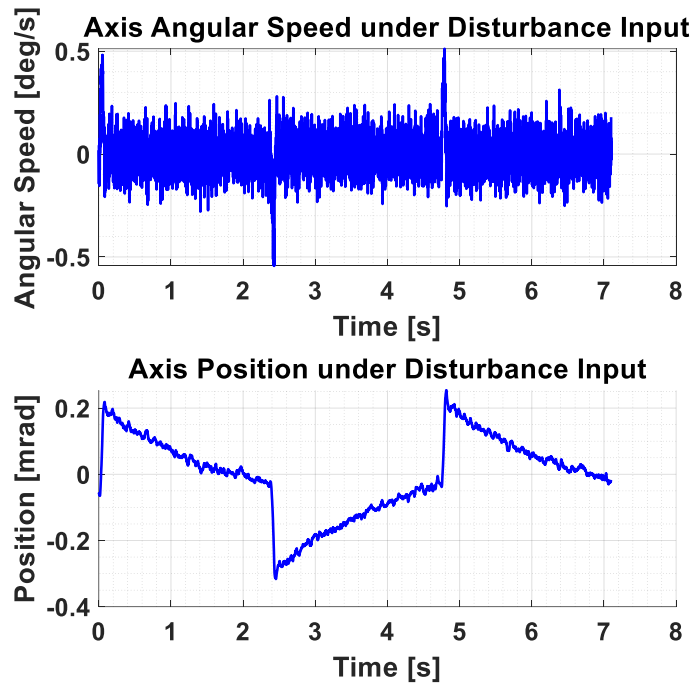
Figure 6.14. Stabilization performance of the fixed-order model-based H_∞ controller

6.2.3. Fixed-Order Data-Driven H_∞ Controller

The experimental reference tracking and stabilization performances of the fixed-order data-driven H_∞ controller are shown in Figure 6.15 and Figure 6.16, respectively.
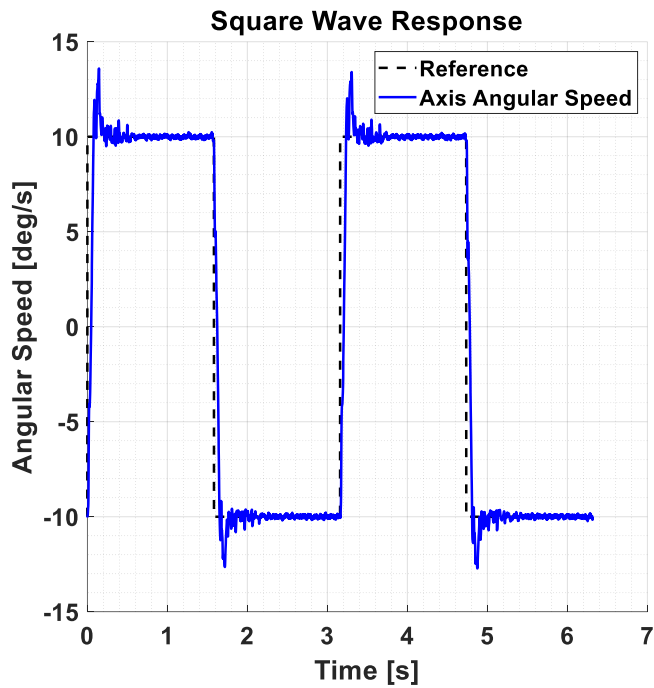
Figure 6.15. Reference tracking performance of the fixed-order data-driven H_∞ controller
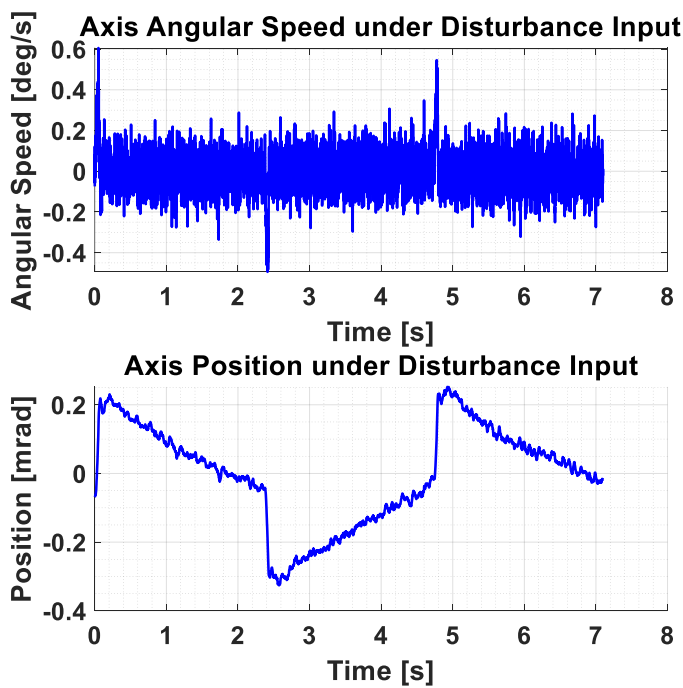
Figure 6.16. Stabilization performance of the fixed-order data-driven H_∞ controller

6.2.4. Comparison of the Controllers in Time Domain

In this section, reference tracking and stabilization performances of three different H_∞ controller are analyzed. Comparison of the step responses of the closed-loop systems with different H_∞ controllers is shown in Figure 6.17. Axis angular velocity of the stabilized

platform under disturbance input is shown in Figure 6.18. Reference tracking and stabilization performances of the H_∞ controllers are summarized in Table 6.1.

According to the Figure 6.17 and Table 6.1, although reduced-order model-based H_∞ controller provided step response with lower maximum overshoot rise time of the closed-loop system obtained with this controller is slightly higher than fixed-order controllers. Response of closed-loop system obtained with fixed-order data-driven H_∞ controller has the highest maximum percent overshoot and its settling time is slightly higher than the other responses.

In stabilization performance tests, disturbance input at $0.2\ Hz.$ is applied to the system. A motion simulator- a Stewart platform- was used to create external disturbance input. Then, standard deviation of traverse axis position of the stabilized platform is calculated to compare performances of the controllers. At low frequencies, reduced-order model-based H_∞ controller has the worst performance according to the theoretical results. Experimental results also show that the full-order model-based H_∞ controller in Design 2 has the lowest disturbance rejection performance. For the applied disturbance input at specific frequency, fixed-order model-based H_∞ controller has the best disturbance rejection performance.

Table 6.1. Time domain performances of designed H_∞ controllers for "System A"

	Rise Time [s]	Settling Time [s]	Max. Overshoot [%]	Standard Deviation of Axis Position [mrad]
Reduced-Order Model-Based H_∞ Controller	0.0624	0.1847	27.7770	0.2098
Fixed-Order Model-Based H_∞ Controller	0.0588	0.1796	31.9740	0.1295
Fixed-Order Data-Driven H_∞ Controller	0.0561	0.1864	35.931	0.1573

Figure 6.17. Comparison of reference tracking performances of closed-loop systems with different H_∞ controllers for "System A"

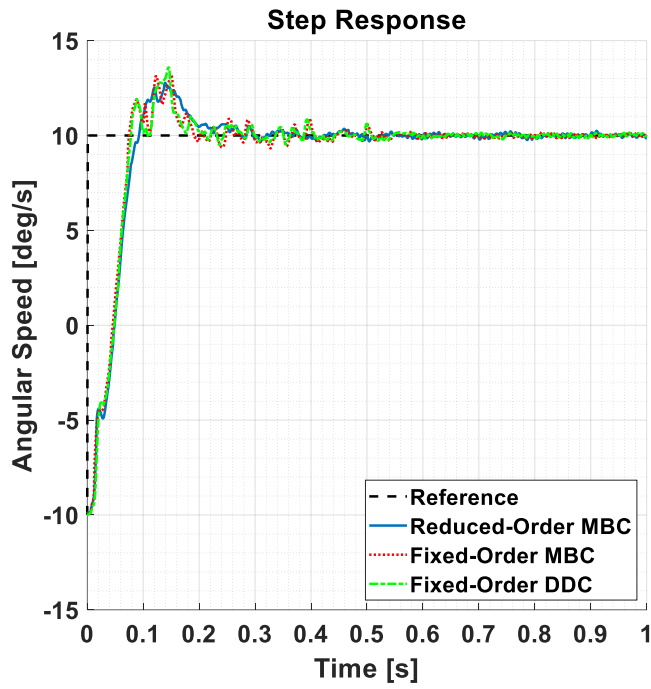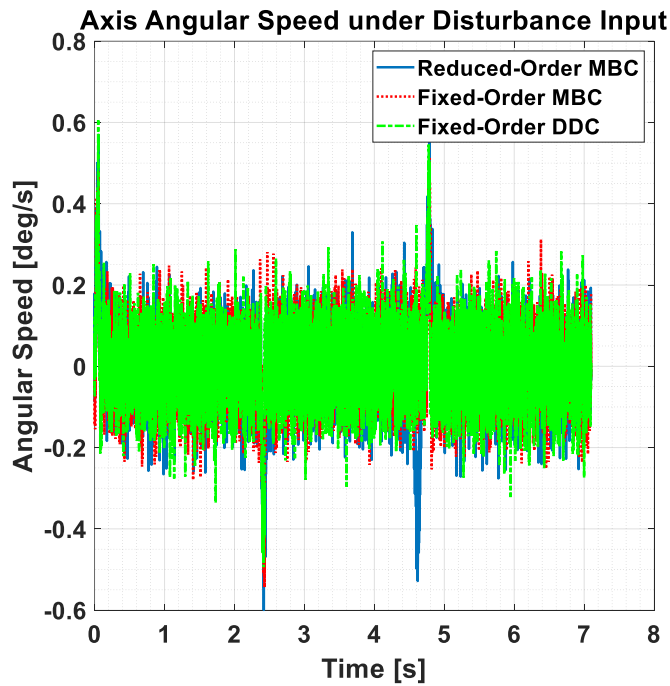Figure 6.18. Comparison of disturbance rejection performances of closed-loop systems with different H_∞ controllers for "System A"

7. CONCLUSION AND FUTURE WORK

7.1. Summary

In this thesis, model-based and data-driven H_∞ controller design methods are used to synthesize robust controllers which are integrated to the speed control loop of stabilized platform used in defense industry.

After introducing the LOS stabilization problem for stabilized platforms and some challenges in this problem, robust control theory is briefly reviewed. The general structure of the feedback control loop, closed-loop transfer functions, and design objectives of the control problem are presented. After defining different representations of uncertainty, nominal stability, nominal performance, robust stability, and robust performance conditions are derived for multiplicative uncertainty case.

After introducing the experimental test setup, system identification method is discussed. First, linearized non-parametric model set is identified by using open-loop system identification tests input/output data. To obtain the non-parametric model set, discrete Fourier transformation based method is performed and non-parametric model set of the stabilized platform is identified in frequency domain. Then, by using mean frequency response function of the system, parametric model of the plant is derived in Laplace domain. In the final step of the system identification procedure, multiplicative uncertainty region between the non-parametric model set and parametric model is calculated.

Firstly, two different full-order model-based H_∞ controllers are designed in $S/KS/T$ mixed-sensitivity framework, with different performance weighting functions. Next, fixed-order model-based controller is designed by using non-smooth optimization technique. To obtain the fixed-order controller, structure of the controller is predetermined as a PI-controller enhanced with asymmetric notch filter. Finally, another fixed-order controller with the same structure is designed by data-driven method. In this method, a novel two-stage approach is performed to calculate the unknown parameters of the controller. Next, comparison of frequency domain performances of the designed controllers is presented by obtaining sensitivity and complementary sensitivity functions for closed-loop systems.

After introducing the order reduction technique for full-order model-based H_∞ controllers, designed controllers are discretized and implemented to the real system.

Finally, reference tracking and disturbance rejection performances of the controllers are measured by real-time tests.

According to the theoretical results for frequency domain, full-order model-based H_∞ controller in Design 1 has the highest disturbance rejection performance in low frequency region. On the other hand, the magnitude of the sensitivity function of closed-loop system obtained with full-order model-based H_∞ controller in Design 2 is larger than the other closed-loop systems up to 5 Hz. In mid frequency region which is in between 5 Hz. and 20 Hz., fixed-order controllers have the worst disturbance rejection performance. In high frequency region, disturbance rejection performances of the closed-loop systems are seen to be similar. Although in mid frequency region, noise attenuation performance and robust stability margin of the fixed-order controllers are seen to be lower than the full-order controllers, in the high frequency region, fixed-order controllers are the best in terms of these metrics. According to the actuator constraints, closed-loop system obtained with full-order model-based H_∞ controller in Design 1 is produced control input which is close to the maximum motor torque limit in high frequency region.

Reference tracking performances of the obtained closed-loop systems are determined experimentally by measuring the square wave responses of the closed-loop systems. According to the real-time reference tracking tests, although the maximum percent overshoot of the response which is obtained with full-order model-based H_∞ controller is the lowest, rise time of the closed-loop system obtained with this controller is slightly higher than the fixed-order controllers. Response of the closed-loop system obtained with fixed-order data-driven H_∞ controller has the highest maximum percent overshoot and its settling time is slightly higher than the other responses.

To measure the disturbance rejection performances of the designed controllers, disturbance input at specific frequency is applied to the system. A motion simulator- a Stewart platform- was used to create external disturbance input. Then, standard deviation of traverse axis position of the stabilized platform is calculated to compare performances of the controllers. According to tests real-time test results, full-order model-based H_∞ controller has the lowest disturbance rejection performance. For the applied disturbance input at specific frequency, fixed-order model-based H_∞ controller has the best disturbance rejection performance.

7.2. Future Work

In this thesis, control design methods are applied to a SISO system. As the most essential future study, one may consider the application of the proposed model-based and data-driven H_∞ robust controller design methods on MIMO systems.

The main non-linear effect on the system is considered as the friction and the linearized non-parametric and parametric models are obtained by eliminating this effect. However, there may also be another non-linear effects on the system arising from backlash or unbalance. Another future work may be to find a method for identification of these effects on the system.

In real-time reference tracking and disturbance rejection tests, angular position of the elevation axis is fixed its natural position. Another future work may be to analyze the effect of the angular position of the elevation axis on controller performances.

8. REFERENCES

[1]   J.M. Hilkert, Inertially Stabilized Platform Technology Concepts and Principles, IEEE Control Syst. (2008). doi:10.1109/MCS.2007.910256.

[2]   A. Preumont, Vibration control of active structures, Solid Mech. Its Appl. (2011). doi:10.1007/978-94-007-2033-6_1.

[3]   M.J. Balas, Active control of flexible systems, J. Optim. Theory Appl. (1978). doi:10.1007/BF00932903.

[4]   B. Niu, H. Zhang, Linear parameter-varying modeling for gain-scheduling robust control synthesis of flexible joint industrial robot, in: Procedia Eng., 2012. doi:10.1016/j.proeng.2012.07.252.

[5]   O.J.M. Smith, Posicast Control of Damped Oscillatory Systems, Proc. IRE. (1957). doi:10.1109/JRPROC.1957.278530.

[6]   W.E. Singhose, W.P. Seering, Control of flexible manipulators with input shaping techniques, in: Flex. Robot Manip. Model. Simul. Control, 2008. doi:10.1049/PBCE068E_9.

[7]   N.C. Singer, W.P. Seering, Preshaping command inputs to reduce system vibration, J. Dyn. Syst. Meas. Control. Trans. ASME. (1990). doi:10.1115/1.2894142.

[8]   L.Y. Pao, W.E. Singhose, Robust minimum time control of flexible structures, Automatica. (1998). doi:10.1016/S0005-1098(97)00178-7.

[9]   M. Kenison, W. Singhose, Concurrent design of input shaping and proportional plus derivative feedback control, J. Dyn. Syst. Meas. Control. Trans. ASME. (2002). doi:10.1115/1.1486009.

[10]   A. Piazzi, A. Visioli, Minimum-time system-inversion-based motion planning for residual vibration reduction, IEEE/ASME Trans. Mechatronics. (2000). doi:10.1109/3516.828585.

[11]   M.N. Sahinkaya, Input shaping for vibration-free positioning of flexible systems, Proc. Inst. Mech. Eng. Part I J. Syst. Control Eng. (2001). doi:10.1243/0959651011541247.

[12]   M.J. Balas, Direct velocity feedback control of large space structures, J. Guid. Control. Dyn. (1979). doi:10.2514/3.55869.

[13]   T.K. Caughey, On the stability problem caused by finite actuator dynamics in the collocated control of large space structures, Int. J. Control. (1985). doi:10.1080/0020718508961163.

[14]   J. Shan, H.T. Liu, D. Sun, Slewing and vibration control of a single-link flexible manipulator by positive position feedback (PPF), Mechatronics. (2005). doi:10.1016/j.mechatronics.2004.10.003.

[15]   S.S. Aphale, A.J. Fleming, S.O. Reza Moheimani, Integral resonant control of collocated smart structures, Smart Mater. Struct. (2007). doi:10.1088/0964-1726/16/2/023.

[16]   W. Ji, Q. Li, B. Xu, J.J. Tu, D.A. Zhao, Cascade servo control for LOS stabilization of opto-electronic tracking platform-design and self-tuning, in: 2009 IEEE Int. Conf. Inf. Autom. ICIA 2009, 2009. doi:10.1109/ICINFA.2009.5205070.

[17]   T.Y. Kuc, W.G. Han, Adaptive PID learning control of robot manipulators, Automatica. (2000). doi:10.1016/S0005-1098(99)00198-3.

[18]   T.P. Blanchett, G.C. Kember, R. Dubay, PID gain scheduling using fuzzy logic, ISA Trans. (2000). doi:10.1016/S0019-0578(00)00024-0.

[19]   P. Schmidt, T. Rehm, Notch filter tuning for resonant frequency reduction in dual inertia systems, in: Conf. Rec. - IAS Annu. Meet. (IEEE Ind. Appl. Soc., 1999.

doi:10.1109/ias.1999.805973.

[20] D.J. Gordon, K. Erkorkmaz, Accurate control of ball screw drives using pole-placement vibration damping and a novel trajectory prefilter, Precis. Eng. (2013). doi:10.1016/j.precisioneng.2012.09.009.

[21] J. Lou, J. Liao, Y. Wei, Y. Yang, G. Li, Experimental identification and vibration control of a piezoelectric flexible manipulator using optimal multi-poles placement control, Appl. Sci. (2017). doi:10.3390/APP7030309.

[22] G.F. Franklin, J.D. Powell, A. Emami-Naeini, Feedback control of dynamic systems., 2002.

[23] M. Athans, TUTORIAL ON THE LQG/LTR METHOD., in: Proc. Am. Control Conf., 1986. doi:10.23919/acc.1986.4789131.

[24] G. Stein, M. Athans, The LQG/LTR Procedure for Multivariable Feedback Control Design, IEEE Trans. Automat. Contr. (1987). doi:10.1109/TAC.1987.1104550.

[25] K.J. Seong, H.G. Kang, B.N. Yeo, H.P. Lee, The stabilization loop design for a two-axis gimbal system using LQG/LTR controller, in: 2006 SICE-ICASE Int. Jt. Conf., 2006. doi:10.1109/SICE.2006.315268.

[26] S. Skogestad, Multivariable Feedback Control: Analysis and Design, 2005.

[27] L. Cui, J. Zhang, L. Gao, F. Wang, A robust controller of a flexible manipulator using genetic algorithm, in: 9th Int. Conf. Control. Autom. Robot. Vision, 2006, ICARCV '06, 2006. doi:10.1109/ICARCV.2006.345428.

[28] M. Baskin, K. Leblebicioglu, Robust control for line-of-sight stabilization of a two-axis gimbal system, Turkish J. Electr. Eng. Comput. Sci. (2017). doi:10.3906/elk-1606-435.

[29] J. V. Burke, D. Henrion, A.S. Lewis, M.L. Overton, Stabilization via nonsmooth, nonconvex optimization, IEEE Trans. Automat. Contr. (2006). doi:10.1109/TAC.2006.884944.

[30] P. Apkarian, D. Noll, Nonsmooth H∞ synthesis, IEEE Trans. Automat. Contr. (2006). doi:10.1109/TAC.2005.860290.

[31] M. Rezac, Inertial stabilization, estimation and visual servoing for aerial surveillance, Ph.D. Program. Electr. (2013).

[32] D.-H. Nguyen, V.-H. Nguyen, Robust Control of Two-Axis Gimbal System, in: 2019 Int. Symp. Electr. Electron. Eng., 2019.

[33] R.E. Skelton, Model error concepts in control design, Int. J. Control. (1989). doi:10.1080/00207178908559735.

[34] Z.S. Hou, Z. Wang, From model-based control to data-driven control: Survey, classification and perspective, Inf. Sci. (Ny). (2013). doi:10.1016/j.ins.2012.07.014.

[35] J.C. Spall, Multivariate Stochastic Approximation Using a Simultaneous Perturbation Gradient Approximation, IEEE Trans. Automat. Contr. (1992). doi:10.1109/9.119632.

[36] Zhongsheng Hou, Wenhu Huang, The model-free learning adaptive control of a class of SISO nonlinear systems, in: 2002. doi:10.1109/acc.1997.611815.

[37] M.G. Safonov, T.-C. Tsao, The unfalsified control concept: A direct path from experiment to controller, in: Feed. Control. Nonlinear Syst. Complex., 2005. doi:10.1007/bfb0027678.

[38] H. Hjalmarsson, S. Gunnarsson, M. Gevers, Convergent iterative restricted complexity control design scheme, in: Proc. IEEE Conf. Decis. Control, 1994. doi:10.1109/cdc.1994.411185.

[39] A. Karimi, L. Mišković, D. Bonvin, Iterative correlation-based controller tuning, Int. J. Adapt. Control Signal Process. (2004). doi:10.1002/acs.825.

[40] G.O. Guardabassi, S.M. Savaresi, Virtual reference direct design method: an off-line approach to data-based control system design, IEEE Trans. Automat. Contr. (2000). doi:10.1109/9.855559.

[41] A. Karimi, K. Van Heusden, D. Bonvin, Non-iterative data-driven controller tuning using the correlation approach, in: 2007 Eur. Control Conf. ECC 2007, 2007. doi:10.23919/ecc.2007.7068802.

[42] K. Van Heusden, A. Karimi, D. Bonvin, Data-driven controller tuning with integrated stability constraint, in: Proc. IEEE Conf. Decis. Control, 2008. doi:10.1109/CDC.2008.4739326.

[43] M. UCHIYAMA, Formation of High-Speed Motion Pattern of a Mechanical Arm by Trial, Trans. Soc. Instrum. Control Eng. (1978). doi:10.9746/sicetr1965.14.706.

[44] S. Arimoto, S. Kawamura, F. Miyazaki, Bettering operation of Robots by learning, J. Robot. Syst. (1984). doi:10.1002/rob.4620010203.

[45] Y. Xie, C. Wang, H. Shi, J. Shi, A data driven control method for structure vibration suppression, Acta Astronaut. (2018). doi:10.1016/j.actaastro.2017.11.046.

[46] Y. Xie, H. Shi, F. Bi, J. Shi, A MIMO data driven control to suppress structural vibrations, Aerosp. Sci. Technol. (2018). doi:10.1016/j.ast.2018.03.023.

[47] S. Khadraoui, H.N. Nounou, M.N. Nounou, A. Datta, S.P. Bhattacharyya, A Measurement-Based Approach for Designing Fixed-Order Controllers for Unknown Closed-Loop Architecture, Asian J. Control. (2016). doi:10.1002/asjc.1069.

[48] E. van Solingen, J.W. van Wingerden, T. Oomen, Frequency-domain optimization of fixed-structure controllers, Int. J. Robust Nonlinear Control. (2018). doi:10.1002/rnc.3699.

[49] A. Karimi, G. Galdos, Fixed-order H∞ controller design for nonparametric models by convex optimization, Automatica. (2010). doi:10.1016/j.automatica.2010.05.019.

[50] D. Mutlu, Platform Motion Disturbance Decoupling by Means of Inertial Sensors for a Motion Stabilized Gimbal, Middle East Technical University, 2015.

[51] E. Çandır, Cascaded Proxy-Based Sliding Mode Control Enhanced with Disturbance Observer for the Stabilization and Control of A Gun-Turret Platform, Middle East Technical University, 2014.

[52] Ö. Hastürk, The Stabilization Of A Two Axes Gimbal Of A Roll Stabilized Missile, Middle East Technical University, 2011.

[53] M. Baskın, LQG/LTR, H-Infinity And Mu Robust Controllers Design For Line Of Sight Stabilization, Middle East Technical University, 2015.

[54] K. Zhou, J.C. Doyle, Essentials of robust control, Prentice Hall, 1999. http://linkinghub.elsevier.com/retrieve/pii/S0005109801002722.

[55] J.C. Doyle, SYNTHESIS OF ROBUST CONTROLLERS AND FILTERS., in: Proc. IEEE Conf. Decis. Control, 1983.

[56] J.C. Doyle, K. Glover, P.P. Khargonekar, B.A. Francis, State-Space Solutions to Standard H2and H∞, Control Problems, IEEE Trans. Automat. Contr. (1989). doi:10.1109/9.29425.

[57] H. Akçay, B. Ninness, Orthonormal basis functions for modelling continuous-time systems, Signal Processing. (1999). doi:10.1016/S0165-1684(99)00039-0.

[58] R. Pintelon, J. Schoukens, System Identification: A Frequency Domain Approach, Second Edition, 2012. doi:10.1002/9781118287422.

[59] G. Ellis, R.D. Lorenz, Resonant load control methods for industrial servo drives, in: Conf. Rec. - IAS Annu. Meet. (IEEE Ind. Appl. Soc., 2000.

doi:10.1109/ias.2000.882073.

[60]   B.C. Moore, Principal Component Analysis in Linear Systems: Controllability, Observability, and Model Reduction, IEEE Trans. Automat. Contr. (1981). doi:10.1109/TAC.1981.1102568.

[61]   K. Glover, All optimal Hankel-norm approximations of linear multivariable systems and their L,∞-error bounds, Int. J. Control. (1984). doi:10.1080/00207178408933239.

APPENDICES

APPENDIX A – Experimental Results for "System B"

Controller design methods described in Chapter 3 are performed for another military stabilized platform named as "System B". The reference tracking and stabilization performances of the synthesized data-driven and model-based H_∞ controllers have been measured by real-time tests.

Comparison of the step responses of the closed-loop systems with different H_∞ controllers is shown in Figure A.1. Axis angular velocity of the stabilized platform under disturbance input is shown in Figure A.2. Reference tracking and stabilization performances of the H_∞ controllers are summarized in Table A.1.

According to the real-time reference tracking tests, speed of the response which is obtained with full-order model-based H_∞ controller is the lowest. Although the rise time of the closed-loop system obtained with fixed-order data-driven H_∞ controller is the lowest, its maximum percent overshoot and settling time characteristics are worse than other closed-loop systems. According to the real-time reference tracking and disturbance rejection tests, fixed-order model-based H_∞ controller has the best performance.

Table A.1. Time domain performances of designed H_∞ controllers for "System B"

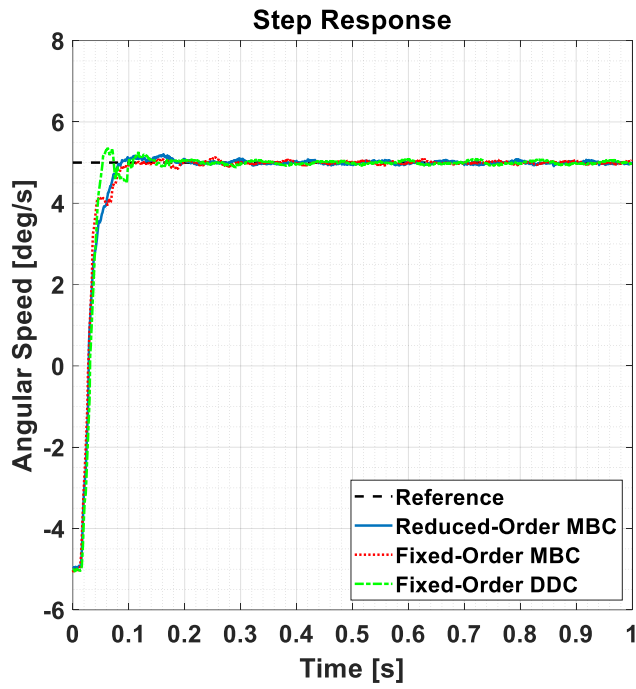|	Rise Time [s]	Settling Time [s]	Max. Overshoot [%]	Standard Deviation of Axis Position [mrad]
Reduced-Order Model-Based H_∞ Controller	0.0425	0.1621	4.156	0.1452
Fixed-Order Model-Based H_∞ Controller	0.0260	0.0845	2.6360	0.0941
Fixed-Order Data-Driven H_∞ Controller	0.0256	0.1292	7.142	0.1228

Figure A.1. Comparison of reference tracking performances of closed-loop systems with different H_∞ controllers for "System B"
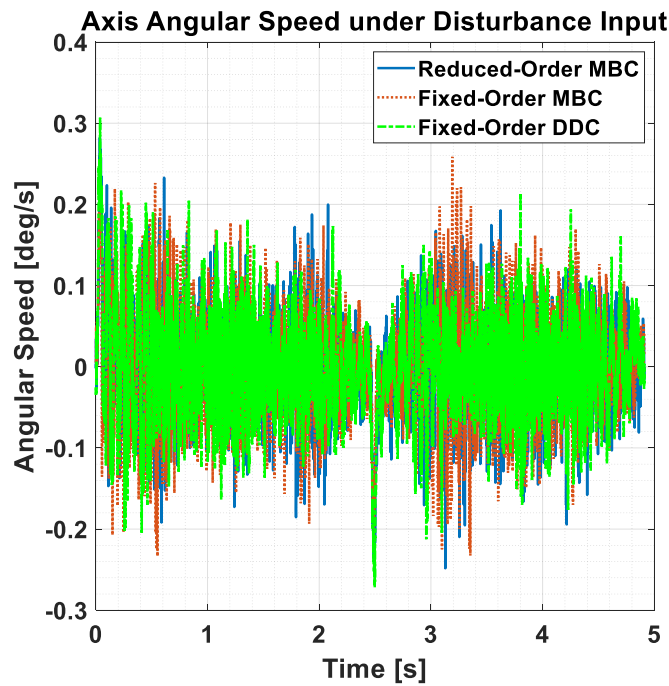

Figure A.2. Comparison of disturbance rejection performances of closed-loop systems with different H_∞ controllers for "System B"

APPENDIX B – Conference Paper

A. Arda Araz, S. Çağlar Başlamışlı, U. Mertcan Özmarangoz, "Two – Stage Data – Driven Fixed Order H_{∞} Controller Design For Flexible Mechanical Systems", TOK '19 National Congress of Automatic Control, 2019, Muğla, Turkey

CURRICULUM VITAE

Name, Surname : Ayhan Arda ARAZ

Place of Birth : Ankara, TURKEY

Date of Birth : 04/12/1991

Marital Status : Married

Address : Çankaya, Ankara, TURKEY

E-mail : ardaaraza@gmail.com

Foreign Language : English

Education

BSc. : Middle East Technical University (2016)

MSc. : -

PhD : -

Work Experience

Mechanical Engineer, Versus Engineering (2017 -)

Publications

A. Arda Araz, S. Çağlar Başlamışlı, U. Mertcan Özmarangoz, "Fixed-Order Data-Driven H_∞ Controller Synthesis for Flexible Mechanical Systems: Two-Stage Approach", *Transaction of the Institute of Measurement and Control (Submitted)*

A. Arda Araz*, S. Çağlar Başlamışlı, "An Adaptable Model for Tracked Vehicle Transient Dynamics", Journal of the Faculty of Engineering and Architecture of Gazi University (Submitted)*

A. Arda Araz, S. Çağlar Başlamışlı, U. Mertcan Özmarangoz, "Two – Stage Data – Driven Fixed Order H_∞ Controller Design For Flexible Mechanical Systems", *TOK '19 National Congress of Automatic Control, 2019, Muğla, Turkey*

S. Çağlar Başlamışlı, A. Arda Araz, Koray Beyaz, "A Black – Box Device For Driver Performance Monitoring And Vehicle Crash Analysis", *OTEKON '16 8th Congress of Automotive Technologies, May 2016, Bursa, Turkey.*